

ANALYSIS OF CONDUCTIVE PROPERTIES OF CORE/ SHELL  
NANOCOMPOSITE STRUCTURES

by

Gayathri Moorthy

A dissertation submitted to the faculty of  
The University of North Carolina at Charlotte  
in partial fulfillment of the requirements  
for the degree of Doctor of Philosophy in  
Electrical Engineering

Charlotte

2012

Approved by:

---

Dr. Kasra Daneshvar

---

Dr. Lee Casperson

---

Dr. Thomas Weldon

---

Dr. Yildirim Aktas



## ABSTRACT

GAYATHRI MOORTHY. Analysis of conductive properties of core/ shell nanocomposite structures. (Under the direction of DR. KASRA DANESHVAR)

Nanostructures have been explored considerably in recent times to ascertain the unique properties they exhibit in the nanoscale regime as opposed to their bulk counterparts. Their characteristic high surface-to-volume ratio coupled with confinement effects contribute to altering physical properties and phenomena as a function of diminishing material dimensions. Core/ shell nanoparticles are fast emerging as a preferred class of nanostructures because of the additional flexibility they offer in providing tailored properties for specific applications.

Electronic conductive properties in composite structures and the parameters responsible for conduction have captivated the interest of researchers for years. Apart from representing a challenging field in a purely academic sense, the method of characterization based on charge transport is seen as a useful tool for efficiently extricating novel behavior exhibited by nanostructures for use in modern technologies.

In this dissertation, the charge transport characteristics of three-dimensional disordered arrays of two different core/ shell nanostructure samples have been analyzed. A copper core/ copper oxide shell sample representing metal core/ metal oxide shell architecture, and a gold core/ silicon dioxide shell sample with the metal core/ insulator shell type of architecture have been used. Careful experimentation on charge transport through the samples reveal non-ohmic conduction trends in both the cases. Furthermore, it is also found that while the Cu/Cu<sub>x</sub>O sample displays a sharp increase in conductivity after a certain threshold temperature, the Au/SiO<sub>2</sub> sample exhibits a gradual increase in

conductivity without any abrupt transition. Various theoretical models have been analyzed to establish the nature of charge transfer mechanisms that predominate in the samples over the wide range of experimental conditions they are exposed to, while considering parameters like the type of core and shell materials considered, particle dimensions, and their structure.



## DEDICATION

I dedicate this dissertation to my family, and to all the people who have influenced me for the better, in various stages of my life.

## ACKNOWLEDGMENT

First and foremost, I would like to thank my advisor, Dr. Kasra Daneshvar, for his insight, constant support and valuable guidance throughout my dissertation work. I would also like to thank my committee members Dr. Lee Casperson, Dr. Thomas Weldon and Dr. Yildirim Aktas for their valuable time and inputs.

Thanks to Dr. Lou Deguzman, Mr. Terence Goveas, and Mr. John Hudak for introducing me to various Clean Room techniques and helping me develop systems that were necessary for carrying out experiments related to my dissertation.

My sincere appreciations to the Graduate & Professional Student Government (GPSG) organization and the IEEE organization at UNC Charlotte for providing students like me a platform to showcase our research on a wider scale through research fairs, and also for monetarily supporting my conference presentations through travel awards. I would also like to express my gratitude to UNC Charlotte for having supported me financially through my PhD degree.

Most of all, I would like to thank my family for their unwavering support and encouragement through my years at UNC Charlotte.

## TABLE OF CONTENTS

CHAPTER 1: INTRODUCTION	1
1.1 Scope of this Introduction	1
1.2 The Era of Nanotechnology	1
1.2.1 The Nanometer scale	1
1.2.2 The Emergence, Impact and Applications of Nanotechnology	1
1.3 Nanostructure Processing Techniques	6
1.3.1 Top-Down Approach	8
1.3.2 Bottom-up Approach	9
1.4 Characteristics of Nanostructures – Size Dependent Phenomena	11
1.4.1 Large Surface to Volume Ratio	11
1.4.2 Quantum Confinement Effects	13
1.5 Types of Nanostructures	16
1.5.1 Geometrical Classification	16
1.5.2 Core Shell Nanostructures	17
1.6 This Dissertation	22
1.6.1 Dissertation Objective	22
1.6.2 Dissertation Layout	23
CHAPTER 2: ELECTRONIC CHARGE TRANSPORT IN NANOSCALE SYSTEMS	25
2.1 Introduction	25
2.2 Charge Transport	26
2.2.1 The Classical Concept	26

2.2.2 Physical Considerations and Characteristic Lengths	27
2.2.3 General Classification of Charge Transport Regimes	30
2.3 Charge Transfer Mechanisms in Nanoscale Systems	34
2.3.1 Tunneling Mechanisms	34
2.3.2 Temperature Assisted Mechanisms	40
2.3.3 Hopping Conduction	45
2.4 Experimental Objectives of this Work	49
CHAPTER 3: EXPERIMENTAL ANALYSIS OF ELECTRICAL CONDUCTION THROUGH CORE/ SHELL NANOCOMPOSITES	50
3.1 Introduction	50
3.2 Experimental Work	50
3.2.1 Samples used	50
3.2.2 Photolithographic Patterning of Electrodes	53
3.2.3 Measurement Setup for Electrical Characterization	54
3.3 Results And Discussion	57
3.3.1 Sample 1: Copper/ Copper oxide core/ shell structure	57
3.3.2 Sample 2: Gold/ Silicon dioxide core/ shell structure	59
3.3.3 Comparisons and Discussion	60
3.4 Conclusion	61
CHAPTER 4: MODELING OF CHARGE TRANSPORT BEHAVIOR	63
4.1 Introduction	63
4.2 Charge Transport Models	64
4.2.1 Crossover from Macroscopic to Microscopic regime	64
4.2.2 Classical Model – Drift-Diffusion Model	65

4.2.3 Semiclassical Model - Boltzmann Transport Equation	67
4.2.4 Quantum Transport Models	70
4.3 Theoretical Modeling Objectives of this Work	71
4.3.1 Proposed Models for Different Nanoscale Systems	72
4.3.2 Modeling the Behavior of Samples used in this Study	80
4.4 Conclusion	89
CHAPTER 5: FINAL REMARKS AND FUTURE DIRECTIONS	92
REFERENCES	95
VITA	108

## CHAPTER 1: INTRODUCTION

### 1.1 Scope of this Introduction

This chapter serves as an introduction to nanotechnology and nanomaterials. It provides a basic background of this field, along with some essential terminology and definitions used in this study. This chapter would enable a novice to appreciate the various facets of nanotechnology and highlight the significance of this research work related to the study of conductive properties exhibited by specific types of nanostructures.

### 1.2 The Era of Nanotechnology

Nanotechnology literally means any research and technology development carried out on a nanoscale that provides a fundamental understanding of phenomena manifested in nanoscale materials, which in turn could have applications in the real world.

#### 1.2.1 The Nanometer scale

A nanometer is 1 billionth of a meter ( $10^{-9}\text{m}$ ), and a nanostructure is any structure with at least one characteristic dimension lying between 1nm and 100nm, putting nanostructures as intermediate in size between a molecule and a bacterium. Figure 1.1 shown below helps us get a better idea of the nanoscale by comparing it with some common recognizable objects.

#### 1.2.2 The Emergence, Impact and Applications of Nanotechnology

The origin of Nanotechnology is often traced to Richard Feynman's famous speech "There's Plenty of Room at the Bottom" in 1959 [2], where he foresaw the possibility of

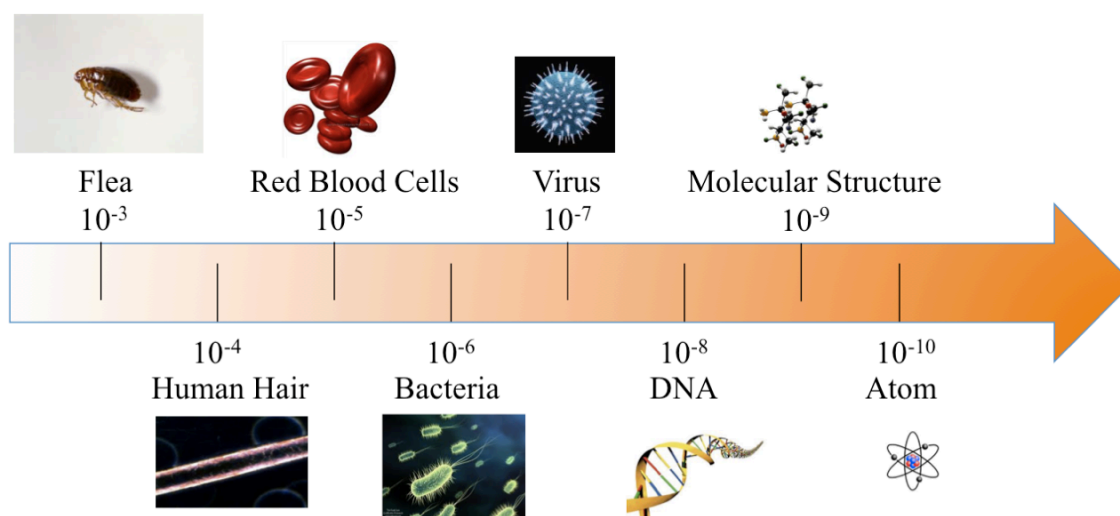


Figure 1.1: Length scale showing size of nanostructures in comparison with other objects [1]

making nanoscale machines that could “arrange atoms” in any way we wanted. Later, Drexler proposed that atoms and molecules could act as self-assembling machinery to perform different tasks at the nanoscale [3]. Though his idea sounded far-fetched at that time, he also pointed out that this is something that has already been put to use by nature. The human body is the best example of a natural machine with multiple nanostructured parts, and specific arrangements dictating their functions. The DNA is one such structure whose only function is to store and replicate information. Photosynthesis in plants is another example where special light sensitive nanoscale pigments inside chloroplasts capture light and trigger a chain of chemical reactions within the plant to produce oxygen and sugar. Following this vision, one area of nanotechnology that developed was concerned with technological feasibility at the nanoscale level and production issues, while another area that dealt with the ‘applications’ aspect of nanotechnology gradually emerged, where the novelties arising from the size-dependent phenomena exhibited by nanoscale materials were exploited.

The realization that there exist small things in the world not visible to the naked eye dates back several centuries, much before the emergence of this dedicated field of study called nanotechnology. Romans used Gold and Silver nanoparticles to color glasses, such that they would give the illusion of being differently colored when illuminated from the front or back. Gold nanoparticles were used for inorganic dyes to introduce red color into their ceramic porcelains. Nanoparticles were also used in hair dyes, cosmetics and for curing several diseases [4, 5].

Despite this, nanotechnology has gained popularity and attracted widespread research attention only in recent times. This is primarily due to the development of new microscopic imaging techniques to expand the direct visibility range, and analytical tools like Transmission Electron Microscope (TEM), Scanning Electron Microscope (SEM), etc., along with new synthesis methods over the last few decades.

In the last 30 years, significant improvements in technology have facilitated manipulation of structures at extremely small scales. Rapid advances in sciences and industrial innovation have fostered interest in miniaturization of the microchip to produce faster, efficient and smaller devices [6]. This has been a major driving force for the advent of microelectronic technologies [7-9], especially in computers where the need for increased computing power has required the number of transistors to increase almost exponentially in the same silicon space (Moore's Law [10]). Though Moore's law is expected to hold for one more decade [11], there will come a point when miniaturization below certain dimensions would bring about a change in the very behavior of components and highlight issues like heat dissipation and power consumption. Thus newer technologies based on Quantum computing and photonics are emerging.



Nanostructures are being manipulated to increase data storage capacities to more than a million times the current capacity with an idea of considering the 'presence' or 'absence' of an atom as a '1' or a '0'. Reaching such a device that works with 1 atom per bit is currently being perceived as the final target [12]. Thus, the constant need for smaller and smarter consumer technology has accelerated advancement not only in the field of nanoelectronics, but nanotechnology in general.

In the medical field, advances in diagnostic tools and the development of efficient therapeutics have brought the goal of combining these two areas to create nanodevices called nanobots one step closer [13]. One of the interesting ideas being researched upon is using nanomaterials for targeted delivery of drugs to certain organs or tissues. These drugs are extensively being researched on for treatment of cancer cells at the affected site rather than using the highly toxic chemotherapy, and in general this technology can lead to drugs with more effective cures and lesser side effects. In the area of renewable energy, nanoparticles may be useful in providing alternatives to the current practice of having to burn non-renewable carbon containing fuels. They may also be used for improving storage capacity of rechargeable and non-rechargeable batteries. The latest nanotechnology projects related to renewable energy are storage, energy conversion and improvements in manufacturing techniques. New methods to synthesize different semiconductors have made it possible to develop nano-sized sensor systems to gauge the effect on the environment [14, 15]. Bandgap engineered quantum devices like lasers and heterojunction bipolar transistors have been developed with unique electronic transport and optical effects [16]. Carbon Nanotubes can be used in displays, as electronic connectors, and even as nanoscale drug dispensers [17]. Another huge market for

nanotechnology is the cosmetic industry. Research on certain nanoparticles has shown that they can be used to repair and heal tissues by efficiently getting absorbed by the skin. Nano-Titanium dioxide and Zinc oxide have been found to absorb and reflect UV light, while being transparent to white light. Such particles can be used in sunscreens and other cosmetics for protecting the skin against UV rays. Fullerenes are new nanomaterials that are being used in cosmetics owing to their antioxidant properties [18]. These materials are also being researched on for the delivery of drugs [19], in medical diagnostics [20] and also as nanoscale lubricants [21, 22]. They are also being investigated for applications in optics and as superconductors [23]. Similarly, it has also found its way into the agriculture industry, where nanoparticles can be used to develop systems to help supply pesticides and monitor environmental conditions of different crops. They are being researched upon to enhance nutritive value of foods through addition of nutritive nanocapsules. Nanotechnological approaches are also being examined to help curb environmental degradation and improving quality of air, water and soil. Certain nanoparticles can serve as potent adsorbents, or be used in combinations with other materials for chemical destruction of contaminating agents [24].

As evident from the above examples, nanotechnology has definitely found its way into many different sectors. It is said that technology has made the world seem like a smaller place to live in; and now this very technology is shrinking, in a literal way. Though research in nanoscale is not new, what has changed over the years is our ability to see and manipulate, image and engineer matter at the nanoscale level [25]. We have entered the era of engineered nanomaterials and devices where controlled manipulation of nanoscale objects is important, especially when dealing with particles below  $\sim 50$  nm,

as size variations could change the basic characteristics of materials like their conductivity, color, solubility, chemical resistance and mechanical strength to name a few. We have to delineate a limit to sample dimensions so as to allow tuning of their properties to our advantage.

### 1.3 Nanostructure Processing Techniques

Since the properties of nanoparticles depend so closely on their size, size distribution and morphology, engineering of materials with novel properties through controlled synthesis and assembly of the material at the nanoscale level is of great interest to researchers today. Different types of nanostructures (powders and compacted solids, organic and inorganic, nanocomposites and nanotubes, self assembled quantum dots and randomly arranged dots, thin films and fibers) are rigorously being studied to assess their size dependent properties. This is a prerequisite to permit manufacturing of materials with tailored properties and sufficient stability. There are various routes for synthesis and assembly of nanostructures, but there are common issues that come to the forefront in different methods.

Primarily, we need to recognize the critical scale lengths that define material structure and organization in the nanometer regime, and that eventually dictates the fundamental macroscopic properties of the material. Improving the ability to control matter has long been the motivation behind research in nanoscale. Progress in science suggests the feasibility of achieving thorough control of the molecular structure of matter via controlled molecular assembly. The consequences of such ability can result in enhanced properties like increased hardness, magnetic coupling, catalytic enhancement, selective adsorption or higher efficiency electronic or optical behavior, and will in turn pay

significant returns in areas as diverse as medicine, computation manufacturing and the environment.

Synthesis and assembly strategies accommodate precursors from liquid, solid or gas phase; employ chemical or physical deposition approaches; or similarly rely on either chemical reactivity or physical compaction to integrate nanostructure building blocks within the final material structure [26]. Despite the broad range of synthesis approaches available, the critical control points fall under two main categories.

- (i) Size and composition control of nanocluster components, whether they are aerosol particles, powders, semiconductor quantum dots or other nano-components.
- (ii) Control of interfaces and distributions of the nano-components within the fully formed materials.

It is important to understand how to exercise separate control over nucleation of nanostructure building blocks and growth of these components throughout the synthesis and assembly processes. For this one needs to comprehend the chemical, thermal and temporal stability of such formed nanostructures, and also take into account the cost effectiveness and stability of large-scale production.

There has been a steady progress in this field especially due to the more general availability of characterization tools having higher spatial, energy and time resolution to clearly identify and trace the nanostructure formation. Innovation in surface engineering techniques and observation of unique size-dependent effects in nanostructures in their electrical, chemical, optical and magnetic properties has surely drawn research interest towards the rich palette of phenomena yet to be technologically exploited.

Two routes have been identified to construct nanomaterials and nanotechnologies; a

top-down approach that refers to ‘sculpting’ or successive slicing of bulk materials to get nano-sized articles, and a bottom-up approach that refers to build up of a material from the bottom: atom by atom or molecule by molecule [25].

### 1.3.1 Top-Down Approach

The top-down approach refers to creating ‘nano-objects’ from a larger parent entity. This approach relies on micromachining materials to the desired size and patterns and in general is subtractive in nature. Popularly used lithography techniques like photolithography, e-beam lithography, X-ray lithography, and other processes like etching, mechanical machining/ polishing also follow the top-down approach. This method is currently the most developed method in fabrication with its base in the semiconductor industry. Another top-down approach is ball milling, that is, the formation of nanostructure blocks through controlled mechanical attrition of the starting bulk material [27]. These techniques have been commonly employed to make mechanical structures like gears and motors, whose dimensions are tens of microns in diameter, many orders of magnitude larger than nanometer scale.

While this line of development has found its place in the micro and nano electromechanical system (i.e. MEMS and NEMS) industry, it has achieved moderate success in nanomaterial synthesis, with its limitations already getting discernable in the case of microchip fabrications where there is enormous commercial pressure for further miniaturization. The biggest problem with the top-down approach is the imperfection of surface structure due to induced stress and significant crystallographic damage to the processed patterns [28]. These imperfections in turn lead to additional challenges in the device design and fabrication. Mass production of such structures is another issue.

Though the top-down approach enables production of complex architectures, it is time consuming and provides limitations in scale and material. Hence a bottom-up approach needs to be considered.

### 1.3.2 Bottom-up approach

The Bottom-up approach first forms the nanostructured building blocks and then assembles them into more complex forms. It starts from the size range 0.1 – 1nm, and extends to the 10 - 100nm scale. There are different technologies that have been developed for this approach. This can be done broadly in two ways – the first being manipulation on the atomic or molecular scale using scanning probe microscopes [29-31], and secondly by allowing self-organization in crystal growth and chemical synthesis. Here, electrons and atoms are allowed to organize themselves into structures, typically called self-assembly. This self-organization process allows spontaneous fabrication of nanostructures using a single and cheap growth procedure, and this has attracted immense attention for its potential to become an alternative route to lithography to push the limits of integration further at a reasonable cost. Growth parameters and the combination of materials are being researched upon to be able to develop self-organized structures of specific dimensions. Colloidal dispersion is a common example of the bottom-up approach, which has also been used in industry for over a hundred years. Examples are the production of salt and nitrate in the chemical industry.

Other common examples of this technology are thin film growth, self and directed assembly of colloidal particles, and spinodal wetting/ dewetting [32]. These nanostructures can then be consolidated in bulk form using techniques like compaction. For example, Wu et al. [33] proposed a method to form powder components through

aerosol techniques followed by compaction of these components into the final material. The degree of control required over the nanostructure size and the nature of their distribution and bonding within the fully formed material varies greatly depending on the ultimate materials application. The bottom-up approach provides a better opportunity to obtain nanostructures with fewer defects and a more homogeneous chemical composition [34]. The quality of interfaces also can be potentially controlled at this scale.

Figure 1.2 shows the difference between these two processing techniques, both of

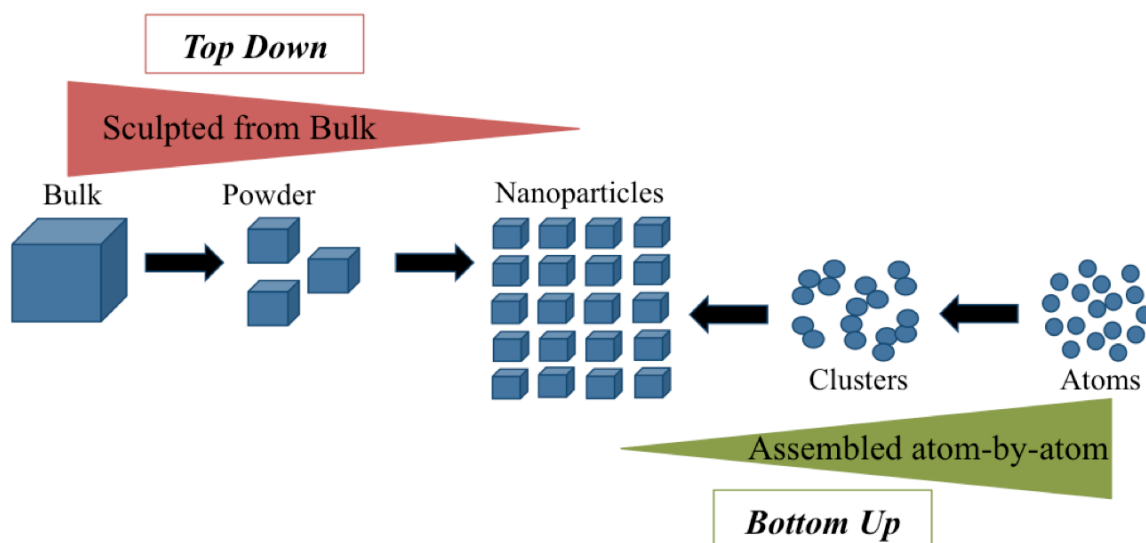


Figure 1.2: Nanostructure processing methods

which are equally efficient concepts with a number of techniques for producing nanostructures. While in a top-down approach, scientists try to improve the concepts in use today like lithography, in a bottom-up approach, one tries to tailor the growth of separate entities like atoms, molecules and clusters up to fabricating patterns. Many current strategies for material synthesis are trying to integrate synthesis and assembly into a single process [35, 36]. The challenges in nanotechnology are slowly entailing an

overlap of both processes wherein top-down approaches like lithography are used to provide a link between the structure and technical environment, while integration of nanostructures to form a functional block uses the bottom-up approach. Thus both these methods have distinct uses in technology and are not always reversible.

#### 1.4 Characteristics of Nanostructures – Size Dependent Phenomena

In nanotechnology, understanding the relation between the physical/chemical properties exhibited by nanostructures and their dimensions are of prime importance. In this size scale, the composition, shape and size of the material can be effectively used to control electronic, optical, mechanical and magnetic properties of the nanostructures. Intensive research has been carried out over the last few decades to study this size-dependent relationship that nanoparticles exhibit different from their bulk counterparts, and still remains a popular research topic in current times. Size effects can be attributed to two main factors (i) Large surface to volume ratio and (ii) Quantum confinement

##### 1.4.1 Large Surface to Volume Ratio

In macroscopic materials, the numbers of atoms on the surface of the material are much smaller than the total number of atoms within the bulk. Hence surface related effects play a minimum role in determining the average properties of the material. This scenario changes as the particles approach nanoscale because the ratio of number of atoms on the surface to the total bulk atoms becomes significant [37, 38]. This is well represented in Figure 1.3.

Surface is an interface between the material and the environment. Hence surface atoms behave differently from bulk atoms. Atoms at the surface have fewer direct neighbors than atoms in the bulk, thus reducing the mean coordination number. Because



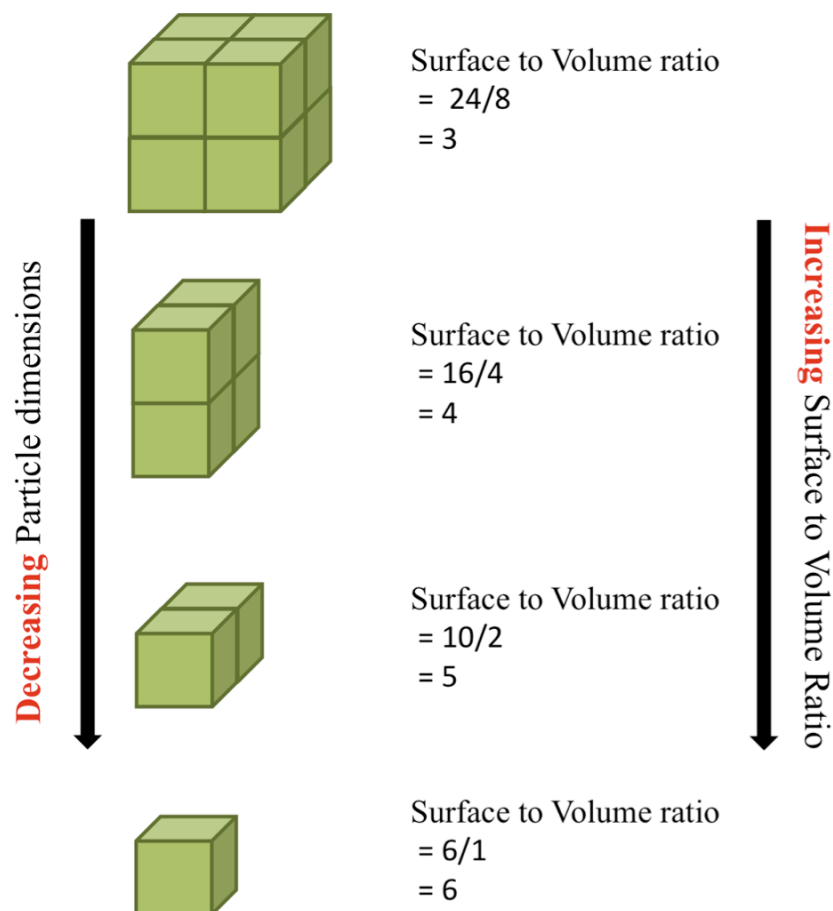


Figure 1.3: Change in Surface to Volume ratio with respect to size of the material

of this, surface atoms tend to be less stabilized than bulk atoms as they get influenced by two different environments; atoms in the nanoparticle core on one side, and influences of the external environment on the other. Some surface atoms of nanoparticles may be able to bind tightly to foreign molecules [39], some may have dangling bonds or other such defects, allowing them to bind with other matrix atoms [40]. There might also be nanoparticles that can limit their thermal expansion, thus increasing their melting point temperatures compared to their bulk counterparts [41]. Thus some form of surface reconstruction always occurs. Depending on the kind of surface atoms, the catalytic

activity of the nanoparticle can change. Surface reconstruction can lead to creation of energy levels in the energetically forbidden gap of the bulk counterpart. This can create trap states for the electrons [42], which can in turn alter optical and electronic properties of these nanoparticles.

#### 1.4.2 Quantum Confinement Effects

In a bulk material, carrier motion is unrestricted in all three spatial directions. When a material is physically made smaller, the size of the region where an electron is free to move goes on reducing. The boundaries of the material begin to squeeze the electrons and holes within the nanostructure, and this is called confinement. Depending on the number of confinement directions, nanostructures are typically classified as quantum wells, wires, and dots, to refer to one, two, and three confinement directions of the structure respectively. When materials are confined by making their dimensions smaller than the excitonic bohr radius of that material, which is typically the average distance between an electron and hole in an exciton, the electronic energy levels of the structure begin to get modified. As the confinement increases, the distance between the allowable electron energy levels goes on increasing, and they become more discrete. Since many of the material properties depend on the electron band structure of the material, a confined particle exhibits properties different from a bulk particle of the same material. Confinement, thus, can be seen as a way to manipulate the organization of energy levels into which the electrons can climb or fall by carefully modifying the nanoparticle size.

The number of energy levels or states per unit energy range is termed as density of states ( $\rho_{DOS}$ ). This attribute of a material is also a function of the degree of confinement. To calculate the density of states, one needs information about the dimensionality of the

material, and the energy 'E' versus wavenumber 'k' relation (dispersion relation) that it obeys. In a bulk material, the density of states is obtained as

$$\rho_{DOS}^{3D} = \frac{1}{(2\pi)^2} \left( \frac{2m^*}{\hbar^2} \right)^{3/2} \sqrt{E} \quad (1.1)$$

Hence this shows a continuous distribution of energies, with the density of states showing a proportional dependence on energy as  $E^{1/2}$ . As the electrons are free to move in all three dimensions, the density of states tend to become smaller near the band edges, and increase with distance from the band edges.

As these materials get confined in one or more dimensions, the density-of-states profile also gets noticeably altered. In 2-dimensional Quantum well structures, the density of states is derived as

$$\rho_{DOS}^{2D} = \frac{m^*}{\pi \hbar^2} \quad (1.2)$$

In these structures the expression shows that  $\rho_{DOS}$  does not depend on energy. Since the motion of electrons is restricted in one direction, this suppresses the increase in density of states with distance from the edges. As a result, the density of states shows a step like behavior, and as soon as the top of the energy gap is reached, there are a lot of available states.

The density of states relation for 1-dimensional Quantum wire structures and 0-dimensional quantum dot structures have been shown in Eq. (1.3) and Eq. (1.4).

$$\rho_{DOS}^{1D} = \left( \frac{2m^*}{\hbar^2} \right)^{1/2} \frac{1}{\pi \sqrt{E}} \quad (1.3)$$

In one-dimensional systems, electron motion is allowed only in one direction, and this causes the energy levels to become more discrete. The density of states show an inverse relation to energy as  $(E)^{-1/2}$ .

$$\rho_{DOS}^{0D} = 2\delta(E) \quad (1.4)$$

In a quantum dot, no free motion of electrons is possible; consequently there is no  $k$ -space that could be occupied by electrons. Each state can only be occupied by two electrons (with different spins), and this leads to the density of states given in the above equation (Eq. 1.4), which is described by a delta function ( $\delta(E)$ ). Figure 1.4 shows schematic diagrams of the dependence of density of states on confinements in one, two and three dimensions, resulting in different density-of-states profiles.

In conclusion, both the factors described above contribute to unique electronic, optical, mechanical and magnetic properties to the nanostructures, which become size dependent. Apart from these modifications in density of states, new scattering effects due to confinement, surface disorder/ roughness and impurities might also manifest themselves in the nanoscale [43]. Hence, understanding the relation between the physical/chemical properties exhibited by nanostructures and their dimensions are of prime importance. All these additional phenomena can be utilized to produce radically

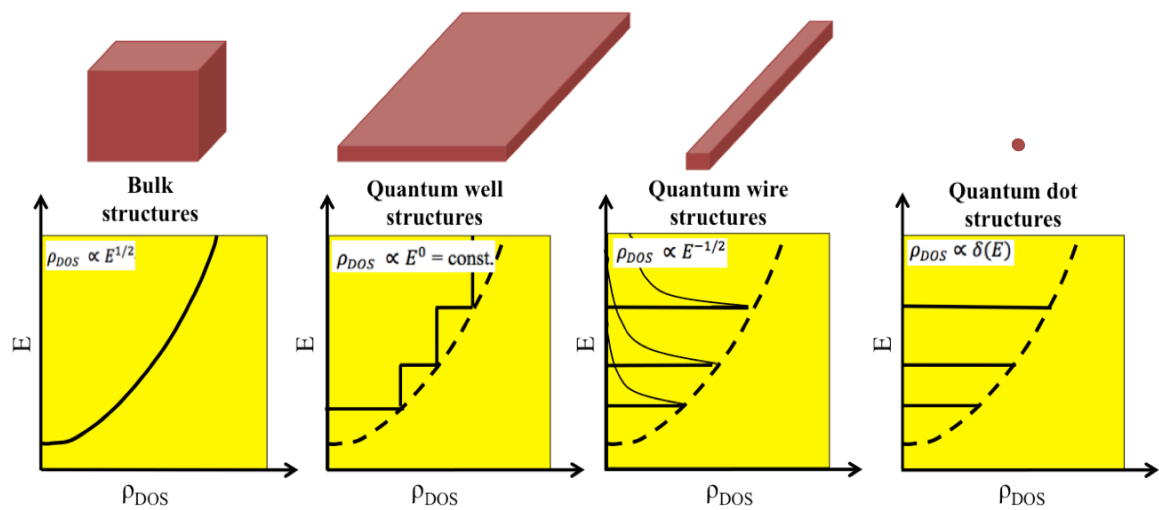


Figure 1.4: Electronic density of states for (a) Bulk material (b) Two-dimensional structures (quantum wells) (c) One-dimensional structures (quantum wires) (d) Zero-dimensional structures (quantum dots)

different types of components for electronic, optoelectronic and information processing applications like resonant tunneling transistors and single electron transistors.

Effect of Quantum confinement on Electrical - Transport properties: The variations in electronic properties as length scales reduce are mainly due to the increasing influence of the wave like property of electrons and the paucity of scattering centers. In macroscopic systems, electronic transport is primarily determined by scattering with phonons, impurities or other carriers. The path of each electron is random, and this represents a diffusive type of transport where the electron wave function cannot be represented by a single phase over the whole sample. When system dimensions become smaller or comparable to the de Broglie wavelength of electrons, the wave nature of electrons become evident. The electronic energy states start becoming more and more discrete, although perfectly discrete states are observed only in nanostructures confined in all three dimensions. This also introduces us to a new localization phenomenon specifically related to phase interference, where charge carriers can travel through the system without randomization of the phase of their wavefunctions if the system is smaller than the mean free path. In some cases, the scatterings can be completely eliminated and the electrons can move ballistically through the entire system, without any resistance.

## 1.5 Types of Nanostructures

### 1.5.1 Geometrical Classification

The properties and specific functions of nanoparticles have been found to be controllable by their shape and size at the nanometer scale [44]. Nanostructures can be classified in many different ways, but as mentioned in Section 1.4.2, they are most commonly classified as:

- (i) Zero-dimensional (0-D) quantum dot structures such as metallic, organic, ceramic quantum dots, nanopowders. These structures have all dimensions in the nanometer range.
- (ii) One-dimensional (1-D) quantum wire structures like nanowires, nanotubes and nanorods. These structures are rod shaped and have one dimension outside the nanometer range.
- (iii) Two-dimensional (2-D) quantum well structures like nano-coatings and thin films. These sheet-like structures have two dimensions beyond nanometer scale.

Figure 1.5, below, shows a bulk structure confined in one, two and three dimensions to the nanometer scale, and the commonly used terms for such structures.

Consequently a lot of improvised mechanisms have contributed to growing nanostructures with a wider variety of geometries resulting in more detailed forms of classifications. They have been subject to a variety of surface engineering techniques to suit different applications. Some of the popular categories include nanobelts, nanoneedles, nanocomposites, nanofabrics, nanofibers, nanoflowers, nanoparticles, nanopillars, nanorods, nanoshells, nanopowders, nanoclusters, and so on [6, 45].

### 1.5.2 Core Shell Nanostructures

With numerous applications being identified in every field, there is considerable attention given to developing a new class of multicomponent, multifunctional nanomaterials integrated in single structures. One result of such technological progress has been the development of core/shell nanostructures.

This new class of complex nanostructures has a central core of one material uniformly encapsulated by a layer of another material called the shell. The shell follows the same geometry as that of the core. This concept of one material surrounded by

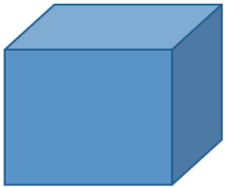



	Number of Confined Dimensions	General Name of Structure
	0	Bulk
	1	Quantum well
	2	Quantum wire
	3	Quantum dot

Figure 1.5: Classification of nanostructures based on geometry : quantum confinement in 0, 1, 2 and 3 dimensions

another has provided researchers the flexibility to experiment with different material combinations, picking from a wide range of materials from metals, oxides, organic/inorganic materials to polymers and insulators. By modifying the size, structure and composition of either of these materials, it is possible to achieve tunable chemical and physical properties with precise control [46-52]. The collective properties exhibited have often been found to be distinct as compared to that of individual components, giving

them a technological edge over conventional materials.

Initially this concept was popularized for its use in making semiconductor heterostructures, where the interface between a semiconductor core and shell creates a step potential, and confines the electrons and holes leading to confinement effects. Such effects could be put to use in lasers and solar cells [32, 53]. The shape of potential in conduction and valence bands is determined in these structures by positions of the corresponding band edges in the materials used as well as by the geometry of the structure. Based on the band alignments, two architectures are recognized, represented as Type I and Type II band alignments (cf. Figure 1.6).

In Type I architecture, the extreme band edges of conduction and valence bands both either lie in the core, or in the shell. Figure 1.6(a) shows the two possible cases, where the electrons and holes are confined in the core or in the shell respectively, and have been tapped for photo-emitting and laser applications that require enhanced emission efficiency. Type II architecture has a staggered band alignment, where the valence band edge or the conduction band edge of shell material is located in the bandgap of the core, as evident from the two cases in Figure 1.6(b). This band alignment renders a spatial separation between the hole and the electron in different regions of the core shell structure and helps suppress non-radiative electron-hole recombination. This also results in a smaller effective bandgap [54, 55] than the individual core and shell materials, and can be manipulated to control the emission wavelengths.

However, this idea has gradually been expanded to many other types of material combinations beyond semiconductors. Sometimes the core is the major component with desired properties for a particular system, and the outer shell acts as a protective layer to



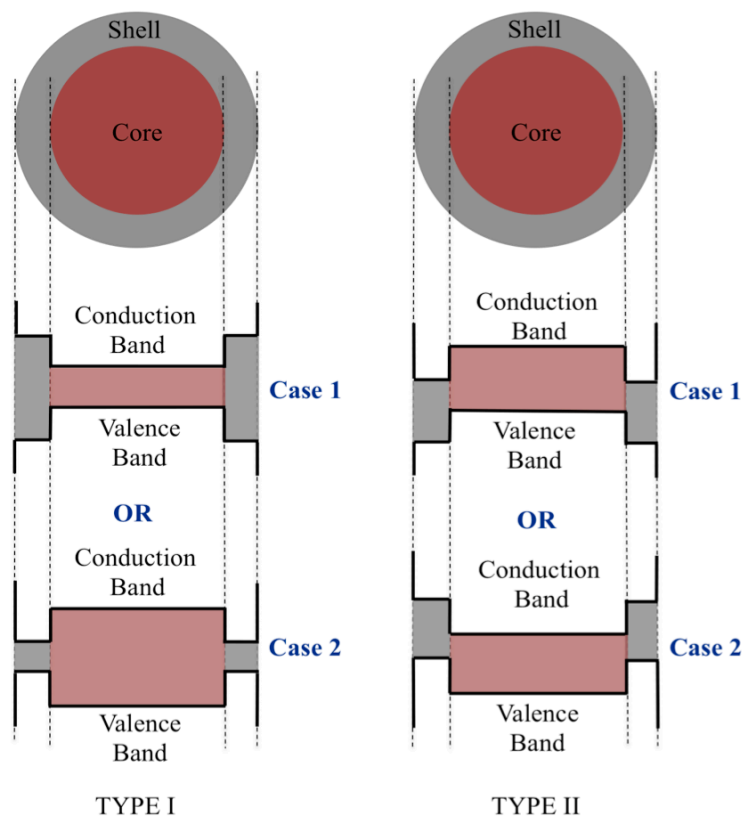


Figure 1.6: Semiconductor Core/ shell heterostructures based on band structure alignments

passivate the core or improve its chemical stability or modify its properties. Often times the surface of a nanoparticle has defects called trap sites or unfinished ‘dangling’ bonds that may reduce chemical reactivity or fluorescence quantum yield [56-58] of the nanoparticle. To overcome this, a concept of coating a ‘dead’ layer or shell over this imperfect nanoparticle core is widely used. This improves the fluorescence and quantum efficiency of nanoparticles significantly [59], because the shell eliminates core surface traps, and confines carrier excitation within the core. Sometimes, shell materials might be selected to consciously create dangling bonds on the surface, and improve the binding capability of the particle to a particular system. This method is strongly being pursued for biological applications including cell targeting and drug delivery. As an example, drug

molecules are encapsulated within biocompatible or biodegradable shell molecules for controlled drug delivery [60-62] to specific sites within the body (cf. Figure 1.7). Materials with a luminescent core can be used as nano-markers that can produce a wide range of colors over a wide pH and temperature range. They can be manipulated to attach to cancer cells or tumor cells to enable cell tracking and selective destruction of the affected cells [63-65]. Multifunctional nanoparticles with a luminescent core can be used in conjunction with a shell conjugated with a biomolecule or drug that can be used for cell targeting, imaging and drug delivery at the same time [66].

Hence, core/ shell structures present a flexible platform for further surface functionalization. Since their properties relate highly to their size specifications, core

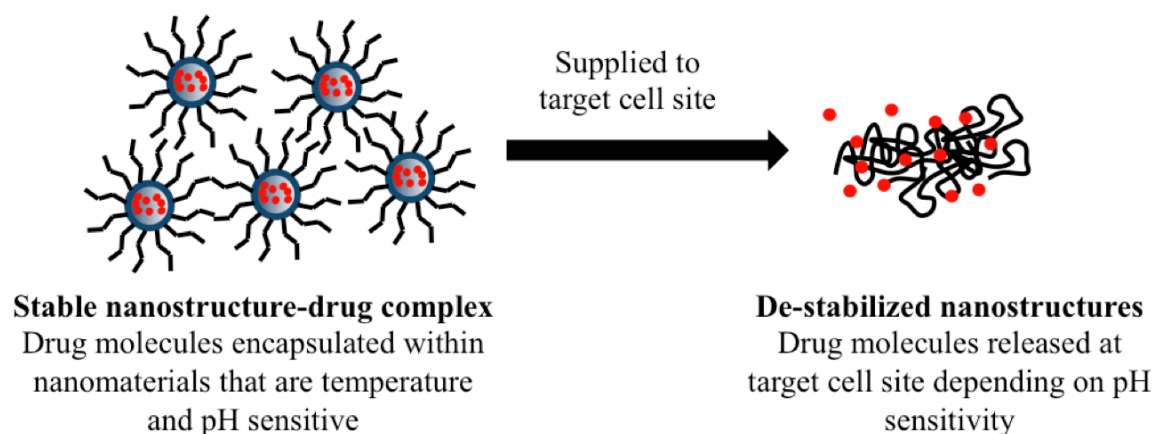


Figure 1.7: Core/ shell applications in the Biomedical field

diameters, shell thicknesses and the nature of interactions between core material and the shell material, extensive experimentation and research criteria need to be established to be able to tap their unique properties in a range of electronic, chemical and biomedical applications.

## 1.6 This Dissertation

### 1.6.1 Dissertation Objective

This work contributes to the goal of exploring the unique properties that nanostructured core/ shell materials could exhibit. Two samples made up of a three dimensional disordered array of monodisperse core/ shell nanostructures have been used for this study; a Copper core/ Copper oxide shell sample with a metal core/metal oxide shell architecture, and a Gold core/ Silicon dioxide shell sample with a metal core/insulator shell architecture. Both samples have a general form of an array of metallic cores surrounded by non-conducting shells. Ordinarily, a bulk structure with similar architecture would not allow any charge transfer through it, because of the non-conducting shell materials isolating the metallic cores from one another.

Hence, the first aim of this study was to experimentally analyze if having such a core/shell architecture in the nanometer scale would instigate any charge transfer mechanism in the structure contrary to our expectations. The experimental part involved building a system to effectively measure conduction through the sample, varying parameters like temperature, voltage and pressure accurately and recording the current flow through the system.

Secondly, charge transfer mechanisms are known to be strongly dependent on particle size and type of interactions between core and shell materials. Consequently, a second aim was to further establish theoretically the reasons behind the observed charge transport traits. Different theoretical models were studied and used to analyze the experimental results theoretically. The main objectives and workflow of this dissertation are as shown in Figure 1.8.

Apart from representing a challenging field in a purely academic sense, material characterization based on charge transport through disordered/ randomly arranged structures is seen as a useful tool for characterizing current and potential nano-devices and systems.

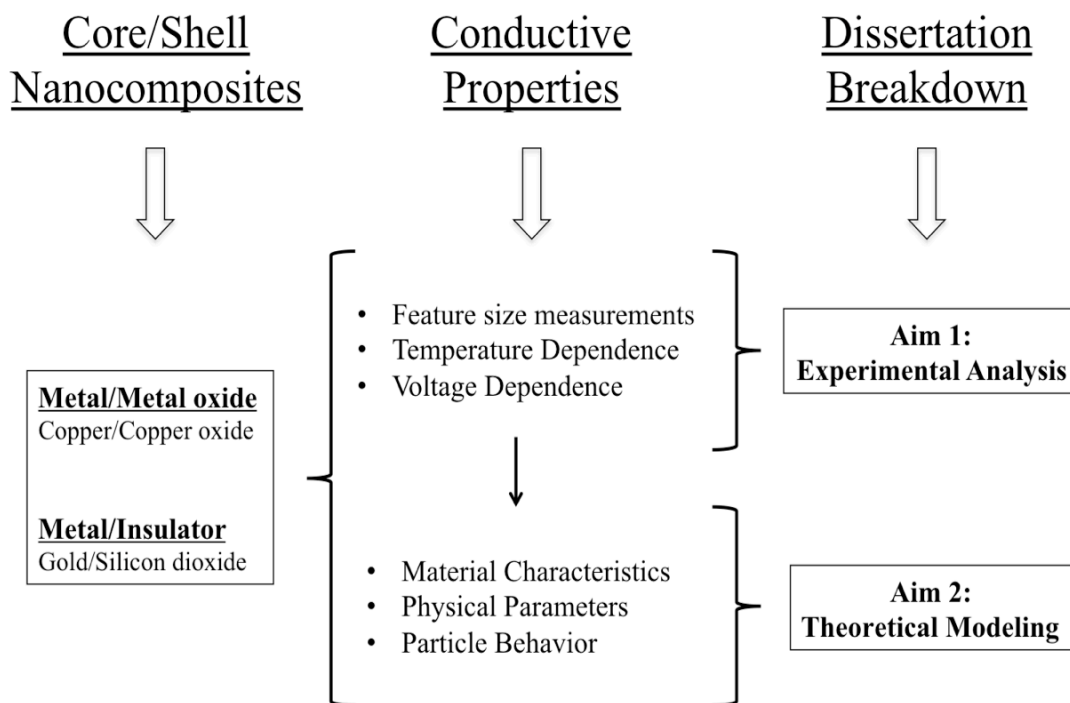


Figure 1.8: Workflow elucidating dissertation breakdown broadly classified into ‘Experimental Analysis’ and ‘Theoretical Modeling’

### 1.6.2 Dissertation Layout

This dissertation has been organized in the following manner. The introduction has aimed at highlighting the significance and advances in nanotechnology, and the challenges involved therein because of the manifestation of unique, and sometimes, unforeseen effects. Chapter 2 gives an overview of the general idea of conduction through bulk materials, followed by the changes in fundamental concepts as dimensions

become smaller than certain critical lengths. It also describes the basis for classifications of prevailing charge transfer mechanisms in low-dimensional structures and their dependence on material and structural parameters. Chapter 3 details the essence of this dissertation, and focuses on the experimental work that has been carried out to successfully uncover some interesting unique electronic phenomena exhibited by the samples under consideration in this study. Chapter 4 gives an account of the hierarchical evolution of charge transport models and discusses the various possible models that could be applicable for the samples under consideration for this study. Experimental data obtained has then been theoretically analyzed and interpreted based on existing models. Chapter 5 gives some remarks about the overall nature and significance of this study, followed by future research directions and possible applications that could tap these unique behaviors for substantial use in this world of advancing technology.

## CHAPTER 2: ELECTRONIC CHARGE TRANSPORT IN NANOSCALE SYSTEMS

### 2.1 Introduction

Nanostructures are typically probed optically (photoluminescence spectroscopy, etc.) or through experiments on charge transport. The term ‘charge carrier transport’ is a broad field that includes traditional ‘bulk’ processes as well as transport through low-dimensional structures. Experimentation on charge transport involves recording the response to an external stimulation (like voltage, temperature) depending on the material characteristics. In bulk materials this relationship between ‘stimulus’ and ‘response’ is usually found to be linear. However, the same cannot be assumed in the nanoscale. Owing to confinement effects, structural defects and disorder, the conductive behavior in nanostructures may demonstrate a deviation from expected behavior. Thus, characterizing materials and matter, especially in terms of the nature of charge transport through them, is a very important prerequisite to understanding the underlying physical principals.

Extensive research has been carried out in recent years in anticipation of useful properties that could be extricated from nanostructures [67-72], and this has resulted in adding several chapters to the history since, with the prefix ‘nano’. This chapter outlines the general idea of conduction through bulk materials, followed by the changes in fundamental concepts as dimensions become smaller than certain critical lengths. It also gives an overview of the prevailing charge transfer mechanisms in low-dimensional

structures and their dependence on material and environmental parameters.

## 2.2 Charge Transport

Charge transport through a material is generally attributed to a net flow of electrons and holes under an electric field. Transport properties of materials can vary significantly depending on the sample dimensions. In order to get an insight on the current flow at nanoscale, we must first understand what happens at the macroscopic scales, and then see the effect of reducing dimensions to the nanoscale.

### 2.2.1 The Classical Concept

In case of macroscopic conductors, due to the presence of impurities and defects in their lattice, electrons move in a diffusive manner with frequent scatterings. This results in an overall reduction in conductivity known as resistance. The motion of electrons between scattering events is essentially free, except for being affected by external forces like electric fields or magnetic fields. There are two velocities that come to the fore while discussing conduction. The first one is the mean speed or the average speed of electrons ' $u$ '. This parameter is used to calculate the mean free path ' $l$ ' of an electron, and this has been detailed in the next section.

When an electric field is applied across a bulk sample, it induces a net movement of electrons and holes in the sample. Generally, the mean free path of such samples is much smaller than material dimensions, and conduction is dominated by scatterings. All these scattering forces help diminish the forces due to accelerating electric fields and render the carriers a steady state velocity called Drift velocity ( $v_d$ ).

Drift velocity is given as

$$v_d(t) = \frac{-eE}{m_e^*} t = -\mu_e E \quad (2.1)$$

where,  $\mu_e$  is a constant referred to as electron mobility. Typically, this drift velocity increases linearly with time and has a value of a few mm per second, which is much smaller than the mean speed  $u$  of electrons of the order  $10^5$ - $10^6$  m/s. This kind of electronic transport typically displays linear response between current and voltage, conforming to the Ohm's law, and is categorized as classical transport.

However, when particle dimensions reduce to the nanometer scale, quantum mechanical nature of electrons become more prominent. Traits like quantization and phase coherence, which are well explained by quantum mechanics, begin to take effect and form the basis of quantum transport.

In quantum mechanics, electrons are described by wave functions, rather than as particles (as in classical transport). The amplitude of a wave function determines the local probability density of the electrons. The wave function is also associated with a certain phase. This allows the waves to interfere, constructively and destructively, and small changes in the material topography, boundary conditions and external environments could significantly affect the interference pattern. These sensitive factors also exist in macroscopic conductors, however since phase coherence is no longer preserved in them due to the multiple scattering events, interference effects average out and vanish, resulting in the familiar Ohmic behavior.

### 2.2.2 Physical Considerations and Characteristic Lengths

Certain confinement lengths that are strongly material dependent have been estimated to define the limits of various transport regimes. These length scales define the distance over which properties such as the electron momentum, phase of wave function, and energy get randomized by scattering events in the sample. Three such critical lengths



have been described below.

(i) Mean Free Path ( $l_e$ )

Electron propagation through real materials is not an uninterrupted process; it is subject to collisions and scattering by other electrons, lattice defects, impurities as well as phonons. This reference to ‘real materials’ is because as per Bloch theorem electrons are capable of propagating without scattering in a perfectly periodic potential like ideal crystals. However, ideal crystals do not exist in reality.

Mean free path is defined as the average distance that an electron can travel before losing its initial momentum. It can be defined in terms of the relaxation time ‘ $\tau$ ’, which is the average time between scattering events or time over which an electron loses the momentum gained from an external field, and mean speed of electrons ‘ $u$ ’ as follows:

$$l = u\tau \quad (2.2)$$

When electrons are scattered from fixed boundaries or impurities, the kinetic energy and momentum of electrons is conserved. The phase of the electrons may be modified, however, by a definite amount. Hence the phase coherence is not lost. These types of collisions are called elastic collisions, and the average distance traversed between two such elastic collisions is termed as elastic mean free path ‘ $l_e$ ’.

Inelastic scatterings, on the other hand, are usually caused by interaction with phonons and other electrons. They depend on many parameters like temperature, material purity and electron concentration among others. These scatterings conserve momentum but not kinetic energy, and lead to a loss of phase coherence. These processes determine the inelastic mean free path,  $l_{in}$ .

(ii) De Broglie Wavelength ( $\lambda_F$ )

This is the Fermi wavelength of the electrons, which is related to the kinetic energy of electrons at Fermi level. It is given by

$$\lambda_F = \frac{h}{p} = \frac{h}{\sqrt{2m^*E_F}} \quad (2.3)$$

where  $m^*$  is the effective electron mass and  $E_F$  is the Fermi energy. It defines the scale on which quantum mechanical effects become important.

Every electron has wave-like properties with a certain phase, which needs to be considered if the Fermi wavelength is the smallest length in the system (i.e.  $\lambda_F \ll L$ ). If the feature sizes become comparable to this value, the wave nature of electrons becomes more pronounced, and their kinetic energies will quantize, leading to size-dependent quantization effects.

### (iii) Phase-coherence Length ( $l_\phi$ )

Also termed as the Phase-breaking length, this is the distance travelled by electrons before their initial phase is destroyed. In quantum mechanics, since an electron state is defined by a wave function that has a phase, phase information becomes important, and this has no analogs in classical physics. Elastic scattering causes a well-defined phase shift, *i.e.* a fixed phase relation can be established between the two paths before and after scattering. This is called phase coherence. However, inelastic scatterings like those due to electron-phonon collisions or electron-electron interactions contribute to a random phase shift and the particle forgets its relation to the phase prior to scattering. In this event the phase coherence is said to be destroyed. Hence it is very important to know the length over which a particle can ‘remember’ its phase. If we assume the carriers to be subject to substantial scattering within a typical time ‘ $\tau_\phi$ ’ such that they move diffusively through the sample, the corresponding phase coherence length scale ‘ $l_\phi$ ’ can then be estimated in

terms of a diffusion constant  $D$  as follows:

$$l_\phi = \sqrt{D\tau_\phi} \quad (2.4)$$

This length scale is especially important at high temperatures. At low temperatures the scattering processes get suppressed, and the phase coherence length becomes strongly material and temperature dependent.

### 2.2.3 General Classification of Charge Transport Regimes

After having defined these length scales, it is possible to classify the systems into distinct transport regimes in comparison with their dimensions and Fermi wavelength, namely, Diffusive transport, Ballistic transport, and Mesoscopic transport. Macroscopic samples much larger than all the defined length scales demonstrate diffusive nature of charge transport. For samples smaller than the mean free path, the quantum mechanical wave nature of the electron under consideration causes the resulting conduction to be assessed as a quantum mechanical issue rather than classical conduction. This is called Ballistic transport. The phase coherence length becomes the most critical scale that defines the boundary between macroscopic and mesoscopic systems. A pictorial representation showing the major differences among the three types of transport regimes is shown in Figure 2.1.

#### (i) Diffusive Transport

Transport is usually diffusive for macroscopic samples that have dimensions much larger than the elastic mean free path ( $l_e < L$ ). The charge carriers undergo multiple scatterings from phonons, boundary scatterings or other lattice/ structural defects while travelling randomly through the device.

For systems where the phase coherence length is less than the elastic mean free path ( $l_\phi <$

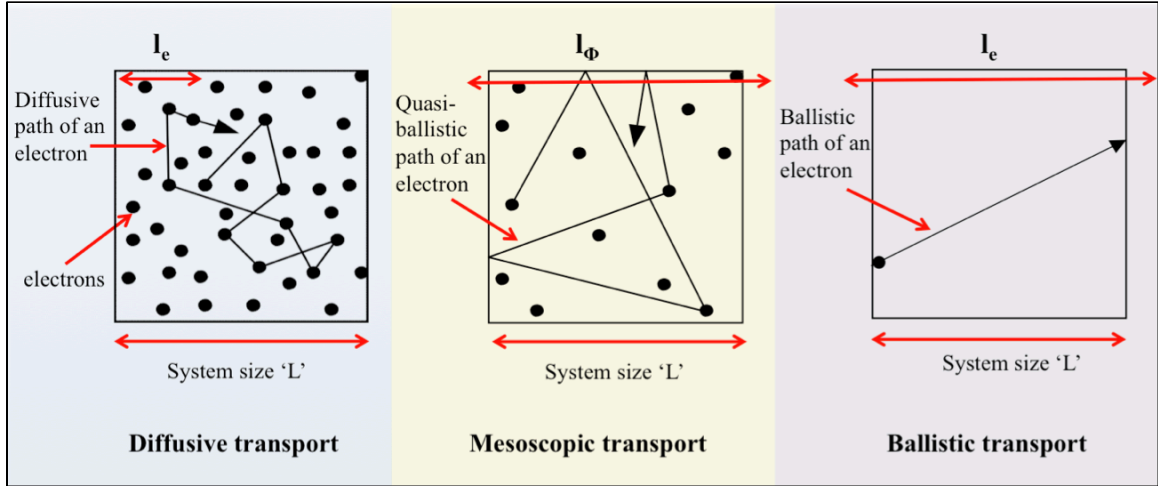


Figure 2.1: Illustration of the effect of critical length scales on transport in nanoscale systems.  $L$  represents the length of the system, ' $l_e$ ' is the elastic mean free path, and ' $l_\phi$ ' is the phase coherence length.

$l_e$ ), interference effects if any, can be neglected. Hence this transport is said to be classically diffusive. In case the phase coherence length is greater than the mean free path ( $l_\phi > l_e$ ), the quantum effects due to wave nature of electrons become evident. Under this condition, the electron interference effects might lead to changes in the resistance or conductance fluctuations even if the system under consideration is very large. This regime is called quantum diffusive regime.

## (ii) Ballistic Charge Transport

Ballistic transport refers to collision-free motion of electron. This type of transport takes place when the material dimensions are small enough to allow charge carriers to travel through them without any scattering. It occurs in small devices where the mean free path or mean scattering length at the operating temperature is longer than the critical device dimensions.

The applied voltage must be sufficiently high, so as to neglect diffusion current and minimize 'inter-band and inter-valley' transitions [73, 74]. Assuming unchanging electric

field ‘E’ and ballistic transport conditions, over a period of time ‘ $\tau$ ’, the electrons can travel with a velocity ‘V’ given by

$$V = \frac{-eE}{m_e^*} \tau \quad (2.5)$$

Though the ballistic electron velocity can ideally have values much larger than drift velocity, because of the higher electric field applied and lack of energy loss by collisions, it becomes practically impossible to have large velocities because ballistic transport takes place over very short time intervals. The time scale over which ballistic transport can occur is determined by comparing the average energy acquired by a ballistic electron with energy at which scattering mechanisms become significant [75]. In this case the resistance of the material becomes independent of its length.

Depending on the magnitude of Fermi wavelength in comparison with sample dimensions, this type of charge transport can also be classified as classical ballistic or quantum ballistic. If the system is larger than the de Broglie wavelength of the electrons, i.e.  $L \gg \lambda_F$ , the band structure of that material is still similar to the bulk, but the scattering events at boundaries will still alter their transport behavior. Hence this is termed as classical ballistic transport. On the other hand, if system dimensions are comparable to the de Broglie wavelength ( $L \approx \lambda_F$ ), the electronic states are significantly altered and begin to affect charge transport through the systems. This is said to be quantum ballistic.

These transport regimes and their classifications based on characteristic lengths have been tabulated as shown in Figure 2.2. In between these two disparate regimes of diffusive transport and ballistic transport lies an intermediate transport regime called the Mesoscopic transport.

Diffusive	Classical	$l_e \ll L$ $l_\phi < l_e$
	Quantum	$l_e \ll L$ $l_\phi > l_e$
Ballistic	Classical	$l_e > L$ $L \gg \lambda_F$
	Quantum	$l_e > L$ $L \approx \lambda_F$

Figure 2.2: Classifications of transport regimes based on characteristic length scales

### (iii) Mesoscopic Transport

This type of charge transport is one that occurs in a system with dimensions less than the phase coherence length ( $L < l_\phi$ ) even though ‘L’ is comparable or greater than the mean free path. Such a sample deviates from the ohmic behavior, and is described as being mesoscopic – one that is bigger than atomic dimensions but small enough to demonstrate non-ohmic trends.

Generally, for incoherent classical transport (in system size greater than ‘ $l_\phi$ ’), the scatterers are known to contribute ‘ohmically’ to conduction. All interference effects within that system would average out, and in effect would allow the conductance to be determined classically by Ohm’s law and related models. However, for a quantum coherent system, interference effects become very pronounced, and affect transport properties [76].

Practically we need to deal with systems having dimensions that require a quantum description of electron dynamics, as well as experience scattering processes that change the coherent dynamics of the system. This regime is termed as mesoscopic regime (intermediate between macroscopic and microscopic), because it requires a quantum

treatment of dynamics and also needs to consider effects due to phonon scattering.

## 2.3 Charge Transfer Mechanisms in Nanoscale Systems

Diverse charge transport phenomena have been reportedly exhibited by different samples, with a close dependence on structure and material characteristics. Because of the multiple charge transfer mechanisms possible, it becomes imperative to know when we can no longer apply the physics we know. Moreover, transport phenomena in disordered lattices are different from those in crystalline structures because of the absence of well-defined energy band structures as in the latter. Depending on the nature of materials being analyzed for charge transport, if the material is highly crystalline it would have minimum trap sites and conduction would occur by electron excitation from valence to the conduction band, while a disordered, non-crystalline system would have many trapped or localized states to assist in conduction. In such systems, an electron might initially get trapped in a bandgap state, and then escape later, or hop from one state to another and contribute to conduction.

In general, charge transport can be the consequence of scattering, free flight or escape from a localized state. Numerous charge transfer mechanism have been demarcated considering all these effects, however, accurate and stringent demarcations are difficult to obtain owing to their dependence on numerous factors like extent of disorder, local temperature and structural defects. Charge transfer mechanisms can be broadly classified into two groups as shown in Figure 2.3.

### 2.3.1 Tunneling Mechanisms

Due to the constant downscaling of materials in electronic devices, tunneling has gained a lot of relevance in describing charge transport through devices with reduced

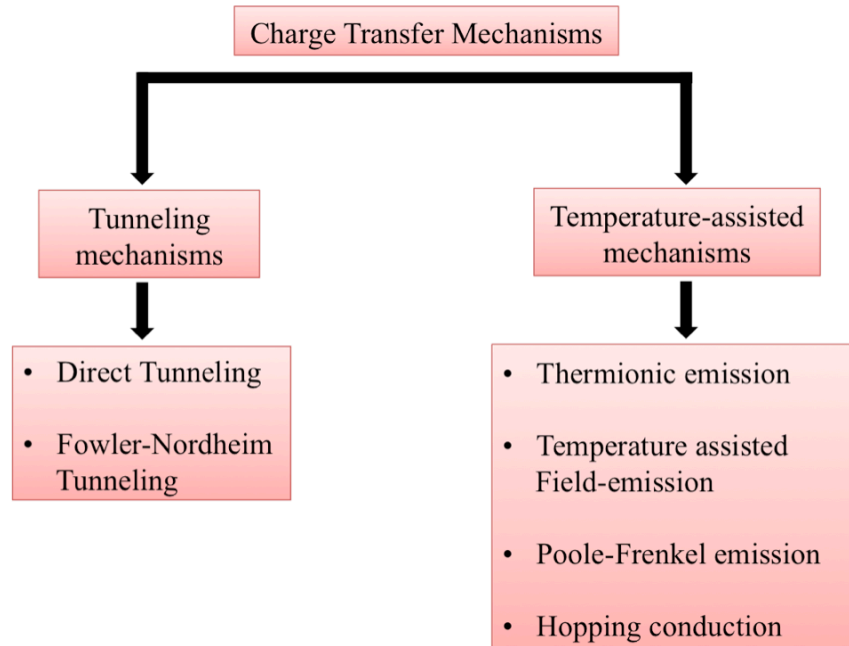


Figure 2.3: Classification of charge transfer mechanisms

dimensions. Charge carriers in the quantum scale are said to exhibit wavelike behavior, with a wave function that defines the probability of finding an electron in a certain position in space. Sometimes electrons in certain systems get confined in a potential well because of barriers formed by the energy difference between Fermi level of the particle and the lower edge of the conduction band of an adjacent or surrounding material in contact with the particle. If the barrier is thin enough, the wave function might penetrate the barrier, and be able to ‘leak’ out to the other side of the barrier. This allows them to pierce through an obstacle even when the particle’s energy is lower than the height of the potential barrier of that obstacle. This phenomenon of allowing crossovers over a classically forbidden barrier is called tunneling. It does not depend on temperature, but strongly depends on barrier thickness and voltage.

A simple representation of a particle tunneling through a barrier can be explained



using the Schrodinger equation. Consider the case of a particle approaching a one-dimensional rectangular potential barrier as shown in Figure 2.4, with a potential of height ' $V_0$ ', and width ' $w$ '.

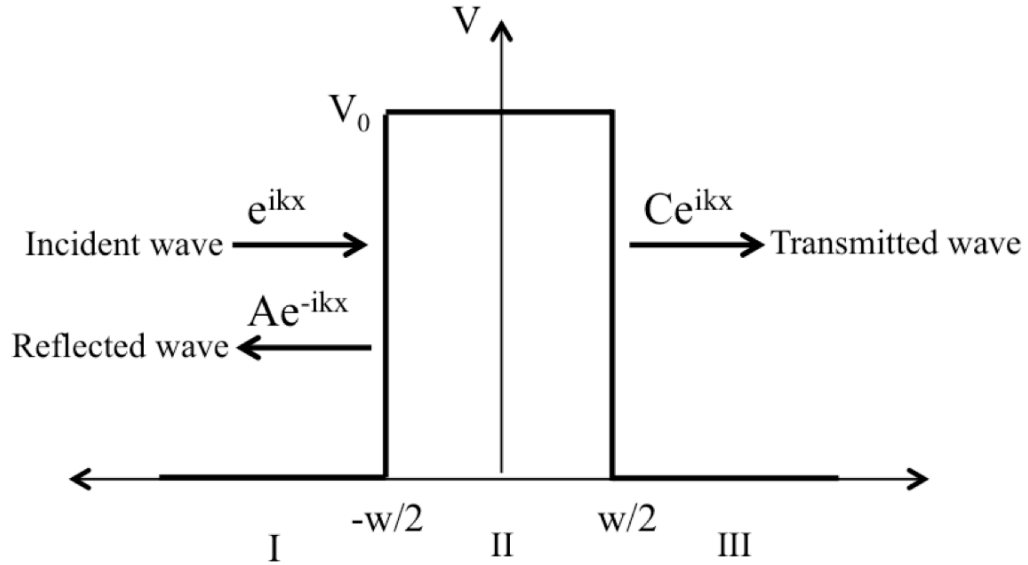


Figure 2.4: Generic description of a particle tunneling through a rectangular potential barrier of height  $V_0$  and width  $w$ .

The potential is 0 everywhere, except in the region of width ' $w$ ' where it has a potential of ' $V_0$ '. Classically this particle can in no way penetrate through the barrier, and should get reflected back, however, quantum mechanically, it has a finite probability of tunneling through the barrier.

An electron in such a system will obey the 1-D Schrodinger equation:

$$-\frac{\hbar^2}{2m} \frac{d^2}{dx^2} \Psi(x) + V(x)\Psi(x) = E\Psi(x) \quad (2.6)$$

where the first term represents the Kinetic energy with  $m$  being the electron mass and  $\hbar$ , the Plank's constant.  $V(x)$  is the potential and  $E$  is the energy of the particle.

These equations would translate to  $(-\frac{\hbar^2}{2m} \frac{d^2}{dx^2} \Psi = E\Psi)$  in regions I and III, and to  $(-\frac{\hbar^2}{2m} \frac{d^2}{dx^2} \Psi = (E - V_0) \cdot \Psi)$  in region II within the potential barrier.

The potential remains constant in each of the three regions, and the solution of the Schrodinger equation can be written as a superposition of the left and right moving waves, given as:

$$\Psi = \begin{cases} e^{ik_0x} + Ae^{-ik_0x}, & x < -w/2 \\ Be^{k_1x} + B'e^{-ik_1x}, & -w/2 < x < w/2 \\ Ce^{ik_0x}, & x > w/2 \end{cases} \quad (2.7)$$

where the wavenumbers  $k_0$  and  $k_1$  are calculated as

$$k_0 = \sqrt{\frac{2mE}{\hbar^2}} \quad \text{for } x > \pm w/2, \text{ and}$$

$$k_1 = \sqrt{\frac{2m(E-V_0)}{\hbar^2}} \quad \text{for } -w/2 < x < w/2$$

The constants A, B, B' and C are coefficients to represent amplitudes of the waves propagating in the different regions in either direction, and are determined by assuming continuity of the wave functions across boundaries of the regions. These equations can then be solved further to give the Transmission probability when  $E < V_0$  as

$$T = \frac{4k_0^2 k_1^2}{(k_0^2 + k_1^2)^2 \sinh^2(k_1 w) + 4k_0^2 k_1^2} \quad (2.8)$$

In the thick Barrier limit  $k_1 w \gg 1$ , the probability of tunneling reduces to

$$T = \frac{4k_0^2 k_1^2}{(k_0^2 + k_1^2)^2} e^{(-2k_1 w)} \quad (2.9)$$

The tunneling expression is now dominated by an exponential term. Assuming the prefactor to be close to unity ( $\sim 1$ ), it becomes clear that tunneling probability decreases exponentially with increase in barrier width. Outside the barrier, the particle oscillates

with wave vector  $k_0$ , and within the barrier it falls off exponentially over a distance  $1/k_I$ . It shows how a particle, that could not have overcome the barrier in classical case, can manage to tunnel its way through the barrier.

In general, two scenarios may exist for tunneling of electrons. Figures 2.5(a) and 2.5(b) represent the two cases, where 'E' is the energy of an electron and  $V_r$  is the potential barrier. The first case is where the particle that is initially in a 'free' state

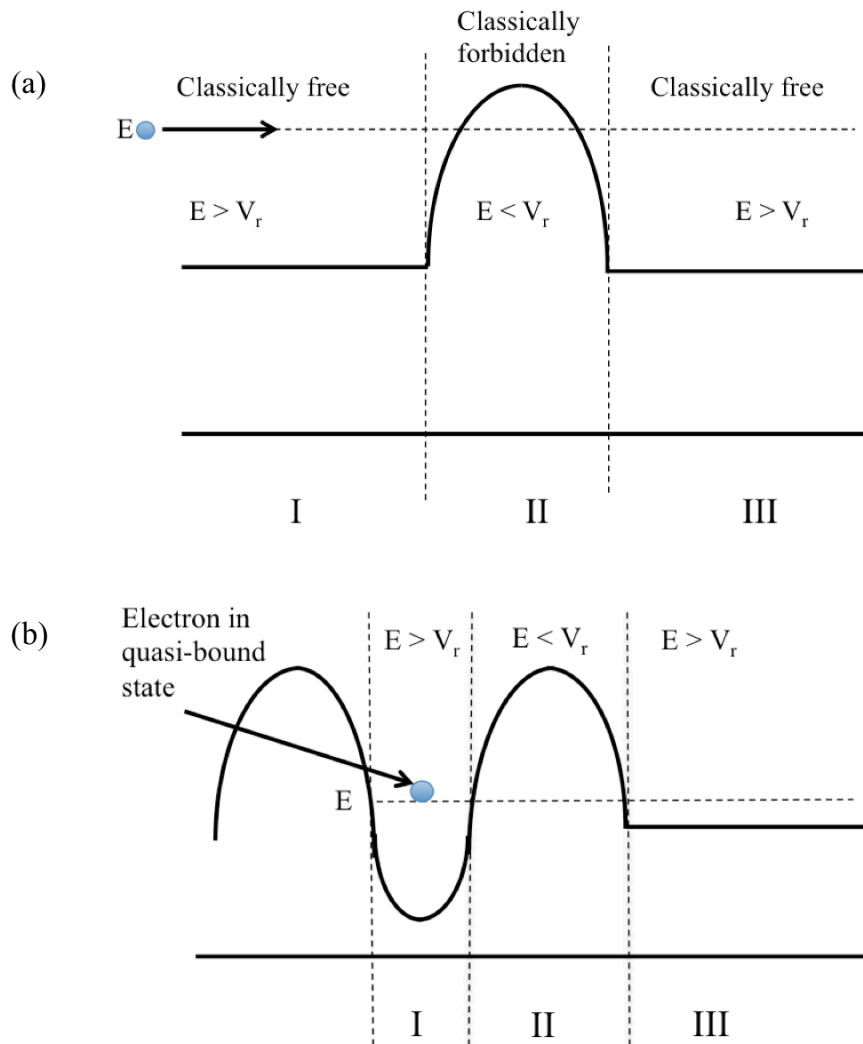


Figure 2.5: (a) Schematic view of electron starting from unbound state tunneling through a classically forbidden barrier (b) Schematic view of electron initially in bound state tunneling through a classically forbidden barrier.

strikes the potential barrier with a finite probability of the electron tunneling through the barrier, or getting reflected back. The second case is that when the electron is initially confined in a quantum well region, with a finite probability to tunnel through the barrier into free space, or into another ‘quantum’ well.

Tunneling can also occur between localized or trap states, if the electronic wave functions of the two states effectively overlap. These sites may be formed as a result of impurities, dangling bonds or other defects. This is also the kind of structure prevalent in nanocomposite structures with alternating dielectric/ metallic materials.

There are different forms of tunneling mechanisms that assist in conduction. They are classified based on the shape and thickness of the barrier they interact with.

#### (i) Direct Tunneling

This is a quantum mechanical phenomenon when carriers are able to tunnel through the barrier directly from one region to the other. When barriers are very thin, their energy levels become quantized. As the thickness of barrier varies, electrons on one side of the barrier may be able to line-up with one of the quantized levels in the barrier, and tunnel through it to the other side of the barrier. This process strongly depends on the thickness of the barrier while it is relatively independent of the electric field across the barrier. Equation for the current density  $J_{DT}$  is given by Simmon’s equation [77].

$$J_{DT} = \frac{q^2 V}{\hbar^2 w} (\sqrt{2m} \Phi^{1/2}) \exp \left( -\frac{4\pi w \sqrt{2m} \Phi^{1/2}}{\hbar} \right) \quad (2.10)$$

where  $q$  is the electron charge,  $\Phi$  is the barrier height,  $w$  is the barrier thickness and  $m$  is the electron mass.

#### (ii) Fowler Nordheim Tunneling

Under high electric fields, the probability of electron tunneling increases, and the

process is termed as Fowler-Nordheim (FN) tunneling. Also called Field emission, as voltage increases, the electrons are able to tunnel through the barrier without having to traverse its entire thickness[78, 79]. The electrons see a triangular barrier due to the band-bending phenomenon at higher voltages, and succeed in tunneling through the barrier, resulting in current flow. Such an emission is called cold emission. For this type of conduction, the Simmons equation is again applicable, however, the shape of the barrier that changes from being rectangular to triangular needs to be accounted for. The tunneling current density in a 3D structure can be given as shown below.

$$J_{FN} = \frac{q^3 E^2}{16\pi^2 \hbar \Phi_B} \exp\left(-\frac{4\sqrt{2m^*}\Phi_B^{3/2}}{3\hbar q E}\right) \quad (2.11)$$

where  $J_{FN}$  is the current density due to FN Tunneling,  $q$  is the electron charge,  $\Phi_B$  is the tunneling barrier height,  $E$  is the electric field applied and  $m^*$  is the effective mass of the tunneling electron. Thus we can see that FN Tunneling is independent of temperature, while being inversely related to barrier height and electric field. Its current density is related to applied voltage as  $J \sim V^2 \exp\left(-\frac{1}{V}\right)$  [80, 81].

These two types of tunneling have been shown schematically in Figure 2.6.

### 2.3.2 Temperature Assisted Mechanisms

#### (i) Thermionic Emission

Thermionic emission refers to the process where carriers overcome a potential barrier by thermal agitation. Electrical conduction in solids is known to result from drifting of electrons through them. The electrons are governed by Fermi-Dirac statistics in any conducting material. The highest energy level is called the Fermi energy, denoted by ' $E_F$ ', and at low temperatures all electrons exist at or below this level.

If the temperature of such a material is increased, the distribution function of charge

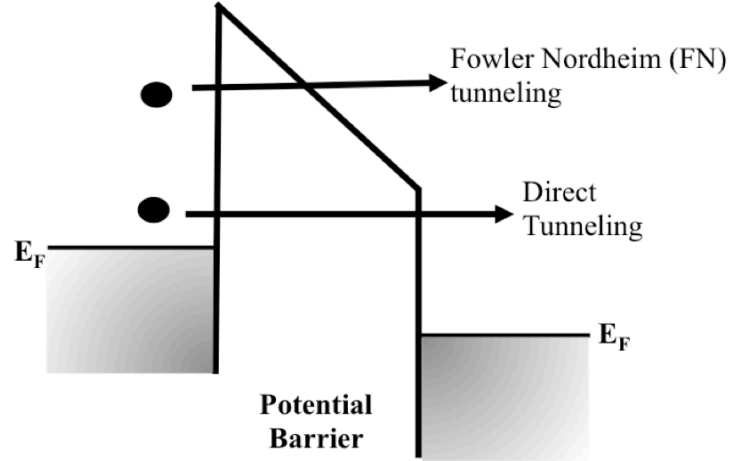


Figure 2.6: Energy-band diagrams showing Direct and Fowler-Nordheim Tunneling mechanisms schematically

carriers undergoes a change, and some of these carriers might be able to acquire enough energy to overcome the surface potential barrier, also called the Work function ' $\Phi_B$ '. It is assumed that the electron would need energy of  $(E_F + \Phi_B)$  to escape from the metal. Once an electron obtains this threshold energy, its probability of getting injected into vacuum/ the neighboring material increases. This process in which free electrons are emitted from a metallic surface by absorption of heat energy supplied to them is called Thermionic emission, and the electrons thus emitted are called thermions. Apart from having the right amount of energy, the carriers must also travel in the right direction to contribute to conduction. Probabilities of the electron suffering reflection can also not be neglected. Taking all these factors into consideration, we arrive at the Richardson equation [82] that gives an expression for the density of current due to thermionic emission mechanism.

$$J_{Th} = A_0 T^2 \exp \left[ -\frac{\Phi_B}{k_B T} \right] \quad (2.12)$$

where  $A_0 = \frac{4\pi emk^2}{h^3} = 1.2 \times 10^6 \text{ A/m}^2\text{K}^2$ , called the Richardson constant,  $J_{Th}$  is the

current density due to Thermionic emission,  $\Phi_B$  is the Work function,  $k_B$  is the Boltzmann constant and  $T$  is the absolute temperature. The exponential term shows the dependence of this phenomenon on temperature and on the actual value of the potential barrier  $\Phi_B$ .

Thermionic emission is usually more significant at high temperatures where the carriers can absorb sufficient thermal energy to jump across the barrier. However, at lower temperatures or when the barrier is very high, thermionic emission loses its importance, and hopping mechanisms may dominate.

#### (ii) Temperature-assisted Field Emission

The relation between the emission of electrons and field strength has been studied for long by Schottky [83], Millikan and Eyring [84], and Millikan and Lauritsen [85], and Richardson [86]. Millikan and his associates have shown that at higher temperatures at which thermionic emission begins, the strong field emission is also affected by temperature, and blends into thermionic. Schottky contributed to better understanding of this model by recognizing certain forces acting on the electron in the opposite direction when it escapes from the surface of a good conductor, called mirror image force [87]. This hindering force was shown to extend over distances larger than the interatomic distances, and Schottky showed that the effect of this force could be offset by application of an external voltage. This external voltage would also serve to aid the electron in escaping the surface by reducing the effective work function, contributing to greater thermionic emission [88].

This is known as Schottky effect and the new formula for overall current density by thermally assisted tunneling can be given by

$$J_{SC} = A_G T^2 \exp\left(\frac{-\left(\Phi_B - \beta_{SC} E^{\frac{1}{2}}\right)}{k_B T}\right); \beta_{SC} = \left(\frac{q^3}{4\pi\epsilon}\right)^{1/2} \quad (2.13)$$

where  $J_{SC}$  is the current density due to Schottky effect,  $\Phi_B$  is the voltage barrier,  $\epsilon$  is the dielectric permittivity and  $A_G = A_O \times \varphi$ , where  $A_O$  is the Richardson constant and  $\varphi$  is the correction factor.

Hence this process termed as Schottky emission is related to electrons that get thermally excited to energy levels above the Fermi level, and get propelled through it at a faster rate by application of external voltage. Depending on the size of the barrier and temperature, thermionic field emission can contribute a significant fraction of the total current.

Figure 2.7 illustrates the mechanisms of thermionic emission and temperature-

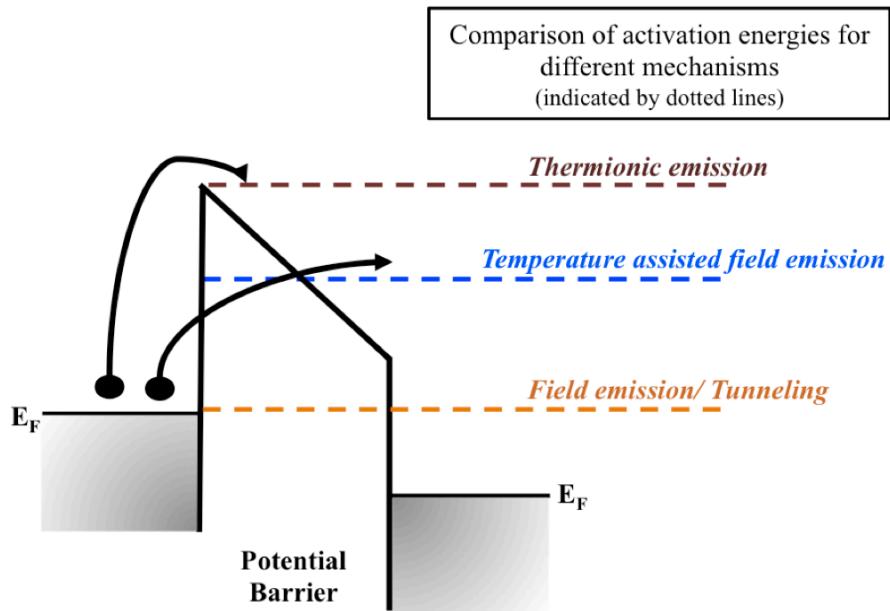


Figure 2.7: Energy-band diagrams showing Thermionic emission and Temperature-assisted field emission mechanisms schematically. Dotted lines indicate relative activation energies required for these two mechanisms relative to tunneling mechanism. Dotted lines are purely representative and not to scale.



assisted field emission, and also shows a comparison of the activation energies that would be required to initiate these mechanisms.

### (iii) Poole- Frenkel (PF) Emission

Electrons sometimes tend to tunnel into, and get confined in trap sites. They are unable to contribute to conduction unless they overcome the potential barrier between the electron sites and the conduction band edge. Depending upon the temperature and electric field applied, electrons may be able to acquire enough energy to get re-emitted to the conduction band of the barrier material.

According to this model, the applied electric field lowers the internal trap barrier heights. This allows the electrons trapped in localized states to escape the trap and overcome the barrier. The expression for the current density is similar to the one for Thermionic emission, however the barrier height is equal to the depth of the trap potential well [81, 89, 90]. Thus the effective barrier height reduces considerably, especially at high electric fields, and this method of conduction becomes significant when the barrier is too thick to exhibit direct tunneling. This process is also called trap-assisted emission and its current density  $J_{PF}$  is given as:

$$J_{PF} = \sigma_0 E \exp\left(\frac{-q\left(\Phi_B - \sqrt{qE/\pi\epsilon}\right)}{k_B T}\right) \quad (2.14)$$

where  $\sigma_0$  is the low fields conductivity,  $\Phi_B$  is the barrier height,  $\epsilon$  is the dielectric permittivity and  $k_B$  is the Boltzmann constant.

### (iv) Hopping Conduction

Hopping conduction is a temperature-assisted conduction process in which localized electrons get thermally energized and drift through a sample by hopping from one site to

another unoccupied site. This topic has been treated separately in the next section because of its high relevance to the work presented here.

Figure 2.8 shows the difference between Poole-Frenkel emission and Hopping conduction. Carriers in the Poole-Frenkel mechanism are mostly trapped; they occasionally get excited to delocalized bands (like the conduction band), from where they can contribute to current. However, for the hopping mechanism, the charges ‘hop’ from trap to trap and contribute to conduction.

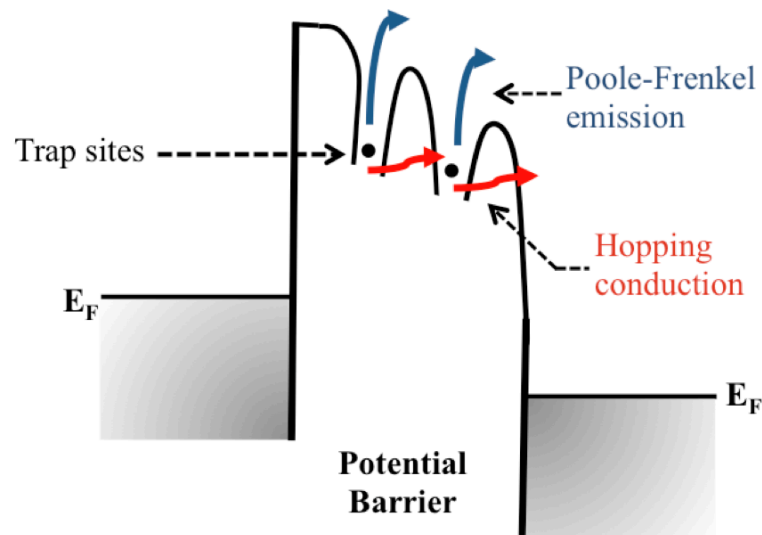


Figure 2.8: Energy-band diagrams showing Poole-Frenkel emission and Hopping conduction mechanisms schematically. For better differentiation both mechanisms have been shown through arrows in different colors.

### 2.3.3 Hopping Conduction

As mentioned above, hopping conduction is a process in which localized electrons get thermally energized and drift through a sample by hopping from one site to another unoccupied site. They need some energy to overcome the potential barrier to hop over the barrier, and this energy usually is supplied via thermal excitation of the material. The

concept of hopping has commonly been used to describe movement of ions within an ionic crystal [91-93]. But it was Frolich [94] who introduced this concept of hopping conduction to explain electron transport with the suggestion that amorphous materials may have electrons in trap states which can contribute to conduction by hopping from one state to another. This concept was then used by Miller-Abraham [95], Anderson[96], Gubanov [97] and many others to explain conduction in different materials structures that may have a high density of localized states where the electrons find it easier to overcome the barrier by hopping between sites, or in cases where the barrier is too thick for tunneling [98-101].

The probability of hopping between two sites depends on the distance between the two sites in consideration, and the energy required for the hop. This hopping process need not be restricted to adjacent sites only. There are two types of hopping conduction mechanisms that differentiate between the distance between the initial and final hop positions of the electrons.

#### (i) Nearest Neighbor Hopping

This is the type of hopping mechanism that occurs if the temperature is very high, because the activation energy required for such hops is rather large. Temperature dependence of conductivity also has the same form as Eq. 2.14, however, the activation energy 'E<sub>H</sub>' would be smaller in this case [102].

$$\sigma = \sigma_1 \exp\left(-\frac{E_H}{k_B T}\right) \quad (2.15)$$

#### (ii) Variable Range Hopping

This mechanism dominates at lower temperatures. In this situation, charge carriers may hop to sites that are further away spatially, but are closer in energy, i.e, requiring

lesser activation energy to increase the probability of hopping [103, 104]. This results in conductivity of the form

$$\sigma = \sigma_0 \exp \left\{ - \left( \frac{T_0}{T} \right)^{1/4} \right\} \quad (2.16)$$

where  $\sigma_0$  is a pre-exponential factor and  $T_0$  is a constant depending on the localization length and the density of states at the Fermi level.

Usually, this process also depends upon the strength of electron-lattice interaction. In a covalently bonded crystal, electrons and holes can be characterized to excellent approximation by assuming that they freely move through a crystal whose atoms are frozen into place. The electrons and holes can scatter off phonons, but when no phonons are present, all ionic displacement is ignored in describing electron and hole transport and properties.

However in ionic or highly polar crystals, where a coulomb interaction between a conduction electron and lattice ions causes a strong electron-phonon coupling, this approach is deemed unsatisfactory. Even with no real phonons present, the charge carriers get surrounded by a cloud of virtual phonons. Physically this relates to a charge carrier, say an electron, pulling positive lattice ions towards it and repelling negative ions away from it. The carriers adjust their position slightly so as to maintain equilibrium with the forces that keep them in place as well as the electrons' pull. This leads to a polarization cloud centered at the charge carrier. This charge carrier, along with the distorted lattice created by it in its vicinity, can be treated as a new quasi-particle called a 'polaron', and this was first suggested by Landau [105]. Depending upon whether the extent of the region over which this polarization causes a distortion in lattice, a polaron can be differentiated as large polaron when the distortion radius is larger than the lattice

constant, or a small polaron when distortion is smaller than the lattice constant. As the electron moves through the polar lattice, it carries the polarization field along with it and contributes to conduction.

As demonstrated in the schematic below (Figure 2.9), there might be vacant sites for the charge carriers to occupy under the influence of an electric field. A charge carrier needs to overcome a barrier of ' $E_i$ ' to hop to the vacant site, which it is able to do at higher temperatures. When no external voltage is applied, hopping events can occur in either direction with the same probability, and such random hoppings do not effectively result in a net current flow. On the other hand, as shown in the second case of Figure 2.9, when external voltage is applied, the likelihood of preferential hopping increases, streamlining the direction of hops resulting in current flow. As in the figure, the external field helps reduce the barrier height for hopping events taking place from left to right by ' $\Delta E_i$ ', but opposes hopping events in the opposite direction.

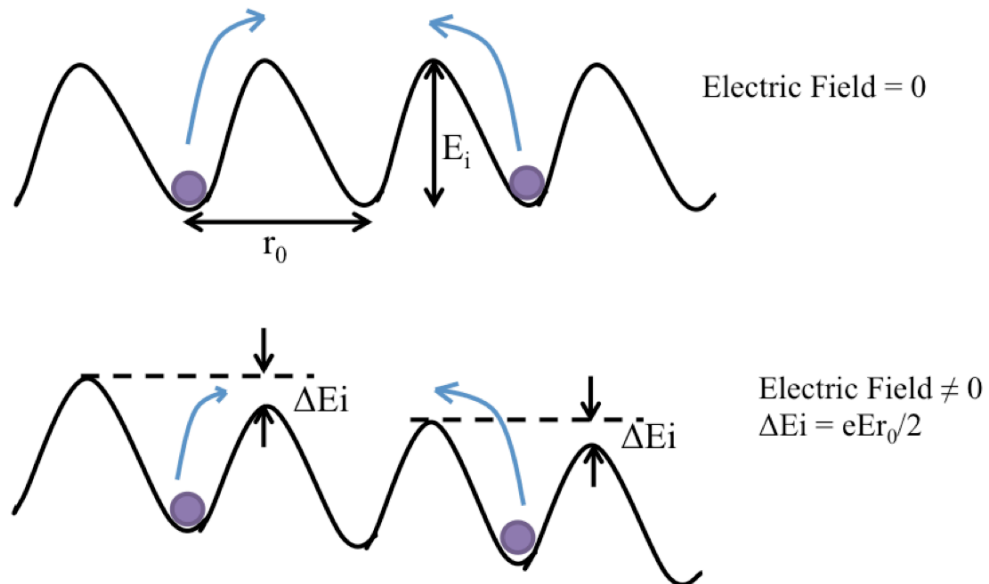


Figure 2.9: Schematic of Polaron hopping mechanism with and without application of an external electric field

## 2.4 Experimental Objectives of this Work

Having seen the numerous possibilities of charge carrier transport through a nanosystem, the significance of characterizing them based on their electronic conductance behavior has been established. Investigations on the effects of change in compositions of different phases of the heterogeneous material, variation in material dimensions, and degree of disorder in a material have attracted a lot of research interest, especially because each of these factors provides a unique platform for nanoscale functionalization.

This dissertation deals with the important issue of characterizing samples of two different core/ shell structure arrays that have different material properties. The primary objectives have been to study charge transport through the chosen samples over a wide range of temperatures and voltages. It is important to analyze the electrical conductivity measurements of these nanostructures to understand the underlying charge transport mechanisms so as to be able to use them in a substantive capacity for any future technology.

## CHAPTER 3: EXPERIMENTAL ANALYSIS OF ELECTRICAL CONDUCTION THROUGH CORE/ SHELL NANOCOMPOSITES

### 3.1 Introduction

This dissertation addresses the significant issue of being able to characterize nanostructures based on the nature of electronic charge transport through them. For this purpose, samples with a particular architecture called core/shell nanostructures have been probed experimentally for the conductive properties they exhibit. The samples under consideration successfully demonstrate the role played by size, disorder and nature of materials chosen, in dictating the universal conductive properties of the material. The first sample chosen is that of Copper metal nanoparticles covered with Copper oxide shells, while the second is that with Gold metal cores surrounded by Silicon dioxide shells.

This chapter describes the overall procedures involved with this study, including sample characterization, system set-up for measurements, measurement procedures and results obtained.

### 3.2 Experimental Work

#### 3.2.1 Samples used

The first sample of Copper core/ copper oxide shell was prepared as described using the sol-gel method by Das et al. [108]. This procedure involved the use of  $\text{CuCl}_2 \cdot 2\text{H}_2\text{O}$ , TEOS (Tetraethoxysilane),  $\text{C}_2\text{H}_5\text{OH}$  and  $\text{HCl}$ . Two solutions were prepared; the first one was made with 60 ml of Ethyl alcohol mixed with 10ml distilled water with 1ml  $\text{HCl}$  and stirred for 10 minutes after which 12.5 ml of TEOS was added to it and further stirred.

Another solution was prepared with 14.26 g of  $\text{CuCl}_2 \cdot 2\text{H}_2\text{O}$  and 60 ml of Ethyl alcohol in 15 ml distilled water. These two solutions were mixed and stirred for 1 hour. The mixture was allowed to stand for a few days and the gel thus formed was reduced with hydrogen to precipitate out metallic copper nanoparticles within the gel matrix. The resulting powders were hot-pressed at  $650^\circ\text{C}$  for 5 minutes and then heated in air at temperatures varying from 700 to  $850^\circ\text{C}$  to form a solid bulk. The Raith 150 Scanning Electron Microscope (SEM), as pictured in Figure 3.1, was used to study the microstructures of



Figure 3.1: Raith 150 e-beam exposure tool used for imaging the nanostructures

the specimen.

The high-resolution SEM image of the Copper/ Copper oxide core/ shell sample shown in Figure 3.2 indicates that these metal-insulator arrays are significantly disordered. A histogram of the particle sizes in the inset of Figure 3.2 shows the sample to have diameters of about  $100\text{nm} \pm 20\text{ nm}$ , with shell thickness of  $10\text{ nm} \pm 1\text{nm}$ .

The second sample with the Gold core and Silicon dioxide shell was purchased from Tedpella Inc. (Redding, CA) in colloidal form. These samples were determined to have



core diameters of 40-50 nm and shell thickness of 10 nm  $\pm$ 1nm using SEM characterization [106]. This has been shown in Figure 3.3, and histogram of particle sizes

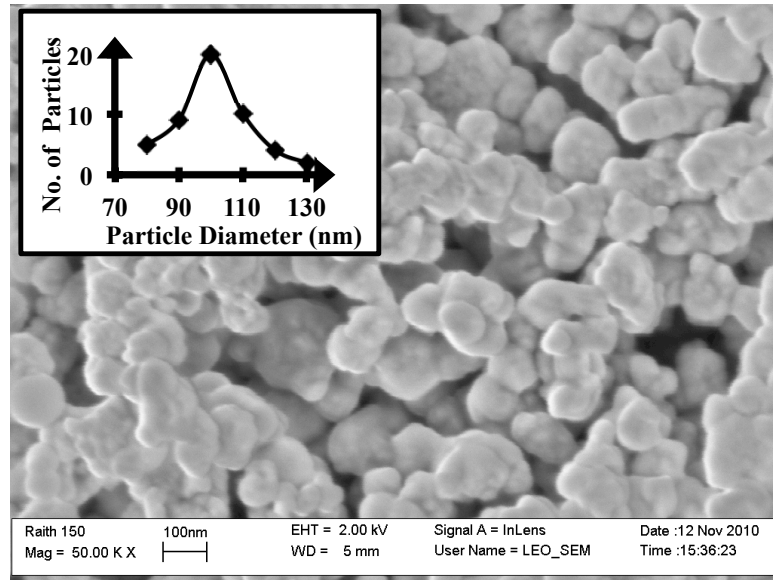


Figure 3.2: SEM micrographs of the hot pressed Copper/ Copper oxide array [106] with the histogram of particle sizes [inset]

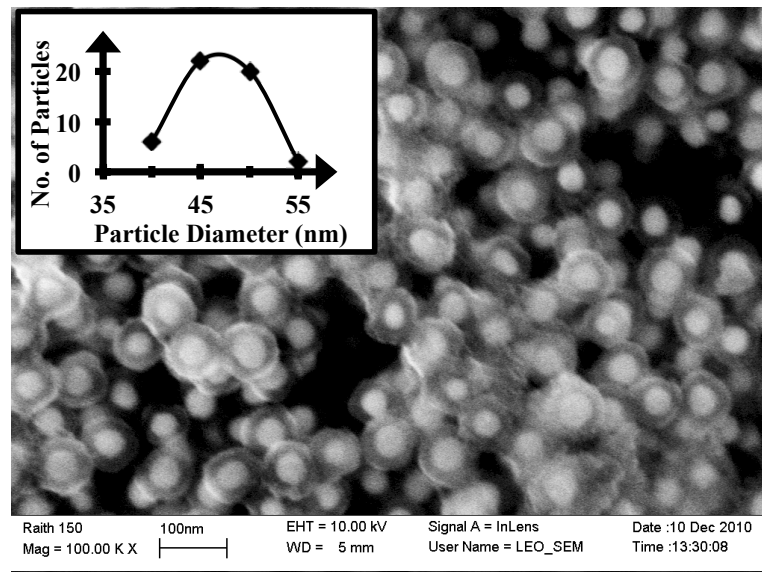


Figure 3.3: SEM micrographs of the Gold/ Silicon dioxide nanostructures of the order of  $\sim$ 50 nm with the histogram of particle sizes [inset] as published in [107]

have been plotted.

### 3.2.2 Photolithographic Patterning of Electrodes

To allow accurate and repeatable experimental studies on the charge transport mechanisms through the core/shell nanostructures, developing two metal electrodes with a minimal separation in which to place the sample under study seemed to be the most effective arrangement.

To serve our purpose, pure and thin rectangular quartz slides with dimensions of 7.5 cm by 2.5 cm were cleaned and coated with a 500Å thin layer of Titanium dioxide ( $\text{TiO}_2$ ) and a 2000Å layer of Gold (Au). Electrodes for metal contact were patterned using photolithography. Photolithography is a popularly used method for microfabrication. It provides a simple and accurate way to fabricate micron-sized features capable of replication. A mask which has partial opaque and partial transparent sections drawn with a computer software (AUTOCAD) is created and used to quickly transfer patterns onto the substrate. However, these patterns are limited to the micron-scale, and do not provide nanoscale resolution. Since our electrodes were not required to be size-limited, and as the separation of a few microns between electrodes was acceptable, photolithography was suitable for our electrode patterning. Figure 3.4 shows the mask used for this purpose. The shaded areas represent opaque parts that cannot be seen through, while the other areas were clear.

The substrate was first cleaned and dried with pure nitrogen gas and placed on the vacuum chuck of a spin coater. A few drops of positive tone photoresist Shipley 1813 were deposited on the substrate, and spun at 4000 rpm for 60 seconds. After soft-baking the sample at 115°C, the mask was carefully aligned over the photoresist-covered slide

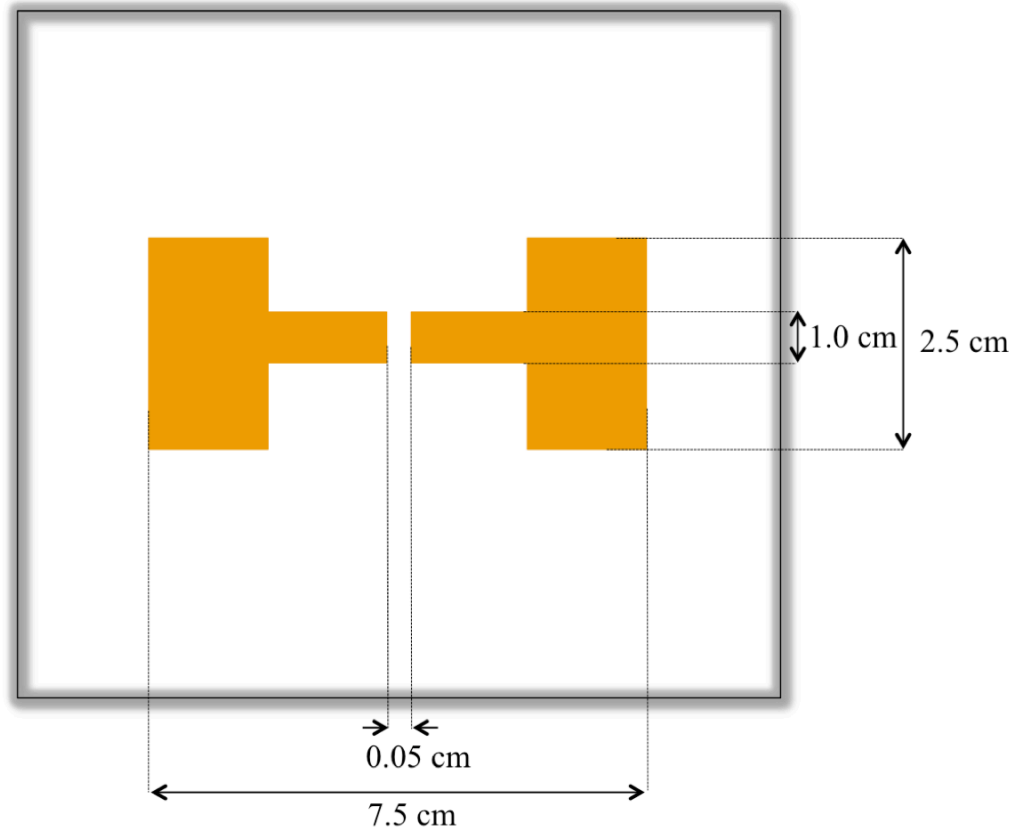


Figure 3.4: Mask used for photolithographic patterning of electrodes (not to scale)

and exposed to UV rays for 15 seconds. The transferred pattern was then verified after developing the photoresist, and hard baked in an oven at 90°C. This step was to ensure photoresist quality for next stage of processing, i.e. etching. These processes of spin coating, exposing and developing had to be repeated multiple times with slight variations in parameters, to ensure proper transfer of pattern before carrying out the last step of etching. After determining successful factors, the final slide was then dipped in Gold etchant, followed by Titania etchant, to get the desired pattern of two gold electrodes with slit 500 microns wide running vertically through the center of the substrate, as illustrated in Figure 3.5. The layer of Titania had to be used because Gold does not adhere to Quartz surfaces, and needs a buffer layer, such as Titania, to hold it in place.

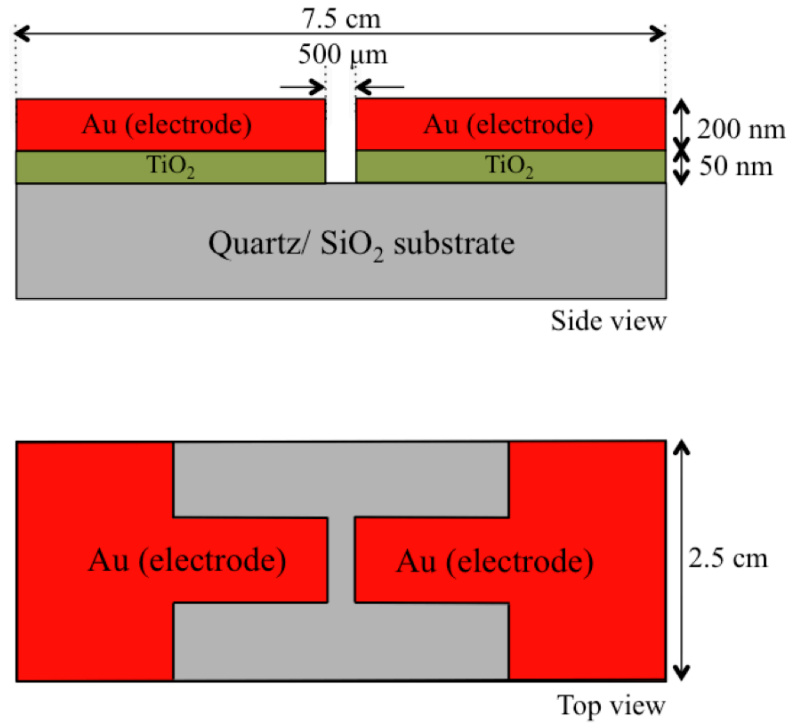


Figure 3.5: Layout of device used in the following work (not to scale)

### 3.2.3 Measurement Setup for Electrical Characterization

Multiple sets of gold electrodes were manufactured as described in the section above. The main purpose of the electrodes was to assist in making external connections. The first sample, namely, the hot-pressed Copper/Copper oxide was placed in the gap between the electrodes for further experimentation. The second sample of the Gold/Silicon dioxide array was purchased in colloidal form; hence a few drops of this solution, that would consist of numerous Gold/ Silica nanostructures, were deposited between a second pair of electrodes and left to dry. This setup has been shown in Figure 3.6.

Both samples were held firmly in place by clamping a thin microscopic glass slide over the gold-coated quartz slides. This method not only applied a uniform lateral pressure on the sample, but also allowed us to make external connections without

annealing. The downward compression force by the glass slide also ensured stability of external contacts.

The entire assembly was placed in a Lindberg tube furnace, which allowed controlled heating and temperature measurements within a range of 300K to 650 K with  $\pm 5$  K accuracy. A sensitive Keithley 2000 model was used for sensing minor variations in current. The overall experimental setup has been demonstrated in Figure 3.7.

### 3.3 Results And Discussion

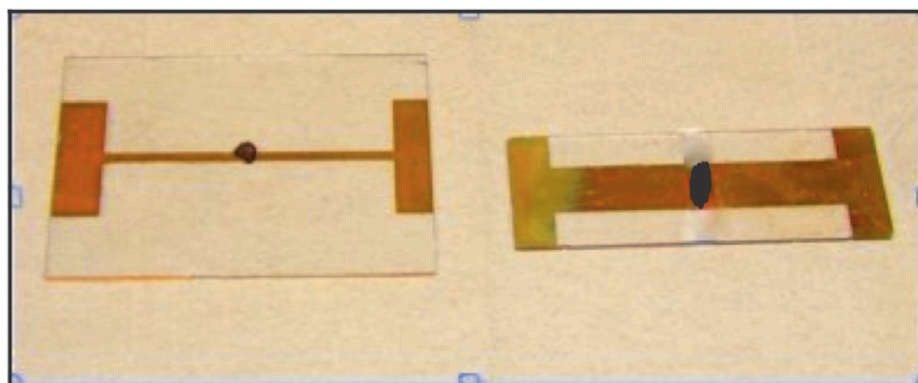


Figure 3.6: Sample setup to measure electrical conductivity

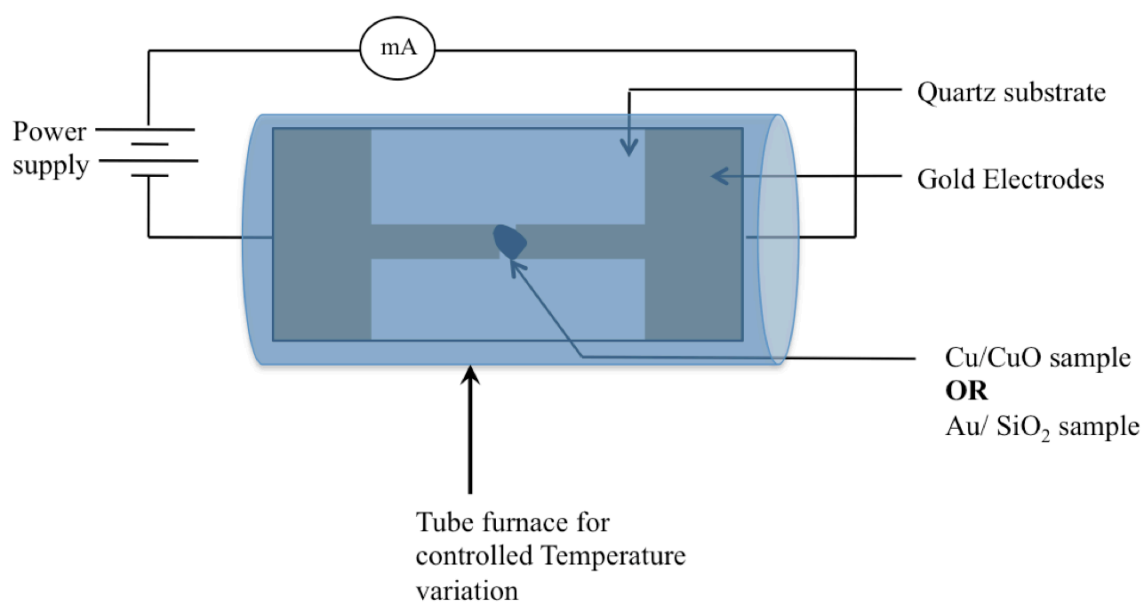


Figure 3.7: Overall experimental setup to measure electrical conductivity

Our experimental study was aimed at determining the dependence of electrical conductivities of the two samples on temperature and external voltage.

Firstly, to ensure reliability of the contacts, measurements were carried out for known bulk samples of conductive, insulating and semi-conductive nature using the aforementioned setup. All the measurements exhibited normal behavior, clearly indicating that contact limiting effects, if any, were beyond the sensitivity of our instruments.

Both samples essentially consist of a random array of metal (conducting) cores encased in non-conducting or semiconducting shells. Ideally, every metal sphere is insulated from adjacent metal spheres by its shell as demonstrated in Figure 3.8, resulting in a sample that exhibits a very high resistance and behaves like an insulator on the whole.

This was experimentally verified at room temperature, where the samples were

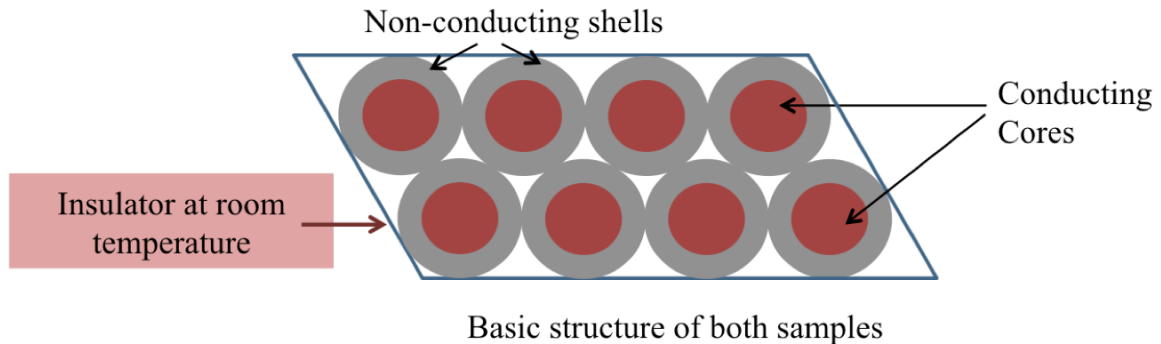


Figure 3.8: Overall structure of both samples

established as perfect insulators. Our aim was to observe if any current flow could be detected through the sample, and if yes, to record it as a function of applied voltage and increasing temperature.

### 3.3.1 Sample 1: Copper/ Copper oxide core/ shell structure

Measurements were first carried out with the Copper/Copper Oxide sample. Figure 3.9

shows the general trend of current through the circuit at increasing temperatures at various constant voltages. These experiments were conducted over a range of 5V to 70V, with voltage being increased in steps of 5V.

Figure 3.9(a) shows the experimental data for only three constant voltages of 15, 30 and 60 volts for purpose of clarity, and also because it adequately underlines the characteristic behavior of the sample.

As observed from these characteristic curves, for the 15 volts data set, the current flowing through the circuit is near zero and remains constant up to a critical threshold temperature of 613 K. Thereafter, we observe a sudden surge in the current flowing through the circuit, which gradually settles down and fluctuates about a certain high current value. When we move to a higher voltage, for example the data set 30 volts, the current remains negligible till 503 K and then shoots up, thus creating a short in the circuit then onwards. It is clearly evident from the graphs that as the voltage levels increase, the threshold temperature at which the current hike is observed reduces.

When we compare all the threshold temperatures with their corresponding voltages, a definite pattern is observed between them, as presented in Figure 3.9(b). It is found that this relation gives a very high correlation of 0.96.

These trends obtained suggest that as we increase the constant voltage at which we carry out our measurements, the Copper/ Copper oxide sample is more disposed to becoming a conductor at a lower threshold temperature. The transition takes place instantly, a characteristic that can be tapped for many viable applications like high temperature sensors, embedded interconnects, etc.

### 3.3.2 Sample 2: Gold/ Silicon dioxide core/ shell structure



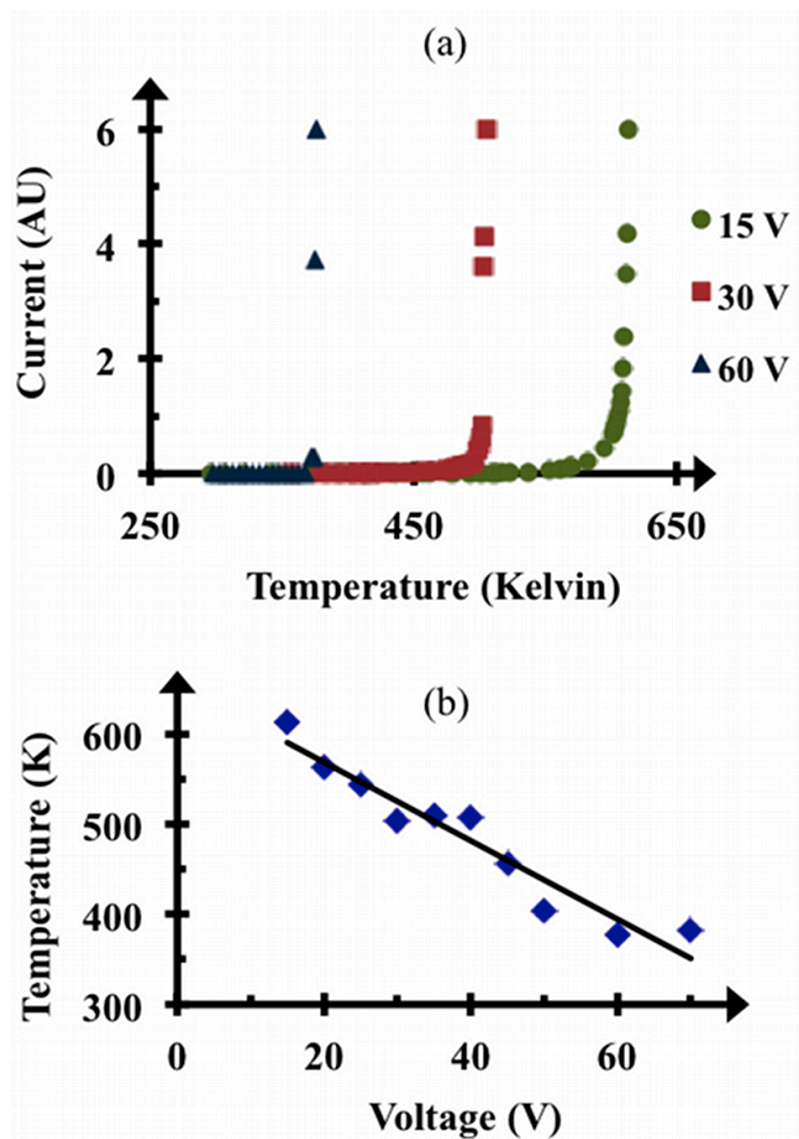


Figure 3.9: Conductive trends for Copper/ Copper oxide sample (a) Dependence of current through sample on temperature at 15, 30 and 60 Volts (b) Plot of threshold temperature versus corresponding experimental voltages. Correlation obtained = 0.96, which substantiates the fact that temperature and voltage play an important role in the conductive properties of core/shell arrays.

As the next step, the general tendency of current flowing through the Gold/Silicon dioxide sample at increasing temperatures and various constant voltages ranging from 5 volts to 70 volts is recorded. To better understand the pattern followed, data for three constant applied voltages have been presented in Figure 3.10.

It is evident that the Au/SiO<sub>2</sub> sample also shows some degree of conduction, contrary to the insulating behavior expected from such a sample. However, it does not demonstrate a sudden change in conductivity like the Copper sample. Consider the data recorded for 15 volts applied. A gradual increase in current flow is observed with increasing temperature. When we move to higher voltages of 30 Volts, and then to 60 Volts, the current versus temperature graph follows the same trend, with the current values being higher than the

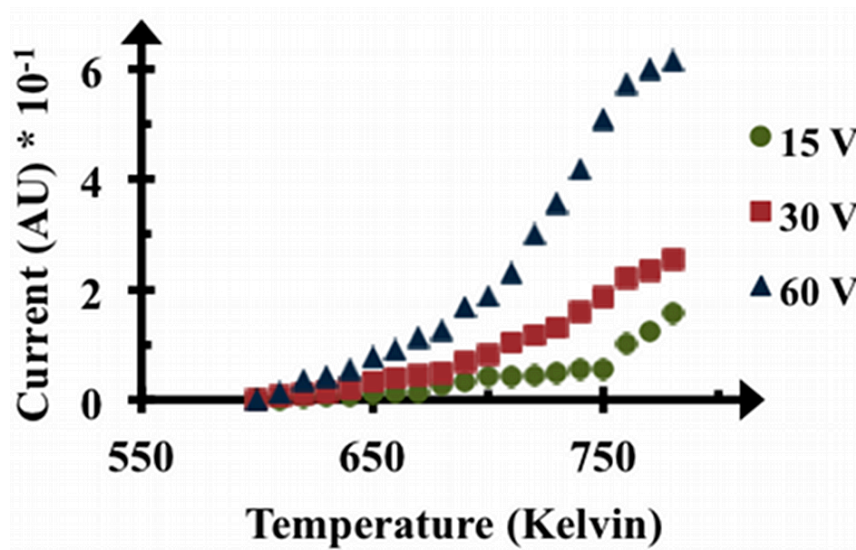


Figure 3.10: Dependence of current through Gold/ Silicon dioxide sample on temperature at 15 Volts, 30 Volts and 60 Volts.

previous data sets, and a slight acceleration in current increase.

These trends obtained suggest that at all values of applied voltages, the conductivity increases proportionally with temperature, however as the values of applied voltages become higher, the rise in current is also faster.

### 3.3.3 Comparisons and Discussion

For the two samples considered in this work, the electrical conductivity trends have

been measured, and have been established to demonstrate a unique non-ohmic behavior. The Copper/Copper oxide sample is seen to exhibit sudden insulator/metal transition at specific temperatures, while the Gold/Silicon dioxide sample shows a gradual increase in current with temperature.

Some important observations made during the experimentation are listed below. The experimental data obtained for both samples are found to be reversible and repeatable, which conform to the sample structurally remaining the same. SEM images of our post-measured samples also support this claim. Repeated measurements on the same samples do not yield any noticeable discolorations or damages on the sample surface. The experiments are repeated with different samples having the same essential structure and size distribution, with minor or no variations, and all results are established to be consistent.

### 3.4 Conclusion

Experimental analyses of the chosen samples clearly display unique electrical conductivity trends over the selected range of temperatures and voltages. Since different parameters affect different samples in dissimilar ways, it is very important to determine which transport mechanism controls the conductivity, as well as sets a limit on conductivity in specific nanocomposite structures. A major task is to ascertain the exact type of charge transport phenomena that dominate each of these core shell structures, where both the shell materials have different characteristics in terms of their chemical bonds and energy band levels. This is a very significant step necessary to capitalize on the unique properties obtainable and take advantage of the transport physics not only for device engineering, but also to correlate electronic transport with fundamental material

issues. Ongoing analysis on this data with proposed theoretical models will help develop a better understanding of underlying mechanisms.

## CHAPTER 4: MODELING OF CHARGE TRANSPORT BEHAVIOR

### 4.1 Introduction

With unique and interesting phenomena like confinement effects [109, 110], electron tunneling [111-113], ballistic transport [114], etc. coming to the fore with shrinking dimensions, characterization based on charge transport has become the basis for many technological advances today. After having outlined various charge transfer mechanisms in Chapter 2, it becomes necessary to model the behavior of different nanoscale systems based on the conductive behavior they exhibit. Moving from the macroscopic bulk scale to the ballistic regime changes the very fundamentals on which transport properties are based. It goes from following an Ohmic classical transport model to one where distinct quantum effects have to be accounted for. Various charge transport models have been developed to help understand and simplify the processes of studying transport mechanisms, that can account for both traditional bulk processes as well as transport in low dimensional or quantized structures.

This chapter starts with a brief overview of the hierarchy of existing charge transport models and then summarizes some of the models proposed over the past few decades by researchers studying electrical conductivity through nanostructures similar to the ones used in this study, having metallic structures separated by a variety of non-conducting structures including insulators, semiconductors, oxides and organic materials. Experimental data obtained for the samples under study has then been theoretically

analyzed and interpreted based on existing models.

## 4.2 Charge Transport Models

### 4.2.1 Crossover from Macroscopic to Microscopic regime

In case of classical descriptions of particle physics, probability distribution functions that define position and momentum of carriers over phase space are used to predict macroscopic quantities of the device like charge and current densities. While classical mechanics can be used to describe motion of particles at a macroscopic level, it is no longer applicable at the microscopic scale of atoms. Nanometer scale objects usually lie in the boundary of these two regimes where ballistic or quantum confinement effects come under scrutiny, and describing charge transport through such structures often requires approaching the realms of quantum mechanics.

Models encompassing the semi-classical and quantum approach tend to violate the assumptions and implications of existing classical models. Particle dynamics now need to be specified by equations for the wave functions or quantum mechanical descriptions in terms of probability density matrices [115]. Semi-classical models require information about the band structure and scattering mechanisms as input parameters, and make assumptions from the classical physics as well as quantum transport theory to get answers with close approximation. However there are many charge transport features like non-local scattering processes, small systems and strong influence of electric fields [116] that are neglected. Hence quantum transport models are required to take into account the complete quantum transport phenomena.

Today, the highly improved manufacturing techniques have facilitated manufacture of a large number of nanostructured devices that demand quantum mechanical treatment

[117, 118]. It thus becomes necessary to use higher-level transport models that can capture transport effects more accurately, albeit at the cost of higher computational complexity.

Over the last few years, increasingly sophisticated charge transport models have been developed. Simpler models give less accurate results but have faster processing speeds, while complex models yield greater accuracy but require longer processing time [119]. All these factors need to be considered by the user to select an apt model for a specific requirement.

The charge transport models can be hierarchically classified into three categories as shown in Figure 4.1, namely, (i) The classical description including the Drift-Diffusion (DD) model (ii) The semi classical approach including the Boltzmann Transport equation (BTE) and (iii) Quantum mechanical formulation including the Schrödinger or Heisenberg equations of motion.

#### 4.2.2 Classical Model – Drift-Diffusion Model

The two main concepts of drift and diffusion lay the foundations of the ‘Drift-diffusion transport model’. This model is based on the assumption that the charge carriers exhibit classical behavior and can undergo multiple scatterings before the electric field driving them changes significantly [120]. It also assumes negligible variation in temperature through the device. This implies that the carriers are able to remain at local equilibrium with their surroundings and are affected only by local conditions. Hence this model has validity when device dimensions are typically much greater than the mean free paths, and under steady state conditions like at low electric field where the carriers are able to acquire a net velocity while maintaining a distribution function characterized by

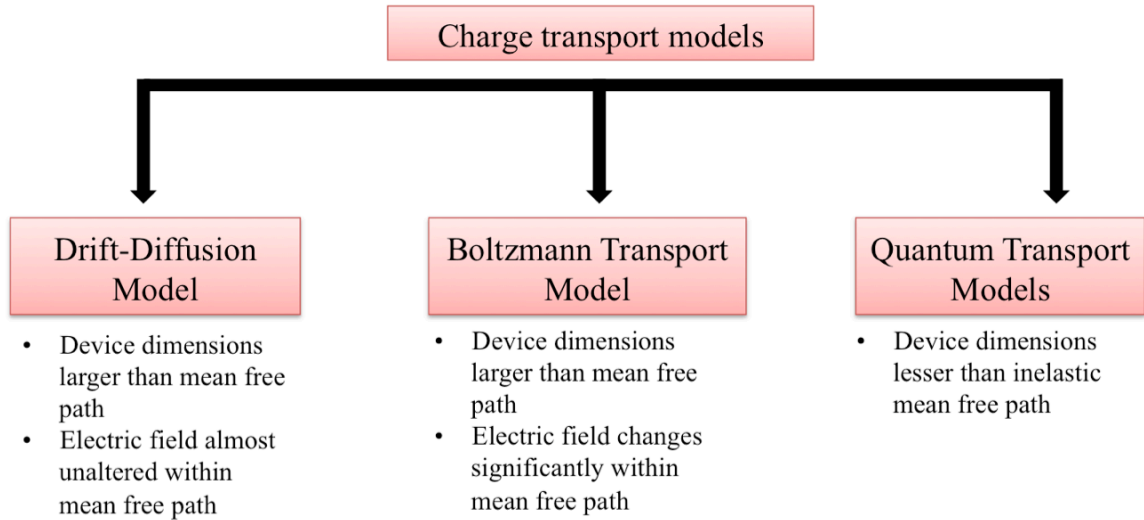


Figure 4.1: Hierarchical classification of charge transport models

thermal equilibrium and normal Fermi energy (the highest occupied energy level).

In nanoscale devices, factors like higher electric fields and temperatures, or drastic compositional variations in the device cause non-local transport effects, where behavior of a charge carrier at one location might be influenced by local surroundings as well as random events occurring at remote sites. Electric fields tend to change significantly in space and the linear relationship between electric field and drift velocity is lost. If the device dimensions become comparable to or smaller than the mean free path, the carriers can traverse the solid with zero or minimal collisions with other carriers and impurities (as in the case of ballistic or quasi-ballistic transport). In such cases, as there is not enough scattering to restore the local equilibrium of carriers, assumptions of the drift diffusion model get violated and non-local hot electron effects begin to affect the charge transport [121]. The Drift Diffusion model does not account for non-local behavior. The transport of electrons and holes then is governed by the Boltzmann transport equation (BTE).



#### 4.2.3 Semi Classical Model - Boltzmann Transport Equation

In the semi-classical domain, theoretical treatments of charge transport are usually based on a ‘one electron transport’ equation, the most popular of which is the Boltzmann Transport Equation (BTE). This BTE is more general than the drift-diffusion model, and provides a detailed description of transport in semi-classical theory. It is more advanced compared to the drift-diffusion model in that it accounts for non-local effects [122]. According to this model, electrons are treated as classical particles having a well-defined position and momentum as a function of time, represented by a distribution function  $f(r, k, t)$  which describes the average distribution of carriers in position ‘ $r$ ’ and momentum ‘ $k$ ’.

It is possible to calculate the probability of finding the particle with a specific momentum ‘ $k$ ’ at a specific position ‘ $r$ ’ and time ‘ $t$ ’ by solving the Boltzmann transport equation. If an external force of ‘ $F(r)$ ’ is applied to a system, the electronic transport properties can be completely determined by solving the steady state Boltzmann transport equation given as

$$\frac{\partial f(r, k, t)}{\partial t} + \frac{1}{\hbar} \nabla_k E(k) \cdot \nabla_r f(r, k, t) + \frac{F}{\hbar} \nabla_k f(r, k, t) = \left( \frac{df(r, k, t)}{dt} \right)_{col.} \quad (4.1)$$

where,  $f(r, k, t)$  is the one particle distribution function,  $\left( \frac{df(r, k, t)}{dt} \right)_{col.}$  is a collision term that accounts for scatterings in momentum space due to lattice or ionized impurity scattering. Free charge carriers within a crystal interact with each other through a number of scattering processes, which relax the momentum and energy of the particle. The scattering probabilities appearing in the collision integrals are accounted for quantum mechanically by the application of Fermi’s golden rule according to which the probability ‘ $P$ ’ of transition per unit time from an initial state  $k$  in band  $m$  to final state  $k'$  in band  $n$  is

described as

$$P_{n,k;m,k'} = \frac{2\pi}{\hbar} |\langle f | (V(r) | n, k \rangle|^2 \delta(E_{k'} - E_k \mp \hbar\omega) \quad (4.2)$$

where ‘ $V(r)$ ’ is the scattering potential of the process and  $E_{k'}$  and  $E_k$  are the initial and final state energies of the particle. This rule is only valid when the initial state has not been significantly depleted by scattering into final states. The delta function results in conservation of energy for long times after the collision is over and  $\hbar\omega$  is the energy absorbed or emitted due to scattering.

The Boltzmann equation plays an important role in the theory of diffusive electronic transport. Even though electron-electron interactions and phase coherence are neglected, the general version of BTE is an integro-differential equation of motion for the probability distribution function for particles in 6D phase space of position and momentum. While the left hand side of the equation represents Newton mechanics, the right side denotes a quantum mechanical scattering operator. Only after some approximations and assumptions does the equation give a clear picture of how charge carriers are affected by an electric field.

In the low electric field regime, the concept of Relaxation time ‘ $\tau$ ’ is usually used as an approximation to simplify the BTE. Relaxation time is defined as the typical time taken by carriers within the steady state distribution  $f(r,k,t)$  to go back to their equilibrium value after the external fields are switched off. This approximation is called the Relaxation Time Approximation (RTA) [123] and provides a simplification for the collision integral to help provide quick analytical solutions to the BTE. It yields the following equation:

$$\left. \frac{\partial f}{\partial t} \right|_{col.} = - \frac{(f - f_0)}{\tau} \quad (4.3)$$

where ' $f$ ' and ' $f_0$ ' are the initial and final equilibrium distribution functions, and ' $\tau$ ' is the relaxation time. This equation describes the rate of change of distribution due to all possible collisions, and only slightly deviates from the one in equilibrium. Hence it assumes that the charge carriers are able to acquire a net velocity while maintaining a distribution function characterized by thermal equilibrium and normal Fermi energy [124]. This approximation assumes that the energy gained by carriers from the external fields is negligible compared to the mean energy of the carriers.

However, the BTE has its own limitations. While the BTE involves calculation of a distribution function under equilibrium forces, in practice, multiple carriers per cubic unit of the device have to be dealt with, and it becomes difficult to arrive at the transport equations and the various transport coefficients for that distribution. Secondly, though it encompasses the non-local effects, it cannot handle quantum mechanical effects, such as those arising from interference effects of electron waves. BTE is based on the assumption that scattering forces are instantaneous both in space and time. However, Fermi's golden rule accounts for prolonged interactions or scatterings, which suggest an infinite time. Under higher electric fields and temperatures, because of the quick variations in local electric field and reduced number of scattering events, carriers are unable to reach a steady state. The external energy supplied leads to an increase in kinetic motion of carriers as well as provides a specific direction of motion for carriers.

Moreover, there exist certain discrepancies within Fermi's Golden rule as well. While this rule requires electron energy to remain constant during scattering events [120], having prolonged interactions (as assumed in Fermi's golden rule) would only cause the energy of charge carriers to change distinctly while scattering if placed in an electric

field. Despite such discrepancies within Fermi's Golden rule as well as with the BTE assumptions, this rule is commonly used to calculate scattering rates as it helps simplify complicated calculations. The idea of infinite mean time (infinite collisions) is however consistent with the fact that electron energy before and after the scattering can be precisely defined. Instantaneous scattering (as assumed in BTE) violates the Heisenberg uncertainty principle, while the infinite collision as per Fermi's Golden rule adheres to this principle. Despite all the contradictions, the BTE model has been an often-used semi-classical transport theory, and can be applicable as long as quantum mechanical effects like interference effects are absent.

BTE needs to take into account this effect of external field on electrons due to quantum confinement and other confining potentials like surface roughness and scattering. There are other kinetic equations that exist to describe the one-electron probability in momentum and space, however they need additional assumptions to be made to converge with the BTE. Since these transport equations don't hold true in high electric fields and also in constrained geometries in nanostructures [125], new transport models need to be formulated to replace BTE.

#### 4.2.4 Quantum Transport Models

These are the most advanced of all models, and predictably, can handle classical as well as quantum mechanical effects. They can be used to study properties of a variety of devices exhibiting quantum behavior like quantum interference, carrier confinement, tunneling, etc. This is especially important when particle dimensions become smaller than the phase coherence length.

Unlike the familiar one-particle Schrodinger equations in the presence of an

independent Coulomb potential, quantum transport in nanostructures requires considering multi-particle interactions and many types of scattering [126, 127]. This demands very complex computational solving, or simplification using approximations. However, there are other solutions to solve the problem of quantum transport like Wigner transformation [128] and Green's Function method [129], that are capable of accounting for the effects like those of scattering and phase-breaking events more easily.

Most of the transport equations are derived from the quantum mechanical Liouville-von Neumann equation [122, 130] , which takes into account various scattering events due to electrons, phonons and impurities. The density matrix ' $\rho$ ' is given as

$$i\hbar \frac{\partial \rho}{\partial t} = [H_0, \rho] + [V, \rho] + [F, \rho] \quad (4.4)$$

where ' $H_0$ ' is the Hamiltonian for carriers and lattice vibrations, ' $V$ ' is the electron scatter interaction and ' $F$ ' is the Hamiltonian that couples the effect of external field on electrons.

It is obvious that coming up with a full many-body quantum mechanical description of transport considering the particles in the device, in the immediate environment and external environment, is beyond the scope of any computational model. However step-by-step approximations help us get a fair idea of the nature of charge transport, with the model losing information about the system at each step. Among the best models in use today are Green function methods, Liouville-von Neumann equation and Wigner distribution equations. By neglecting the phase information and non-local behavior of electrons it is possible to arrive at BTE, which is yet the most popular model in use. This is simplified further to arrive at the RTA and Drift-diffusion models.

#### 4.3 Theoretical Modeling Objectives of this Work

One of the main objectives of this dissertation has been to try and establish theoretical reasons for charge transport observed experimentally, define a range of existing theoretical models along with their limitations in explaining the experimental results obtained. It is imperative to get a good understanding on charge carrier transport and electrical conduction for proper characterization, selection of materials for device applications, and investigation of atypical transport phenomena arising due to quantum effects. A number of studies have been reported in the past decade describing the charge transport mechanisms predominant in different types of discontinuous thin films and composite nanostructures. Various combinations of materials have been explored, their compositions and phase concentrations have been manipulated, and dimensions of particles have been experimented with. Some of the significant and relevant paths followed by researchers for modeling their samples' electronic behaviors have been reviewed in the following section.

#### 4.3.1 Proposed Models for Different Nanoscale Systems

Perhaps one of the earliest studies was led by Maxwell at the end of the last century, where he studied the conductive properties of a homogeneous conductive medium interspersed with insulating spherical particles [131]. Neugebauer and Webb [132] have extensively studied conduction in composite discontinuous metallic islands and have proposed a model based on tunneling transport of thermally activated charge carrier proportional to their concentrations and drift velocities. The barrier to tunneling is the energy difference between Fermi level of a particle and the lower edge of the conduction band of the substrate. This model suggests an exponential dependence of conductivity on inverse temperature within their temperature range of 373K and an apparent non-

dependence on electric field. They also emphasize the importance of charging energy, which is the energy required to transfer charge carriers from one initially neutral island to another. However it is suggested that high electric fields could defy the model by changing the equilibrium concentration of the charges maintained, leading to a field-dependent activation energy.

Taking this theory further, R.M. Hill [133] has analyzed the mechanisms of electrical conduction of a thin aggregated metal film on dielectric substrates at moderate fields ( $<10^4 \text{ V cm}^{-1}$ ) over a limited temperature range ( $< 600\text{K}$ ), on the basis of quantum mechanical tunneling. This differs from Neugebauer's model in that the activation energy has been estimated based on particle dimensions and interparticle spacing. The concept of substrate conduction, effects of barrier height on electrical properties of the substrate, and temperature dependence on tunneling have been taken into account by Hill. While an activated quantum mechanical tunneling has been determined as the primary mode of transport for charge carriers in films with small particle sizes and inter-particulate gaps less than the mean free path length, an unactivated tunneling is said to predominate for larges particles with small gaps. This is because the charges are more likely to be trapped in the substrate than tunneling through them when the gaps become larger. In such cases, modes of transport are likely to be thermionic emission, where the charge carrier gets emitted from a particle onto the conduction band of the substrate, with subsequent capture of the charge by a second particle or bulk conduction in the substrate. Limits have been set for each mechanism depending on metallic particle sizes and inter-island spacings and this has been effectively summarized by Tick and Fehlner [134] shown in Table 4.1.

Table 4.1: Classification of discontinuous metal films according to Hill, summarized by Tick and Fehlner [134]

Type of film	Island space	Interisland spacing	Predominant type of conduction	Activation Energy
I	Small	Small	Tunneling	Large
II	Small	Large	Thermionic emission	Small
III	Large	Small	Tunneling	Small
IV	Large	Large	Thermionic emission	Small
V	...	...	Oxide-skin conduction	Large

Tick and Fehlner have applied this model to gold-rich islands grown on palladium nuclei on dielectric Silicon-Monoxide substrate. They report small temperature-independent activation energy at low temperatures, leading to negligible conduction through discontinuous films. However as temperature increases, a large number of carriers are activated in the inter-island spaces and activated tunneling becomes the dominant transport process. They have calculated the activation energy for conduction by the same equation used by Neugebauer et al.

$$E = \frac{e^2}{4\pi\epsilon\epsilon_0} \left( \frac{1}{r} - \frac{1}{r+s} \right) \quad (4.5)$$

where ‘ $r$ ’ is the average island radius, ‘ $s$ ’ is the average interisland distance and ‘ $\epsilon$ ’ is the low frequency dielectric constant of the substrate. This shows the dependence of particle dimensions as well as the dielectric constant of the material in determining the charge transport. Uozumi *et al.* has however argued that ohmic conductance arises from the non ohmic tunneling currents at high electric fields [135] and derived an expression for the critical electric field over which non-ohmicity occurs.

Mott has introduced a model based on observing the activation energies involved in various conduction behaviors observed in order to determine the nature of charge



transport. It is based on the Arrhenius law, an equation commonly used to determine the temperature dependence of the specific reaction rate constant in chemical reactions. The Arrhenius equation has the general form of

$$\ln(\sigma) = \left( \frac{-E_a}{kT} \right) + \text{constant} \quad (4.6)$$

or, 
$$\sigma = \sigma_0 \exp\left(\frac{-E_a}{kT}\right) \quad (4.7)$$

where ' $\sigma$ ' is the conductivity, ' $E_a$ ' is the activation energy, and ' $T$ ' is the corresponding temperature. The Mott model [136] suggests that the activation energy can be calculated from the plots of conductivity versus temperature that enable one to draw tangents and determine the activation energies from their slopes. Studying the trend of activation energy with varying temperatures can help determine the charge transfer processes involved.

The electrical properties of glasses containing embedded metal and semiconductor ions have been subject to a lot of research [137-141]. A general non-linear trend has been reported in the plots of logarithmic conductivity versus reciprocal temperature, which is suggestive of a temperature dependent activation energy that decreases with temperature. Theoretical analysis has shown a good agreement with Mott's theory of phonon-assisted polaronic hopping conduction for electrical transport [142] at higher temperatures. The expression for small polaron hopping between localized states in glasses containing Transition Metal (TM) ions has been derived by Mott [143, 144] as

$$\sigma = \frac{v_0 e^2 C(1-C)}{kTR} \exp(-2\alpha R) \exp\left(-\frac{W}{kT}\right) \quad (4.8)$$

where ' $v_0$ ' is the phonon frequency, ' $C$ ' is the fraction of sites occupied by an electron or polaron given by the ratio of transition metal ion concentration in the lower valence state to the total ion concentration, ' $\alpha^{-1}$ ' is the localization length parameter, ' $R$ ' is the local

intersite separation and ‘W’ is the activation energy for hopping conduction. The electron is always assumed to move to the nearest empty localized state and the current density is found to be a function of overlap between wavefunctions, density of states at the Fermi level and the effective velocity of transport which is given as the product of phonon frequency and intersite separation ‘R’. This type of transport is especially prevalent when all states are strongly localized.

In cases of lower temperatures and negligible disorder, the behavior is said to conform to the variable range hopping (VRH) model [145] where the polarons are susceptible to hop beyond the nearest neighbors owing to lower polaron binding energy. The density of states per unit energy ‘ $\rho_{DOS}$ ’ near the Fermi level of a sphere of radius ‘R’ is:

$$\rho_{DOS} = \frac{4\pi R^3 N(E_F)}{3} \quad (4.9)$$

This implies that the average separation of level energies or the activation energy ‘ $\Delta E$ ’ will be:

$$\Delta E = \frac{3}{4\pi R^3 N(E_F)} \quad (4.10)$$

This equation shows that the farther the electron hops, the smaller is the activation energy to be overcome. If R is the range of the hop, it will fall exponentially as  $\exp(-2\alpha R)$ . This implies that there would be an ideal hopping distance for which the term ‘ $\exp(-2\alpha R)\exp(-\frac{W}{k_B T})$ ’ is maximized. After necessary calculations and solving for conductivity, the equation for variable range hopping is found to be

$$\sigma = \sigma_0 \exp \left[ -(T_0/T)^{1/4} \right] \quad (4.11)$$

where ‘ $\sigma_0$ ’ is a pre-exponential factor and ‘ $T_0$ ’ is a constant depending on the localization

length and the density of states at the Fermi level.

Some researchers have defined an additional parameter called percolation threshold, specifically to explain electrical properties of heterogeneous materials with conducting grains embedded in insulator substrates. This parameter refers to the critical concentration of the conducting phase necessary to initiate conduction. The behavior of heterogeneous systems can be shown to differ markedly above and below their percolation threshold values [146]. In his study of electrical conductivity of Carbon/Germanium amorphous semiconductors, Kazimierski [147] has shown that for all heterogeneous materials above percolation threshold, conductivity can be described by a generic formula (as given by Hill [148])

$$\sigma(T) = \sigma_0 \exp\left(-\left(\frac{kT_0}{kT}\right)^n\right) \quad (4.12)$$

for which  $n = 1$  makes it equivalent to the Arrhenius equation, with  $kT_0$  being the activation energy. The values of ' $n$ ' change depending on the conducting phase material and its characteristic dimensions, and can range from 0.25 to 1. If  $n = 0.25$ , Eq. 4.12 becomes the same as that derived by Mott for variable range hopping in three-dimensional space.

In their study of electrical conduction in core/shell nanocomposites made of transition metals and their oxides, Das et.al [149] have shown that these samples form a percolative network, and cause conduction by polaron hopping between the nearest  $\text{Cu}^+$  and  $\text{Cu}^{2+}$  ions. They have analyzed their electrical conductivity data based on Mott's model and attributed it to nearest neighbor hopping of phonon assisted polarons at higher temperatures, and variable range hopping at lower temperatures.

Often times, temperature dependence on the log of conductivity may not be

represented by a single slope, rather, it might be represented by a curve with an activation energy that smoothly decreases with decrease in temperature. In this case one can draw multiple tangents to determine the change in activation energies with temperature, as determined by Mott's model. However Gudaev *et al.* [150] have questioned the validity of such a model on the basis that tangents can be drawn in multiple ways, leading to vague conclusions about the activation energies involved. Their published works [150-152] have attempted to classify different transport mechanisms depending on the temperature and nature of material. They have established that charge transport in disordered materials usually obeys inverse Arrhenius law if they are non-polar, and obey a power law in case of polar disordered materials. They have carried out experiments with various disordered materials, and propose that if the conductivity occurs due to electrons hopping from one state to another by a one-phonon process, the transition probability 'P' will depend on temperature as

$$P = \nu_0 \exp\left(\frac{\nu_0}{k_B T}\right) \quad (4.13)$$

with ' $\nu_0$ ' being the phonon frequency. From this, they conclude that the conductivity can be described by the inverse Arrhenius law

$$\sigma = \sigma_0 \exp\left(\frac{T}{\alpha^{-1} T_0}\right) \quad (4.14)$$

where ' $\alpha^{-1} T_0$ ' is a parameter depending on the decay of density-of-states in the exponential region. This usually takes place in non-polar materials.

In case of polar materials, where multiple phonon-electron interactions arise, the transition probability 'P' changes to the form

$$P = \left(\frac{kT}{\hbar \nu_0}\right)^n \quad (4.15)$$

where ‘ $n$ ’ is the number of phonons. In this case the conductivity follows the power law pattern where

$$\sigma = \sigma_0 T^n \quad (4.16)$$

On this basis they have carried out analyses on Boron and its compounds [153, 154], which though crystalline, are known to have a highly defective structure. They have proved the absence of polaron effects in disordered Beta-Boron structures, as well as the strong presence of polaron effects on Boron compounds with metal ions embedded in them, and conformed their hypothesis, considering purely hopping electron transfer through local states and percolation concepts while assuming density of states at the Fermi level exponentially depends on energy. However, they have also touched upon the issue of not being able to differentiate between multi-phonon transitions of electrons and variable range hopping of electrons in case of materials with polar lattices.

Athanassiou *et al.* [155] have prepared carbon coated copper nanoparticles with insulator core- metal shell geometry, and have studied the sensitivity of the insulating carbon layer to external temperature and pressure applied. Comparing their results based on Kazimierski’s universal equation and multiphonon tunneling model [156] to fit their results, they have concluded that materials with smaller band-gaps show greater agreeability to the variable range hopping model, and favor the tunneling based conducting mechanism for their results obtained.

The electrical properties of a metal core/organic shell structure have been studied by Murray *et al.* using interdigitated array (IDA) electrodes [157]. They have reported an increase in material resistivity with increase in chain length of the organic shell material, and a decrease with increasing temperature. This result has been attributed primarily to

thermally activated electron transfer that creates opposite charges in adjacent metal cores, and secondly, to distant-dependent tunneling through the organic shell. Yakimov *et al.* have ascribed their results obtained for their Ge/Si quantum dot samples to the Efros-Shklovskii law [158] at higher temperatures, which transitions to the Arrhenius law as temperature diminishes. Beverly *et al.* [159] have described the temperature dependent charge transport of self-assembled Silver nanoparticles as being a function of particle size. They observe a transition from simple activated conduction to variable range hopping model with change in the degree of disorder. Similarly, conduction through self assembled Gold nanocrystal monolayers as a function of structural disorder have been shown by Parthasarathy *et al.* [160] to exhibit voltage thresholds, and obeying the power law model. A temperature-dependent conductivity has also been reported in Gold nanoparticle/hydrogel composites by X. Zhao *et al.* [161] where the sample exhibits excellent thermo-switchability. This repeatable behavior is attributed to the specific hydrogel material chosen as shell material, which swells and shrinks with temperature variations, thus changing the inter-core distance parameters.

As seen in this section, there has been an immense demand and interest to study the electrical conductivities of different kinds of nanostructures including disordered heterogeneous structures, glass nanocomposites embedded with metal and/or semiconductor ions, and core/ shell structures with different material combinations. Researchers are continually investigating the effects of change in compositions of the different phases of the heterogeneous material, variation in material dimensions, and degree of disorder in a material.

#### 4.3.2 Modeling the Behavior of Samples used in this Study

(i) Sample 1: Copper/ Copper oxide

According to R.M Hill's classifications[148] based on particle size and inter-particle distance of the sample, tunneling and thermionic emission could be highly probable mechanisms in the Copper/Copper oxide system. Considering that the sample has an oxide layer of roughly 10nm thickness, there is a possibility of a few stray electrons tunneling through the oxide barrier at lower temperatures when external voltage is applied. However this would not cause any sizeable surge in current and cannot individually explain the distinctive conduction trend observed. The sudden transition observed in the current - temperature graphs of the sample hint at some additional mechanism coming to the fore when heated beyond a certain threshold temperature.

To interpret the results better, the variation of natural log of conductivity with temperature inverse for the Copper/ Copper oxide sample has been observed. As mentioned earlier, the Arrhenius equation for electrical conduction is given by

$$\sigma(T) = \sigma_0 \exp\left(-\frac{E_a}{k_B T}\right) \quad (4.17)$$

where ' $E_a$ ' is the activation energy and ' $k_B$ ' is the Boltzmann constant. The pre-exponential factor ' $\sigma_0$ ' is a constant that depends on carrier concentration and other material dependent parameters [141]. This expression gives the dependence of conductivity ' $\sigma$ ' on temperature ' $T$ ' and activation energy ' $E_a$ '. According to this equation, the plot of natural log of conductivity ( $\sigma$ ) versus  $1/T$  should typically display a linear dependence, implying that the activation energy is independent of temperature. However, when this dependency is sketched for the Copper/ Copper oxide sample, another uncharacteristic trend presents itself, as shown in Figure 4.2.

Over the entire range of temperatures, a significant change in slope is observed on

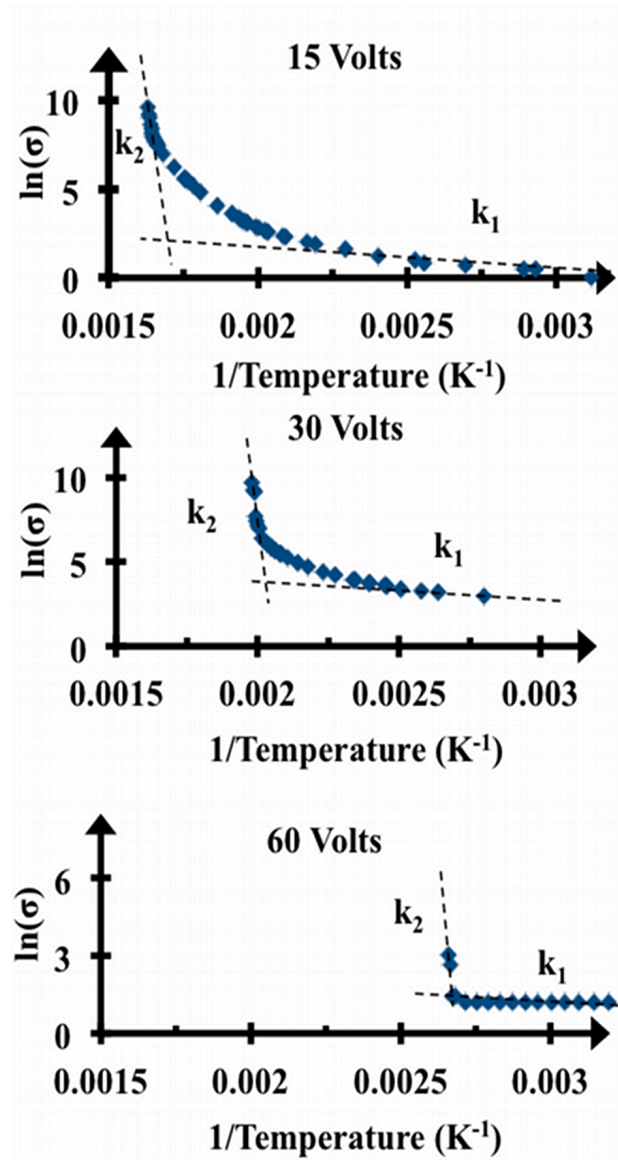


Figure 4.2: Natural log(Conductivity) versus  $1/\text{Temperature}$  plots at different voltages showing two distinct slopes for Copper/ Copper oxide sample

either side of the observed threshold temperatures, which yields two straight lines with two different slopes. This is indicative of certain temperature-dependent conduction mechanisms involving different activation energies dictating the sample's conductive properties. The range of activation energies calculated from the slopes of tangents drawn before and after the threshold temperatures are also seen to differ significantly. These



values have been mapped in Figure 4.3 for comparison.

Moreover, a comparative study undertaken to verify if the transition in activation energies corresponds to the estimated threshold temperatures for various data sets also furnishes a positive result. Figure 4.4 illustrates this study for the data set of 30 volts, showing a current versus temperature trend alongside the graph of variation of natural log of conductivity versus temperature inverse. A very good correlation is obtained on comparing the threshold temperature in the upper graph against the transition temperature in the lower graph at which activation energy changes. Similar conditions are recorded for the data sets of other voltages as well. This verifies that the temperature-dependent

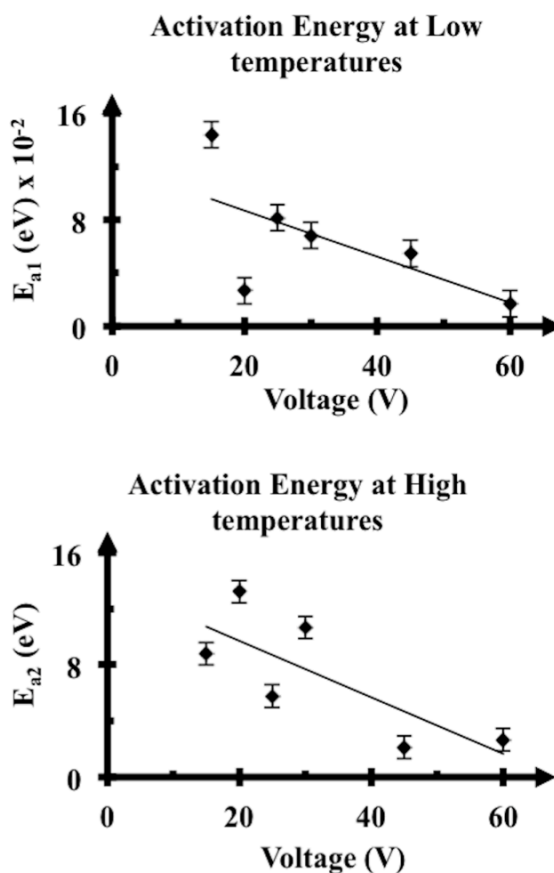


Figure 4.3. Comparison of activation energies obtained from Figure 4.2 for various voltages at low temperatures and high temperatures for the Copper/ Copper oxide sample.

activation energy does have an impact on the conductive trends exhibited by the Copper/ Copper oxide sample.

Copper oxide has a high dielectric constant of 18.1, making it decidedly polarizable in the presence of an external charge. This would be an ideal condition for the formation of polarons. An electron that enters the oxide barrier as a result of thermal emission can create a cloud of polarized medium that serves as a potential well for the charge. Under the influence of an externally applied electric field, the motion of this potential well and the charge trapped inside it can contribute to conduction. An activation energy changing with temperature has been recognized as being one of the characteristics of hopping

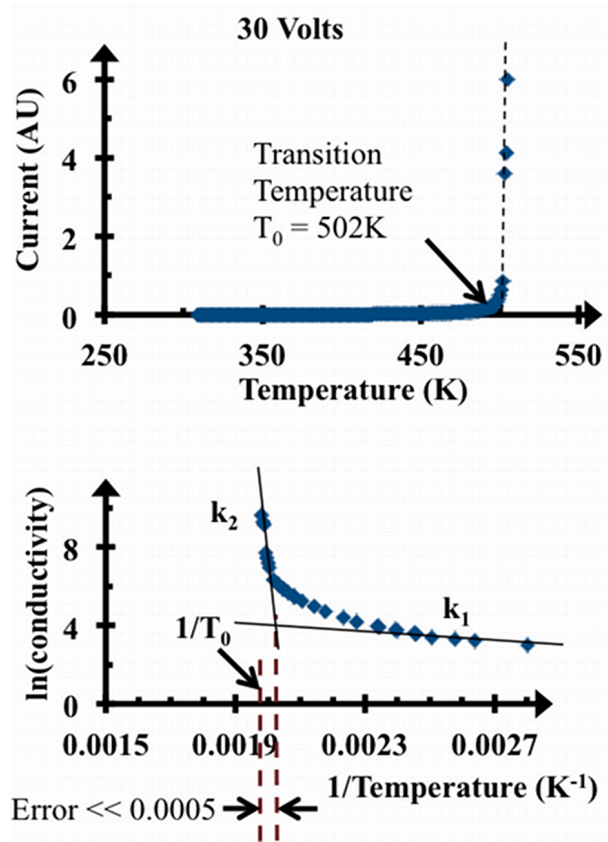


Figure 4.4: Current versus Temperature Characteristics along with  $\ln(\sigma)$  vs  $1/T$  plot for 30 Volts data-set of Copper/ Copper oxide sample.

conductivity according to Mott's model [103], and has been verified by Das *et.al* [108] and Gudaev *et.al* [150]. Considering the high polarizability of the shell material, this theory of polaron hopping seems promising. Apart from this, as pointed out by Gudaev [162], multiphonon-assisted transitions of electrons can also occur from one state to another, and cannot be neglected. With rise in temperature, the acoustic phonon-electron interactions are bound to increase. This may allow additional charge carriers to hop from one trap site to another under the influence of externally applied voltage. All these factors and theoretical studies suggest that the sudden carrier enhancement observed above certain critical temperatures could primarily be the result of temperature-activated hopping mechanisms occurring in the Copper/ Copper oxide sample.

(ii) Sample 2: Gold/ Silicon dioxide

In the Au/SiO<sub>2</sub> sample, a negligible current flow is observed as opposed to the Cu/Cu<sub>x</sub>O sample. A complete lack of a measureable amount of current at low temperatures, and an increase in charge transport as a function of applied voltage shows that the current through Au/SiO<sub>2</sub> sample is a function of both temperature and applied voltage. The relation between the natural log of conductivity ( $\sigma$ ) and temperature inverse ( $1/T$ ) has been plotted as shown in Figure 4.5, to try and interpret the results better.

In this case, a near-linear dependency is observed in the plot of natural log of conductivity ( $\sigma$ ) versus  $1/T$  unlike the Copper/ Copper oxide sample. This proves that the activation energy remains constant throughout the temperature range, implying the dominance of a single conductive mechanism over the entire temperature range. This is also the reason for not observing any sharp transition in the 'current versus temperature' graph, like the one observed in the Copper/ Copper oxide sample.

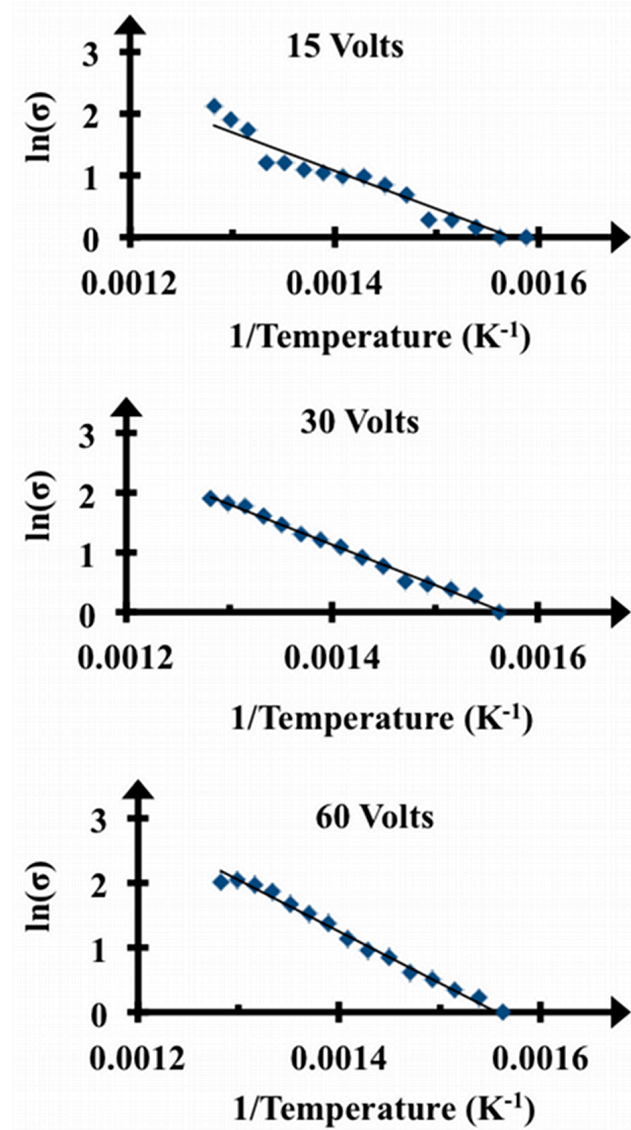


Figure 4.5: Natural log of conductivity versus Temperature inverse at different voltages showing constant slope throughout temperature range for Gold/ Silicon dioxide sample

Generally, the line-up between the metal Fermi level and valence/ conduction bands of the shell material plays an important role in determining the charge transfer mechanism. The metal/insulator/metal type of array structure of the Gold/Silica sample could play an important role, as the insulator barrier height is much higher than the Fermi level for gold. This makes the probability of electrons obtaining enough thermal energy to overcome the

barrier almost negligible, ruling out conduction merely by thermionic emission. Furthermore, Silicon dioxide has a relatively low dielectric constant, and its strong covalent bonds prevent it from getting polarized or forming polarons even at high temperatures, ruling out polaron hopping mechanisms.

At lower voltages, few of these carriers might traverse the oxide via direct tunneling, i.e. through the entire width of the potential barrier between the two metal spheres. As higher voltages are applied, band bending occurs, causing the barrier to taper proportional to the applied voltage. This enables the charge carriers to tunnel through the barrier more easily, since the carriers no longer need to navigate the entire thickness of the insulator layer. Since the probability of tunneling is known to depend on thickness of barrier, barrier height and the structure of the barrier, the current through the sample is also bound to increase at a faster rate with increase in voltage. This is verified from the experimental results presented in Figure 3.10 for three different voltages applied. Another important factor to consider is the temperature dependence of the sample's conductivity. Due to external application of heat, thermally emitted carriers start filling up energy levels above the metal Fermi level. As seen from the temperature-current curve for different voltages, current increases fairly exponentially with temperature, suggesting a temperature-assisted tunneling behavior.

The equation for thermal-assisted field emission (Eq. 2.13) has been used to try and fit the experimental results. This equation is rewritten below:

$$J_{SC} = A_G T^2 \exp\left(\frac{-(\Phi_B - \beta_{SC} E^{\frac{1}{2}})}{k_B T}\right); \beta_{SC} = \left(\frac{q^3}{4\pi\epsilon}\right)^{1/2} \quad (4.18)$$

where  $J_{SC}$  is the current density due to Schottky effect,  $\Phi_B$  is the effective field

dependent Schottky barrier height,  $\epsilon$  is the dielectric permittivity and  $A_G = A_0 \times \varphi$ , where  $A_0$  is the Richardson constant and  $\varphi$  is the correction factor.

The correction factor  $\varphi$  is known to be highly dependent on the sample being used, its dimensions, surface roughness and impurities. Depending on whether the samples under consideration are metals, oxides or composite surfaces the correction factor has been found to vary over a wide range of values [163, 164], from about 0.5 in metals to as low as  $8.3 \times 10^{-5}$  in certain oxides. Because of these ambiguities involved, we have tried to find this factor theoretically by fitting the above equation (Eq. 4.18) to the experimental data.

The values obtained for the three experimental data sets (i.e. for 15, 30 and 60 volts) are found to conform to the range of physicality, being of the order of  $10^{-4}$  (as suggested by [163]), and are found to differ very slightly from each other. We have thus determined the average of  $\varphi$  to be equal to  $8.63 \times 10^{-4}$ , and used this value for the purpose of theoretically modeling the experimental behavior of the sample. Fixing the ' $\varphi$ ' also ensures that the current versus temperature dependencies plotted experimentally and theoretically will solely depend on variations in voltage and temperature. Based on this understanding, the experimental data has been fitted to Eq. 4.18 as shown in Figure 4.6.

From Figure 4.6, it is evident that the equation for temperature-assisted field emission is able to successfully reproduce the experimental data obtained for the various data sets at different voltages. In addition, the value of effective barrier heights in each case has been calculated using the formula  $\Phi_{eff} = \left( \Phi_B - \beta_{SC} E^{\frac{1}{2}} \right)$ . This also yields the expected trend of the effective barrier height decreasing as the applied voltage increases.

From the above considerations regarding the type of sample materials, the

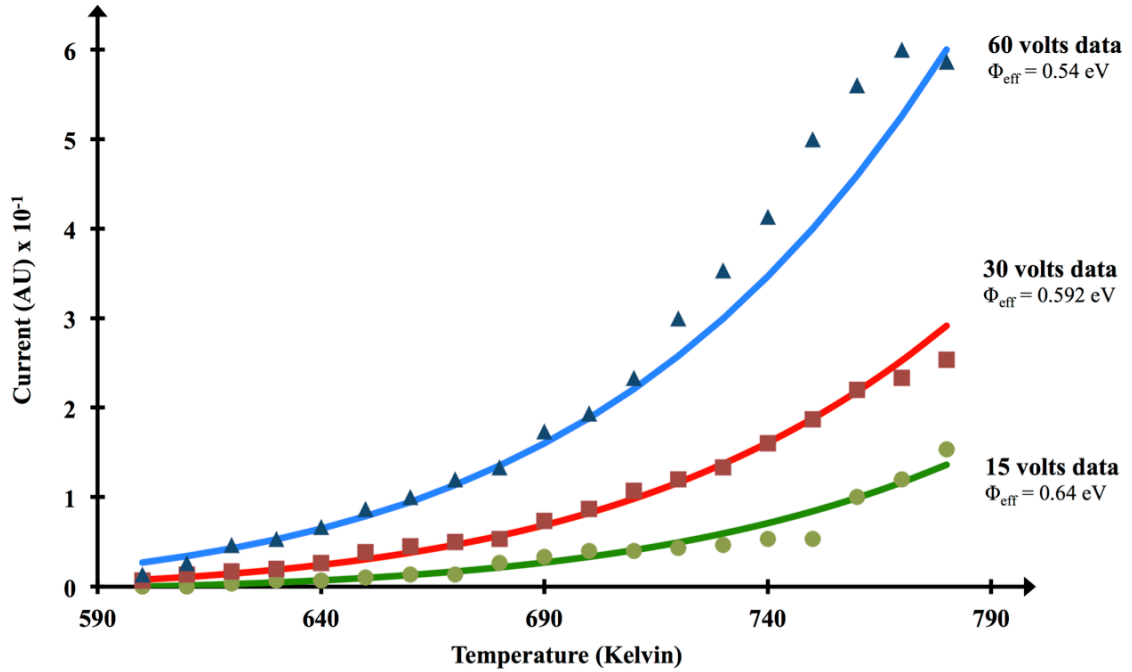


Figure. 4.6: Theoretical fitting to experimental data sets of Gold/ Silicon dioxide sample at 15, 30 and 60 volts. Data points represent experimental data at different voltages, whereas the continuous lines indicate theoretical fits.

experimental parameters being varied, and the fitting parameters obtained from the equation considered, temperature-assisted tunneling seems to be the most dominant mode of conduction in the Gold/ Silicon dioxide sample. Since the same equation cannot be used for fitting the experimental results of the Copper/ Copper oxide sample, it can be concluded theoretically that the inherent conduction mechanisms in both samples are definitely different.

In general, the externally applied voltage has two universal effects. The higher applied voltage compensates for losses in the circuit and draws a higher current into the sample. This increases ohmic thermal dissipation in the sample and results in a higher sample temperature. These two, effectively reduce the critical temperature at increasing voltages.

#### 4.4 Conclusion

On the basis of the experimental results, a careful theoretical analysis has been carried out to estimate the charge transfer mechanisms dominating in both the samples considered. Based on the data analyses as shown in the preceding section, the transfer mechanisms with the highest possibilities of contributing to conduction in both samples have been identified, as shown pictorially in Figures 4.7 and 4.8.

While the charge transport behavior of copper/ copper oxide is attributed primarily to

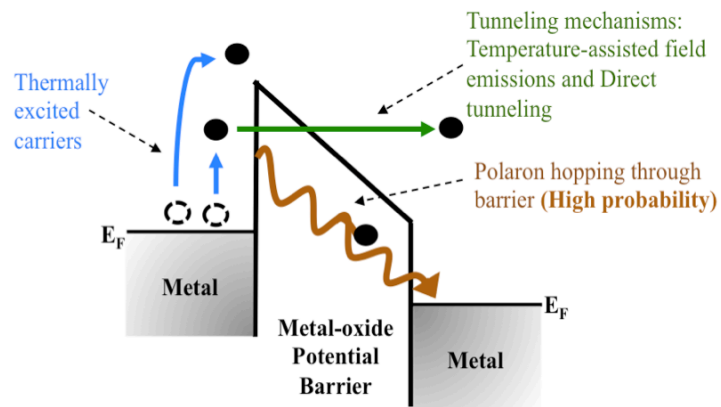


Figure 4.7: Pictorial representation of suggested charge transfer mechanisms in Copper/ Copper oxide core shell array

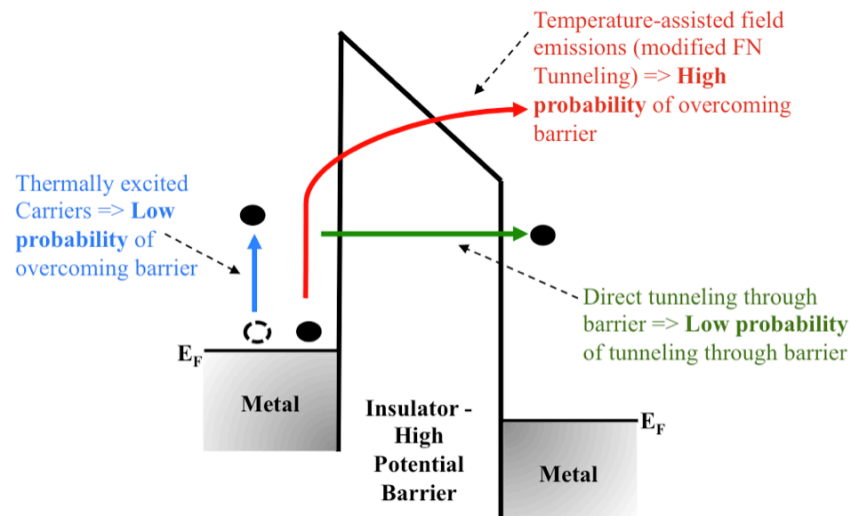


Figure 4.8: Pictorial representation of suggested charge transfer mechanisms in Gold/ Silicon dioxide core shell array



polaron hopping, the behavior of Gold/ Silicon dioxide is believed to be a result of tunneling mechanisms. These conclusions have been based on various factors like the nature of the core and shell materials, their dielectric constants, extent of disorder, structure dimensions, and careful assessment of existing theoretical models. Further refinement in modeling the behavior of these two nanocomposites will surely pave the way for their use in significant applications, as well as encourage further research in core/shell combinations and material transport.

## CHAPTER 5: FINAL REMARKS AND FUTURE DIRECTIONS

In summary, this dissertation has dealt with the important issue of being able to characterize nanostructures on the basis of charge transport through them. Two samples with conducting core and non-conducting shell architectures have been selected for this study. They have been analyzed experimentally and theoretically to try and establish the nature of charge transfer occurring through both samples over a wide range of temperature and electric fields.

Though the two samples considered in this experiment have their metallic cores separated from each other by non-conducting materials, effectively providing a structure that has periodic energy barriers to be overcome by the free charge carriers of the core materials, both samples are seen to exhibit certain conductive properties that are unique to both – their own bulk counterparts, as well as to each other. This is very interesting because:

(i) *It highlights the kind of unique properties that can be expected from nanostructures in general:* The metal core/ metal oxide shell (copper/copper oxide) structure that shows a transition behavior that can find applications in temperature sensing, embedded sensing in IC interconnects [165, 166] and for switching and control purposes. The Gold/Silicon dioxide sample being another unique metal-insulator combination has been shown to exhibit tunable optical properties with varying shell thicknesses [167].

(ii) *It emphasizes the significance of selecting the right materials for the core and shell layers to use it in specific applications.* Depending on the nature of shell materials surrounding the metal cores used in this study, different non-ohmic conductive trends are observed in both samples. Both the behaviors can be tapped for applications in different areas. Hence it is very important to choose the right material combination for use in specific applications.

The metal core/ metal oxide shell structure points to an interesting application for an adjustable thermal switch. That is, the temperature at which switching from insulator to conductor occurs can be manipulated by designing the composite with specific core/shell materials or by varying shell thicknesses and core diameters. This switching temperature can be adjusted over a wide range of temperatures from very low temperature all the way to temperatures below the melting temperatures of the materials in use. As an example, the core/ shell combination presented here can be used as a temperature sensor over high temperatures of 300° C to 400° C which is also the ideal temperature range between the inlet and outlet temperature of water in typical nuclear reactors. Thermal switches at such temperature ranges are expensive, inaccurate, and not readily available. So this work could be a significant step forward for developing such technology.

Secondly, polaron hopping has been shown to be a dominant method of charge transfer in certain types of structures. The charge introduced in a potential well sequentially is transferred throughout the arrays of potential wells and outputted in first-in-first-out order. This is very similar to the process in Charged Couple Devices (CCD) that are used for image processing, with the possible advantage of having ultimate pixels resolution.

Generally, conducting materials are optically opaque and this is due to the massive interaction of electrons and photons in conductors. On the contrary, insulating materials, due to a lack of free electrons, are generally transparent in the optical field. The core/shell composite material discussed in this dissertation has a potential application for switchable windows that could block the solar radiation entering the windows during hot summer days and the switch back to full transparency on cold winter days.

From the above examples, it is clear that the unique conductive properties obtained from core/ shell nanocomposite structures can indeed have a plethora of technological applications. The development of more accurate theoretical models to categorize and distinctly differentiate between the underlying principles leading to charge transfer will surely allow such samples to be tapped in substantive capacity for future applications.

## REFERENCES

- [1] S. Stevens, L. A. Sutherland, and J. S. Krajcik, *Big Ideas of Nanoscale Science and Engineering*: NSTA Press, 2009.
- [2] R. P. Feynman, "There's plenty of room at the bottom [data storage]," *Microelectromechanical Systems, Journal of*, vol. 1, pp. 60-66, 1992.
- [3] K. E. Drexler, *Engines of creation*: Anchor Press/Doubleday, 1986.
- [4] Z. Huaizhi and N. Yuantao, "China's ancient gold drugs," *Gold Bulletin*, vol. 34, pp. 24-29, 2001.
- [5] J. Turkevich, "Colloidal gold. Part II," *Gold Bulletin*, vol. 18, pp. 125-131, 1985/12/01 1985.
- [6] M. Köhler and W. Fritzsche, *Nanotechnology: An Introduction to Nanostructuring Techniques*: John Wiley & Sons, 2008.
- [7] I. Venkatesh and V. C. Venkatesh, *Precision Engineering*: McGraw-Hill Education (India) Pvt Limited, 2007.
- [8] R. S. Muller and T. I. Kamins, *Device electronics for integrated circuits*: Wiley, 1986.
- [9] R. S. Muller and T. I. Kamins, *Device Electronics for Integrated Circuits*: John Wiley & Sons, 2002.
- [10] R. R. Schaller, "Moore's law: past, present and future," *Spectrum, IEEE*, vol. 34, pp. 52-59, 1997.
- [11] H. Wong and I. Hiroshi, *The road to miniaturization* vol. 18. Bristol, ROYAUME-UNI: IOP, 2005.
- [12] F. Kreupl, "Carbon Nanotubes in microelectronic applications," in *Carbon Nanotube Devices: Properties, Modelling, Integration and Applications*, C. Hierold, Ed., ed Weinheim: Wiley-VCH, 2008, pp. 1-41.
- [13] C. A. Haberzettl, "Nanomedicine: destination or journey?," *Nanotechnology*, vol. 13, p. R9, 2002.
- [14] B. Gulson and H. Wong, "Stable Isotopic Tracing—A Way Forward for Nanotechnology," *Environ Health Perspect*, vol. 114, 2006.
- [15] C. G. Granqvist, A. Azens, P. Heszler, L. B. Kish, and L. Österlund, "Nanomaterials for benign indoor environments: Electrochromics for “smart windows”, sensors for air quality, and photo-catalysts for air cleaning," *Solar*

*Energy Materials and Solar Cells*, vol. 91, pp. 355-365, 2007.

- [16] F. Capasso, "Band-Gap Engineering: From Physics and Materials to New Semiconductor Devices," *Science*, vol. 235, pp. 172-176, January 9, 1987 1987.
- [17] M. J. O'Connell, *Carbon Nanotubes: Properties And Applications*: CRC/Taylor & Francis, 2006.
- [18] M. Lens, "Use of Fullerenes in Cosmetics," *Recent Patents on Biotechnology*, vol. 3, pp. 118-123, 2009.
- [19] C. T. Vogelson, "Advances in drug delivery systems," *Modern Drug Discovery*, vol. 4, pp. 49-50, April 2001 2001.
- [20] T. Da Ros and M. Prato, "Medicinal chemistry with fullerenes and fullerene derivatives," *Chemical Communications*, pp. 663-669, 1999.
- [21] E. Ōsawa, *Perspectives of Fullerene Nanotechnology*: Kluwer Academic Publishers, 2002.
- [22] W. Kratschmer, L. D. Lamb, K. Fostiropoulos, and D. R. Huffman, "Solid C60: a new form of carbon," *Nature*, vol. 347, pp. 354-358, 1990.
- [23] M. Eddaoudi and J. F. Eubank, "Periodic Nanostructures Based on Metal–Organic Frameworks (MOFs): En Route to Zeolite-Like Metal–Organic Frameworks (ZMOFs)," in *Organic Nanostructures*, ed: Wiley-VCH Verlag GmbH & Co. KGaA, 2008, pp. 251-274.
- [24] J. Theron, J. A. Walker, and T. E. Cloete, "Nanotechnology and Water Treatment: Applications and Emerging Opportunities," *Critical Reviews in Microbiology*, vol. 34, pp. 43-69, 2008.
- [25] Y. W. Guozhong Cao, *Nanostructures and nanomaterials: synthesis, properties and applications*, 2 ed. vol. 1,2. Singapore: World Scientific Publishing, 2010.
- [26] E. L. Hu and D. T. Shaw, "Synthesis and Assembly," Loyola College in Maryland, MarylandSep 1999 1999.
- [27] C. C. Koch, "Materials Synthesis by Mechanical Alloying," *Annual Review of Materials Science*, vol. 19, pp. 121-143, 1989.
- [28] F. Ashby, P. J. S. G. Ferreira, and D. L. Schodek, *Nanomaterials, Nanotechnologies and Design: An Introduction for Engineers and Architects*: Butterworth-Heinemann, 2009.
- [29] A. A. G. Requicha, S. Meltzer, F. P. T. Arce, J. H. Makaliwe, H. Siken, S. Hsieh, D. Lewis, B. E. Koel, and M. E. Thompson, "Manipulation of nanoscale components with the AFM: principles and applications," in *Nanotechnology*,

2001. *IEEE-NANO 2001. Proceedings of the 2001 1st IEEE Conference on*, 2001, pp. 81-86.
- [30] J. Loos, "The Art of SPM: Scanning Probe Microscopy in Materials Science," *Advanced Materials*, vol. 17, pp. 1821-1833, 2005.
  - [31] D. Cojoc, E. Di Fabrizio, L. Businaro, S. Cabrini, F. Romanato, L. Vaccari, and M. Altissimo, "Design and fabrication of diffractive optical elements for optical tweezer arrays by means of e-beam lithography," *Microelectronic Engineering*, vol. 61, pp. 963-969, 2002.
  - [32] C. B. Murray, D. J. Norris, and M. G. Bawendi, "Synthesis and characterization of nearly monodisperse CdE (E = sulfur, selenium, tellurium) semiconductor nanocrystallites," *Journal of the American Chemical Society*, vol. 115, pp. 8706-8715, 1993/09/01 1993.
  - [33] J. E. B. Katari, V. L. Colvin, and A. P. Alivisatos, "X-ray Photoelectron Spectroscopy of CdSe Nanocrystals with Applications to Studies of the Nanocrystal Surface," *The Journal of Physical Chemistry*, vol. 98, pp. 4109-4117, 1994/04/01 1994.
  - [34] N. C. Seeman and A. M. Belcher, "Emulating biology: Building nanostructures from the bottom up," *Proceedings of the National Academy of Sciences of the United States of America*, vol. 99, pp. 6451-6455, April 30, 2002 2002.
  - [35] M. K. Wu, R. S. Windeler, C. K. R. Steiner, T. Bors, and S. K. Friedlander, "Controlled Synthesis of Nanosized Particles by Aerosol Processes," *Aerosol Science and Technology*, vol. 19, pp. 527-548, 1993/01/01 1993.
  - [36] K. D. Sattler, *Nanoparticles and Quantum Dots*: Taylor & Francis, 2010.
  - [37] E. Roduner, "Size matters: why nanomaterials are different," *Chemical Society Reviews*, vol. 35, pp. 583-592, 2006.
  - [38] K. D. Sattler, *Handbook of Nanophysics: Nanoparticles and Quantum Dots*: CRC Press, 2010.
  - [39] H. Modrow, "Tuning Nanoparticle Properties - The X-ray Absorption Spectroscopic Point of View," *Applied Spectroscopy Reviews*, vol. 39, pp. 183-290, 2004/12/31 2004.
  - [40] L. L. Araujo, R. Giulian, D. J. Sprouster, C. S. Schnohr, D. J. Llewellyn, and K. P., "Size-dependent characterization of embedded Ge nanocrystals: Structural and thermal properties," *Physical Review B*, vol. 78, p. 15, 2008.
  - [41] Q. Xu, I. D. Sharp, C. W. Yuan, D. O. Yi, C. Y. Liao, A. M. Glaeser, A. M. Minor, J. W. Beeman, M. C. Ridgway, P. Kluth, J. W. Ager, III, D. C. Chrzan, and E. E. Haller, "Large Melting-Point Hysteresis of Ge Nanocrystals Embedded

- in SiO<sub>2</sub>," *Physical Review Letters*, vol. 97, p. 155701, 2006.
- [42] A. P. Alivisatos, "Perspectives on the Physical Chemistry of Semiconductor Nanocrystals," *The Journal of Physical Chemistry*, vol. 100, pp. 13226-13239, 1996/01/01 1996.
  - [43] A. Korkin and F. Rosei, *Nanoelectronics and Photonics: From Atoms to Materials, Devices, and Architectures*: Springer, 2008.
  - [44] B. J. Jankiewicz, D. Jamiola, J. Choma, and M. Jaroniec, "Silica-metal core-shell nanostructures," *Advances in Colloid and Interface Science*, vol. 170, pp. 28-47, 2012.
  - [45] U. Müller, "Nanostructures," in *Inorganic Structural Chemistry*, ed: John Wiley & Sons, Ltd, 2007, pp. 241-245.
  - [46] M. L.M., *Composites with Nanomaterials in Functional Nanomaterials*. California: American Scientific Publishers, 2006.
  - [47] R. Davies, G. A. Schurr, P. Meenan, R. D. Nelson, H. E. Bergna, C. A. S. Brevett, and R. H. Goldbaum, "Engineered Particle Surfaces," *Advanced Materials*, vol. 10, pp. 1264-1270, 1998.
  - [48] H. Ow, D. R. Larson, M. Srivastava, B. A. Baird, W. W. Webb, and U. Wiesner, "Bright and Stable Core-Shell Fluorescent Silica Nanoparticles," *Nano Letters*, vol. 5, pp. 113-117, 2005/01/01 2004.
  - [49] N. Sounderya and Y. Zhang, "Use of Core/Shell Structured Nanoparticles for Biomedical Applications," *Recent Patents on Biomedical Engineering*, vol. 1, pp. 34-42, 2008.
  - [50] C. Sanchez, B. Julian, P. Belleville, and M. Popall, "Applications of hybrid organic-inorganic nanocomposites," *Journal of Materials Chemistry*, vol. 15, 2005.
  - [51] S. M. Kang, K.-B. Lee, D. J. Kim, and I. S. Choi, "Biomimetic approach to the formation of gold nanoparticle/silica core/shell structures and subsequent bioconjugation," ed: Institute of Physics, 2006.
  - [52] L. M. Liz-Marzán, M. Giersig, and P. Mulvaney, "Synthesis of Nanosized Gold-Silica Core-Shell Particles," *Langmuir*, vol. 12, pp. 4329-4335, 1996/01/01 1996.
  - [53] L. Wendler and R. Pechstedt, "Dynamical Screening, Collective Excitations, and Electron-Phonon Interaction in Heterostructures and Semiconductor Quantum Wells. Application to Double Heterostructures," *Physica Status Solidi (b)*, vol. 141, pp. 129-150, 1987.



- [54] P. Reiss, M. Protière, and L. Li, "Core/Shell Semiconductor Nanocrystals," *Small*, vol. 5, pp. 154-168, 2009.
- [55] S. A. Ivanov, A. Piryatinski, J. Nanda, S. Tretiak, K. R. Zavadil, W. O. Wallace, D. Werder, and V. I. Klimov, "Type-II Core/Shell CdS/ZnSe Nanocrystals - Synthesis, Electronic Structures, and Spectroscopic Properties," *Journal of the American Chemical Society*, vol. 129, pp. 11708-11719, 2007/09/01 2007.
- [56] B. O. Dabbousi, J. Rodriguez-Viejo, F. V. Mikulec, J. R. Heine, H. Mattoussi, R. Ober, K. F. Jensen, and M. G. Bawendi, "(CdSe)ZnS Core/Shell Quantum Dots - Synthesis and Characterization of a Size Series of Highly Luminescent Nanocrystallites," *The Journal of Physical Chemistry B*, vol. 101, pp. 9463-9475, 1997/11/01 1997.
- [57] A. Burns, H. Ow, and U. Wiesner, "Fluorescent core-shell silica nanoparticles: towards "Lab on a Particle" architectures for nanobiotechnology," *Chemical Society Reviews*, vol. 35, pp. 1028-1042, 2006.
- [58] S. Wang, B. R. Jarrett, S. M. Kauzlarich, and A. Y. Louie, "Core/Shell Quantum Dots with High Relaxivity and Photoluminescence for Multimodality Imaging," *Journal of the American Chemical Society*, vol. 129, pp. 3848-3856, 2007/04/01 2007.
- [59] P. Reiss, J. I. Bleuse, and A. Pron, "Highly Luminescent CdSe/ZnSe Core/Shell Nanocrystals of Low Size Dispersion," *Nano Letters*, vol. 2, pp. 781-784, 2002/07/01 2002.
- [60] J. Kim, J. E. Lee, S. H. Lee, J. H. Yu, J. H. Lee, T. G. Park, and T. Hyeon, "Designed Fabrication of a Multifunctional Polymer Nanomedical Platform for Simultaneous Cancer-Targeted Imaging and Magnetically Guided Drug Delivery," *Advanced Materials*, vol. 20, pp. 478-483, 2008.
- [61] C.-Y. Huang and Y.-D. Lee, "Core-shell type of nanoparticles composed of poly[(n-butyl cyanoacrylate)-co-(2-octyl cyanoacrylate)] copolymers for drug delivery application: Synthesis, characterization and in vitro degradation," *International Journal of Pharmaceutics*, vol. 325, pp. 132-139, 2006.
- [62] J. M. Chan, L. Zhang, K. P. Yuet, G. Liao, J.-W. Rhee, R. Langer, and O. C. Farokhzad, "PLGA-lecithin-PEG core-shell nanoparticles for controlled drug delivery," *Biomaterials*, vol. 30, pp. 1627-1634, 2009.
- [63] M. Chu, X. Song, D. Cheng, S. Liu, and J. Zhu, "Preparation of quantum dot-coated magnetic polystyrene nanospheres for cancer cell labelling and separation," *Nanotechnology*, vol. 17, p. 3268, 2006.
- [64] J. L. Arias, M. Lopez-Viota, M. A. Ruiz, J. Lopez-Viota, and A. V. Delgado, "Development of carbonyl iron/ethylcellulose core/shell nanoparticles for biomedical applications," *International Journal of Pharmaceutics*, vol. 339, pp.

237-245, 2007.

- [65] F. Pinaud, D. King, H.-P. Moore, and S. Weiss, "Bioactivation and Cell Targeting of Semiconductor CdSe/ZnS Nanocrystals with Phytochelatin-Related Peptides," *Journal of the American Chemical Society*, vol. 126, pp. 6115-6123, 2004/05/01 2004.
- [66] E. M. Goldys, *Fluorescence Applications in Biotechnology and Life Sciences*: John Wiley & Sons, 2009.
- [67] G. Schmid, *Clusters and Colloids: From Theory to Applications* NY: VCH Publishers, 1994.
- [68] S. G. Penn, L. He, and M. J. Natan, "Nanoparticles for Bioanalysis," *Current Opinion in Chemical Biology*, vol. 7, pp. 609-615, 2003.
- [69] L. J. d. Jongh, *Physics and chemistry of metal cluster compounds : model systems for small metal particles*. Dordrecht [etc.]: Kluwer Academic Publishers, 1994.
- [70] M. Valden, X. Lai, and D. W. Goodman, "Onset of catalytic activity of gold clusters on titania with the appearance of nonmetallic properties," *Science*, vol. 281, pp. 1647-50, Sep 11 1998.
- [71] R. A. Pala, K. T. Shimizu, N. A. Melosh, and M. L. Brongersma, "A Nonvolatile Plasmonic Switch Employing Photochromic Molecules," *Nano Letters*, vol. 8, pp. 1506-1510, 2008/05/01 2008.
- [72] M. E. Franke, T. J. Koplin, and U. Simon, "Metal and Metal Oxide Nanoparticles in Chemiresistors: Does the Nanoscale Matter?," *Small*, vol. 2, pp. 36-50, 2006.
- [73] C. M. Snowden and E. Snowden, *Introduction to Semiconductor Device Modelling*: World Scientific Publishing Company (1998).
- [74] K. T. Tsen, *Ultrafast Dynamical Processes in Semiconductors*: Springer, 2004.
- [75] M. A. Reed, *Nanostructured Systems*: Academic Press, 1992.
- [76] A. Tschersich, "Quantum interference and charge fluctuations in quantum dots and granular metals," Ph. D., Ruhr University Bochum Bochum, 2001.
- [77] J. G. Simmons, "Conduction in thin dielectric films," *Journal of Physics D: Applied Physics*, vol. 4, p. 613, 1971.
- [78] H. Fowler R, "Electron Emission in Intense Electric Field," *Proc. Roy. Soc. (London) A*, vol. 119, pp. 173-181, 1928 1928.
- [79] L. D. Filip, D. J. Carey, and S. R. P. Silva, "Electron tunneling from a 3D nanosphere," in *Vacuum Nanoelectronics Conference (IVNC), 2010 23rd*

*International*, 2010, pp. 179-180.

- [80] S. R. Pollack and C. E. Morris, "Electron Tunneling through Asymmetric Films of Thermally Grown  $\text{Al}_2\text{O}_3$ ," *Journal of Applied Physics*, vol. 35, pp. 1503-1512, 1964.
- [81] S. M. Sze and K. K. Ng, *Physics of Semiconductor Devices*: John Wiley & Sons, 2006.
- [82] O. W. Richardson, "LI. Some applications of the electron theory of matter," *Philosophical Magazine Series 6*, vol. 23, pp. 594-627, 1912/04/01 1912.
- [83] W. Schottky, "Cold and Hot Electron Discharges," *Phys. Zeits.*, vol. 14, p. 63, 1923.
- [84] R. A. Millikan and C. F. Eyring, "Laws Governing the Pulling of Electrons out of Metals by Intense Electrical Fields," *Physical Review*, vol. 27, pp. 51-67, 1926.
- [85] C. C. Millikan and C. C. Lauritsen, "Relations of Field-Currents to Thermionic-Currents," *Proceedings of the National Academy of Sciences*, vol. 14, pp. 45-49, January 1, 1928.
- [86] O. W. Richardson, "The Emission of Secondary Electrons and the Excitation of Soft X-Rays," *Proceedings of the Royal Society of London. Series A*, vol. 119, pp. 531-542, July 2, 1928 1928.
- [87] W. Monch, *Electronic Properties of Semiconductor Interfaces*: Springer, 2004.
- [88] W. B. Nottingham, "Thermionic Emission," Massachusetts Institute of Technology, Cambridge, December 10, 1956.
- [89] J. J. O'Dwyer, *The theory of electrical conduction and breakdown in solid dielectrics*: Clarendon Press, 1973.
- [90] K. C. Kao and W. Hwang, *Electrical transport in solids: with particular reference to organic semiconductors*: Pergamon Press, 1981.
- [91] D. L. Sidebottom, B. Roling, and K. Funke, "Ionic conduction in solids: Comparing conductivity and modulus representations with regard to scaling properties," *Physical Review B*, vol. 63, p. 024301, 2000.
- [92] H. L. Tuller, "Ionic Conduction in Nanocrystalline Materials," ed, 2002.
- [93] Choi, B. C., Kim, J. B., Kim, and J. N., "Ionic conduction associated with polaronic hopping in  $\text{KTiOPO}_4$  single crystal," *Solid State Communications*, vol. 84, pp. 1077-1080, December 1992.
- [94] H. Frohlich, "On the Theory of Dielectric Breakdown in Solids," *Proceedings of*

- the Royal Society of London. Series A. Mathematical and Physical Sciences*, vol. 188, pp. 521-532, February 25, 1947.
- [95] A. Miller and E. Abrahams, "Impurity Conduction at Low Concentrations," *Physical Review*, vol. 120, pp. 745-755, 1960.
  - [96] P. W. Anderson, "Absence of Diffusion in Certain Random Lattices," *Physical Review*, vol. 109, pp. 1492-1505, 1958.
  - [97] A. I. Gubanov, *Quantum electron theory of amorphous conductors Semiconductors*: Consultants Bureau, 1965.
  - [98] R. L. McCreery, "Molecular Electronic Junctions," *Chemistry of Materials*, vol. 16, pp. 4477-4496, January 11, 2004.
  - [99] D. Segal, A. Nitzan, M. Ratner, and W. B. Davis, "Activated Conduction in Microscopic Molecular Junctions," *The Journal of Physical Chemistry B*, vol. 104, pp. 2790-2793, April 1, 2000.
  - [100] G. R. Hutchison, M. A. Ratner, and T. J. Marks, "Hopping Transport in Conductive Heterocyclic Oligomers: Reorganization Energies and Substituent Effects," *Journal of the American Chemical Society*, vol. 127, pp. 2339-2350, February 1, 2005.
  - [101] M. Bixon and J. Jortner, "Hole Trapping, Detrapping, and Hopping in DNA," *The Journal of Physical Chemistry A*, vol. 105, pp. 10322-10328, November 1, 2001.
  - [102] A. Popov, *Disordered Semiconductors: Physics and Applications*: Pan Stanford Publishing, 2011.
  - [103] N. F. Mott, "Conduction in glasses containing transition metal ions," *Journal of Non-Crystalline Solids*, vol. 1, pp. 1-17, 1968.
  - [104] N. F. Mott, "Conduction in non-crystalline materials," *Philosophical Magazine*, vol. 19, pp. 835-852, April 1, 1969.
  - [105] L. D. Landau, "Electron motion in Lattices," *Phys. Z. Sowjetunion*, vol. 3, pp. 664-664, 1933.
  - [106] G. Moorthy and K. Daneshvar, "Electrical properties of conductive metal/insulating shell nanocluster array," *Southeastcon, 2011 Proceedings of IEEE*, pp. 38-41, pp. 17-20 March 2011.
  - [107] G. Moorthy and K. Daneshvar, "Conduction in metallic core/shell nanoclusters," in *Southeastcon, 2012 Proceedings of IEEE*, pp. 1-4, 2012.
  - [108] D. Das, T. Kundu, M. Dey, S. Chakraborty, and D. Chakravorty, "Electrical conduction in composites containing copper core-copper oxide shell nanostructure

in silica gel," *Journal of Chemical Sciences*, vol. 115, pp. 341-348, 2003.

- [109] P. M. Petroff, A. Lorke, and A. Imamoglu, "Epitaxially self-assembled quantum dots," *Physics Today*, vol. 54, pp. 46-52, May 2001.
- [110] S. A. Empedocles, R. Neuhauser, K. Shimizu, and M. G. Bawendi, "Photoluminescence from single semiconductor nanostructures," *Advanced Materials*, vol. 11, pp. 1243-1256, October 20 1999.
- [111] T. Lee, W. Wang, and M. A. Reed, "Mechanism of electron conduction in self-assembled alkanethiol monolayer devices," *Annals of the New York Academy of Sciences*, vol. 1006, pp. 21-35, December 2003.
- [112] J. A. E. Strosio, D.M., , "Atomic and Molecular Manipulation with the Scanning Tunneling Microscope," *Science*, vol. 254, pp. 1319-1326, 1991.
- [113] M. G. Schultz and F. von Oppen, "Quantum transport through nanostructures in the singular-coupling limit," *Physical Review B*, vol. 80, p. 033302, 2009.
- [114] T. V. Torchynska, "Ballistic transport and photoluminescence in silicon nanocrystallites," *Journal of Applied Physics*, vol. 92, pp. 4019-4023, 2002.
- [115] F. M. Bufler, *Full-band Monte Carlo Simulation of Electrons and Holes in Strained Si and SiGe*: Utz, Wiss., 1998.
- [116] C. M. Snowden and E. Snowden, *Introduction to Semiconductor Device Modelling*: WORLD SCIENTIFIC Publishing Company (1998).
- [117] B. Kannan, K. Castelino, and A. Majumdar, "Design of Nanostructured Heterojunction Polymer Photovoltaic Devices," *Nano letters*, vol. 3, pp. 1729-1733, December 1, 2003.
- [118] E. Polizzi and N. Ben Abdallah, "Self-consistent three-dimensional models for quantum ballistic transport in open systems," *Physical Review B*, vol. 66, p. 245301, 2002.
- [119] C. Jungemann and B. Meinerzhagen, *Hierarchical Device Simulation: The Monte-Carlo Perspective*: Springer, 2003.
- [120] S. Bandyopadhyay, *Physics of Nanostructured Solid State Devices*: Springer, 2012.
- [121] P. W. Hawkes, *Advances in Electronics and Electron Physics*: Academic Press, 1994.
- [122] M. Lundstrom, *Fundamentals of Carrier Transport*: Cambridge University Press, 2009.

- [123] C. Jacoboni and P. Lugli, *The Monte Carlo Method for Semiconductor Device Simulation*: Springer, 2002.
- [124] D. K. Ferry, *Semiconductor Transport*: Taylor & Francis, 2000.
- [125] D. K. Ferry and S. M. Goodnick, *Transport in Nanostructures*: Cambridge University Press, 1997.
- [126] D. K. Blanks, G. Klimeck, R. Lake, D. Jovanovic, R. C. Bowen, C. Fernando, W. R. Frensley, and L. Manhua, "NEMO: general release of a new comprehensive quantum device simulator," in *Compound Semiconductors, 1997 IEEE International Symposium on*, 1998, pp. 639-642.
- [127] M. V. Fischetti, "Master-equation approach to the study of electronic transport in small semiconductor devices," *Physical Review B*, vol. 59, pp. 4901-4917, 1999.
- [128] P. Bordone, M. Pascoli, R. Brunetti, A. Bertoni, C. Jacoboni, and A. Abramo, "Quantum transport of electrons in open nanostructures with the Wigner-function formalism," *Physical Review B*, vol. 59, pp. 3060-3069, 1999.
- [129] S. Datta, *Electronic Transport in Mesoscopic Systems*: Cambridge University Press, 1997.
- [130] G. Baccarani, F. Odeh, A. Gnudi, and D. Ventura, "A critical review of the fundamental semiconductor equations," *Institute for Mathematics and Its Applications*, vol. 59, p. 19, 1994.
- [131] J. C. Garland and D. B. Tanner, *Electrical transport and optical properties of inhomogeneous media*, 1978.
- [132] C. A. Neugebauer and M. B. Webb, "Electrical Conduction Mechanism in Ultrathin, Evaporated Metal Films," *Journal of Applied Physics*, vol. 33, pp. 74-&, 1962.
- [133] R. M. Hill, "Electrical Conduction in Ultra Thin Metal Films. I. Theoretical," *Proceedings of the Royal Society of London. A. Mathematical and Physical Sciences*, vol. 309, pp. 377-395, March 25, 1969 1969.
- [134] P. A. Tick and F. P. Fehlner, "Electrical Behavior of Composite Discontinuous Films," *Journal of Applied Physics*, vol. 43, pp. 362-&, 1972.
- [135] K. Uozumi, M. Nishiura, and A. Kinbara, "On the field effect of the electrical conductance of discontinuous thin metal films," *Journal of Applied Physics*, vol. 48, pp. 818-819, 1977.
- [136] N. F. Mott, "Conduction in glasses containing transition metal ions," *Journal of Non-Crystalline Solids*, vol. 1, pp. 1-17, 1968.

- [137] L. Murawski, C. H. Chung, and J. D. Mackenzie, "Electrical properties of semiconducting oxide glasses," *Journal of Non-Crystalline Solids*, vol. 32, pp. 91-104, 1979.
- [138] A. Ghosh and D. Chakravorty, "Electrical conduction in some sol-gel silicate glasses," *Physical Review B*, vol. 48, pp. 5167-5171, 1993.
- [139] M. Sayer and A. Mansingh, "Transport Properties of Semiconducting Phosphate Glasses," *Physical Review B*, vol. 6, pp. 4629-4643, 1972.
- [140] A. Ghosh, "Transport properties of vanadium germanate glassy semiconductors," *Physical Review B*, vol. 42, pp. 5665-5676, 1990.
- [141] R. Singh and K. Sethupathi, "Electrical DC conductivity in iron-containing bismuth-vanadate glasses," *Journal of Physics D: Applied Physics*, vol. 22, p. 709, 1989.
- [142] N. F. Mott and E. A. Davis, *Electronic processes in non-crystalline materials*, 2nd ed. Oxford: Clarendon Press, 1971.
- [143] I. G. Austin and N. F. Mott, "Polarons in crystalline and non-crystalline materials," *Advances in Physics*, vol. 18, pp. 41-102, 1969/01/01 1969.
- [144] N. F. Mott, "Metal-Insulator Transition," *Reviews of Modern Physics*, vol. 40, pp. 677-683, 1968.
- [145] N. F. Mott, "Conduction in non-crystalline materials," *Philosophical Magazine*, vol. 19, pp. 835-852, 1969/04/01 1969.
- [146] S. Kirkpatrick, "Percolation and Conduction," *Reviews of Modern Physics*, vol. 45, pp. 574-588, 1973.
- [147] K. P, "Electrical conductivity of plasma-deposited carbon-germanium amorphous semiconductors: correlation with nanostructure," *Journal of Non-Crystalline Solids*, vol. 325, pp. 206-212, 2003.
- [148] R. M. Hill, "On the observation of variable range hopping," *Physica Status Solidi (a)*, vol. 35, pp. K29-K34, 1976.
- [149] D. Das, D. Das, T. Kundu, M. Dey, S. Chakraborty, and D. Chakravorty, "Electrical conduction in composites containing copper core-copper oxide shell nanostructure in silica gel," *Journal of Chemical Sciences*, vol. 115, pp. 341-348, 2003.
- [150] O. Gudaev and V. Malinovskii, "Hopping charge-transfer mechanism in quasi-crystals of boron and of its compounds," *Physics of the Solid State*, vol. 44, pp. 837-842, 2002.

- [151] Gudaev, O. A., Malinovskii, V. K., Tybulewicz, and A., *Electrical conductivity of polar disordered materials exhibiting multiphonon transitions*, vol. 34. New York, NY, ETATS-UNIS: American Institute of Physics, 1992.
- [152] O. Gudaev and V. Malinovskii, "Universal regularities of charged carrier transfer in disordered materials," *Glass Physics and Chemistry*, vol. 26, pp. 364-372, 2000.
- [153] O. A. Golikova, "Semiconductors with complex lattice and the amorphization problem," *physica status solidi (a)*, vol. 101, pp. 277-314, 1987.
- [154] O. A. Golikova, "Quasiamorphous semiconductors," *Soviet Physics Uspekhi*, vol. 32, p. 665, 1989.
- [155] E. K. Athanassiou, C. Mensing, and W. J. Stark, "Insulator coated metal nanoparticles with a core/shell geometry exhibit a temperature sensitivity similar to advanced spinels," *Sensors and Actuators A: Physical*, vol. 138, pp. 120-129, 2007.
- [156] D. Emin, C. Seager, and R. Quinn, "Small-Polaron Hopping Motion in Some Chalcogenide Glasses," *Physical Review Letters*, vol. 28, pp. 813-816, 1972.
- [157] R. H. Terrill, T. A. Postlethwaite, C.-h. Chen, C.-D. Poon, A. Terzis, A. Chen, J. E. Hutchison, M. R. Clark, and G. Wignall, "Monolayers in Three Dimensions: NMR, SAXS, Thermal, and Electron Hopping Studies of Alkanethiol Stabilized Gold Clusters," *Journal of the American Chemical Society*, vol. 117, pp. 12537-12548, 1995/12/01 1995.
- [158] A. Yakimov, A. Dvurechenskii, G. Min'kov, A. Sherstobitov, A. Nikiforov, and A. Bloshkin, "Hopping conductivity and Coulomb correlations in 2D arrays of Ge/Si quantum dots," *Journal of Experimental and Theoretical Physics*, vol. 100, pp. 722-730, 2005.
- [159] K. C. Beverly, J. F. Sampaio, and J. R. Heath, "Effects of Size Dispersion Disorder on the Charge Transport in Self-Assembled 2-D Ag Nanoparticle Arrays," *The Journal of Physical Chemistry B*, vol. 106, pp. 2131-2135, March 1, 2002.
- [160] R. Parthasarathy, X.-M. Lin, and H. M. Jaeger, "Electronic Transport in Metal Nanocrystal Arrays: The Effect of Structural Disorder on Scaling Behavior," *Physical Review Letters*, vol. 87, p. 186807, 2001.
- [161] X. Zhao, X. Ding, Z. Deng, Z. Zheng, Y. Peng, and X. Long, "Thermoswitchable Electronic Properties of a Gold Nanoparticle/Hydrogel Composite," *Macromolecular Rapid Communications*, vol. 26, pp. 1784-1787, 2005.
- [162] O. Gudaev and V. Malinovskii, "Electrical Conductivity of Polar disordered materials exhibiting Multiphonon transitions," vol. 34, 1992.
- [163] B. Wolf, *Handbook of Ion Sources*: Taylor & Francis, 1995.



- [164] C. J. Smithells, *Metals reference book*: Plenum Press, 1967.
- [165] J. Appenzeller, M. Radosavljević, J. Knoch, and P. Avouris, "Tunneling Versus Thermionic Emission in One-Dimensional Semiconductors," *Physical Review Letters*, vol. 92, p. 048301, 2004.
- [166] J. Livage, J. P. Jolivet, and E. Tronc, "Electronic properties of mixed valence oxide gels," *Journal of Non-Crystalline Solids*, vol. 121, pp. 35-39, 1990.
- [167] T. Ung, L. M. Liz-Marzán, and P. Mulvaney, "Optical Properties of Thin Films of Au@SiO<sub>2</sub> Particles," *The Journal of Physical Chemistry B*, vol. 105, pp. 3441-3452, May 1, 2001.

## VITA

EDUCATION

Ph.D.- Electrical and Computer Engineering  
 Aug '09 – Dec '12  
 University of North Carolina at Charlotte, NC  
 GPA: 3.93/4.0

M.S.- Electrical and Computer Engineering  
 Jan '08 – May '09  
 University of North Carolina at Charlotte, NC  
 GPA: 3.9/4.0

B.E. – Electronics Engineering  
 Aug'03 – May '07  
 University of Mumbai, India

PUBLICATIONS

G. Moorthy, and K. Daneshvar, *Conduction in core/shell nano-composites*, Journal of Applied Physics, Volume 111, Issue 12, 124503-124503-5, June 2012

G. Moorthy, K. Daneshvar, Conductive properties in Metal Core/ Shell nanoclusters, Southeastcon, 2012 Proceedings of IEEE, 1 - 4, March 2012

G. Moorthy, K. Daneshvar, Electrical Properties of Conductive Metal/ Insulating Shell nano-cluster array, Southeastcon, 2011 Proceedings of IEEE, 38 – 41, March 2011

EXPERIMENTAL  
TECHNIQUES

Clean Room Experience (Class 100 and Class 1000 facilities)

- Photolithography and E-Beam lithography
  - Mask pattern designing using AUTOCAD
  - Conversant with lithography equipment operation, processing regimes and related metrology
- Process development for nanoimprint template fabrication using E-beam lithography on different substrates

Material Characterization

- Observation and Characterization of nanostructures using the RAITH 150 Scanning Electron microscope (SEM)

Optical and Electrical characterization

- Current/ Voltage measurements for different types of nanostructures under varying experimental parameters

- Photoluminescence measurements of different nanoparticles with laser and conventional light sources

#### Laser technology

- Hands-on experience in Ultra-Violet (UV) laser and Femtosecond laser operation

### AWARDS

1<sup>st</sup> place, Best Research Paper presentation - 12<sup>th</sup> annual Graduate Research Fair Award, UNC Charlotte, 2012

2<sup>nd</sup> place, Best Research Paper presentation – 11<sup>th</sup> annual Graduate Research Fair, UNC Charlotte, 2011

Graduate and Professional Student Government Travel Award, 2012 & 2011

Graduate Assistant Support Plan, Fall 2009- present

### TEACHING EXPERIENCE

Teaching Assistant - University of North Carolina at Charlotte, NC (Fall'09 – present)

Responsibilities included holding short lecture sessions, supervising labs, designing undergraduate projects and guiding students through project implementation, helping students with course material, assigning homework and grading.

- Lab Instructor: Digital Design, Instrumentation and Network Theory, Logic and Networks, Electromagnetic and Electronic Devices
- Recitation Instructor: Analog and Digital Communication, Introduction to Electromagnetic fields, Network Theory

Assistant Instructor – Electronics and Optical Communications course, Summer Venture in Science and Mathematics (SVSM) program held for High school students (Summer'09 – Summer'12)

Graduate Student Assistant- Lithography Workshops organized at University of North Carolina at Charlotte for students at the High school level and undergraduate level (Fall'10 – Fall'11)

### OTHER SKILLS

Computer skills

- Programming skills: C/ C++, MATLAB, JAVA, VHDL

Professional skills

- Experience in writing technical research papers and reports
- Extensive oral presentation experience including conferences and research presentations
- Data organization and strong analytical skills
- Ability to work in a multi-disciplinary environment

PROFESSIONAL  
SOCIETIES

Member of Institute of Electrical and Electronics Engineers (IEEE) (2009-Present)

Secretary and Member of Women in Engineering (WiE) (2011-Present)